Geochemical and microtextural characteristics reflect the formation mechanics of laminated iron deposits at the Perle & Bruse and Troll Wall vent fields

Tarje Javnes Lyngtveit

Master of Science Thesis

Department of Earth Science
University of Bergen

August 2017

Abstract

Located at the southern section of the Artic Mid-Ocean Ridge, the Jan Mayen Vent Fields (JMVF) consist of three main hydrothermal sites, the Troll Wall, Perle & Bruse and Soria Moria. These sites contain numerous Fe-deposits, located distal to high-temperature venting sites. A recent study of such Fe-deposits from the Troll Wall reports of abundant neutrophilic Fe-oxidizing bacteria (FeOB), at locations with active low-temperature venting. The same study suggests that the stratified structure, and textural and chemical variations of the laminae and layers of the deposits reflect changes in physicochemical conditions (i.e. temperature, fluid dynamics, pH, nutrient availability), which govern the formation processes, such as habitability and growth of biomineralizing FeOB, and abiotic mineralization. In this study samples of Fe-deposits from both the Troll Wall and Perle & Bruse vent fields are characterized by scanning electron microscopy (SEM) and geochemical analysis, with the aim of establishing possible intra- and inter-field textural and geochemical variations at these sites, and if such variations can be explained by similar physicochemical changes.

The textural results reveal that the samples from both fields are built up of stacked sequences of five distinct laminae or laminated layers of different colour, thickness, porosity and microtextures, separated by internal cavities. A yellow and a light brown layer with a highly porous framework of 10-50 μm thick, 200μm to >1000μm long bundles of 0.3-1μm wide fibres, which apparently grew inward from an outer glass-like lamina and into the cavities, form the innermost layers in each sequence. The fibres were likely formed through nucleation onto extracellular polymers (EPS). Secondary mineral coating and attached twisted FeOB stalks on the bundles in the light brown layer suggest a further development from the yellow stage through different biotically and abiotically dominated stages. Clusters of 2-3 μm wide, branching tubes (Y-guys) associated with biomineralizing FeOB are mainly converging around the glass-like lamina. Massive, 5-15 μm wide, and 50-300 μm long unidirectional filamentous structures comprising most of the outermost brown and dark brown layer, are likely formed from connecting nodular, abiotic precipitates, indicating periods of poor biotic growth conditions. Lower amount of secondary mineral coating, stronger branching of Y-guys, and greater general abundance of other likely biosignatures of microaerophilic FeOB in the Perle & Bruse sample suggest better growth conditions at this site. The geochemical data confirm that the samples from both vent fields have a similar composition, with approximately 50-80 wt% Fe_2O_3 and 20-35 wt% SiO_2, along with low contents of base metals. Mn is enriched in the surface layer relative to the interior, although the concentration is markedly lower in the Perle & Bruse sample compared to the Troll Wall sample. The enrichment likely reflects Mn-oxyhydroxides precipitation at the oxic surface during periods of hydrothermal quiescence. Thus, the variation in Mn-content between laminae at both sites suggests variations in hydrothermal input throughout the formation of the deposits at both sites, with generally a more intermittent hydrothermal activity at the Troll Wall site than the Perle & Bruse site. Chondrite-normalised REE patterns for the Troll Wall deposit are similar to that of seawater and low-temperature hydrothermal fluid previously reported for this field. However, REE patterns with similarity to Jan Mayen basalts for the Perle & Bruse deposit suggest a higher fluid temperature resulting in stronger leaching of the subsurface rocks at this site. Negative Eu anomalies indicate that the hydrothermal fluid at both sites never reached temperatures above 200-250°C.

This study demonstrates that hydrothermal fluctuations and associated shifts in the position of the redox-gradient and nutrient availability likely explain the formation of the laminated structure and the activity of Fe-oxidizing bacteria in marine hydrothermal Fe-deposits. The study also demonstrates that differences in intra-and inter- field textural and chemical composition do exist between the investigated Fe-deposits, and that these differences are likely caused by variation in the venting styles and physicochemical conditions of the hydrothermal fluids. To this end, conceptual models for the formation of the Perle & Bruse and Troll Wall Fe-deposits and associated microtextures are proposed.

Acknowledgements

Contents

1. Introduction

1.1 Investigating hydrothermal deposits

Estimating fluxes, sizes, and depth of hydrothermal circulation systems at mid-ocean spreading ridges is essential for understanding ocean chemistry, and the mineralization processes occurring within the oceanic crust. The latter could also have important economic consequences in the future as the prospect of large-scale deep-sea mining becomes increasingly viable as technology advances. Understanding the prevalence, microenvironmental habitats and metabolism of biomineralizing bacteria in these systems may also help combat expensive subsea corrosion problems (e.g. McBeth et al., 2010; Lee et al., 2013), and may be useful to the mineral processing industry (e.g. Esther et al., 2015).

However, little is currently known about the microbial diversity associated with Fe-oxidizing bacteria (FeOB) and the diversity of Fe-oxyhydroxide structures produced as a party of their metabolism (e.g. Forget et al., 2010), as cultivating and isolating Fe-oxyhydroxide-producing microorganisms have proven difficult (e.g. Hanert, 1973; Hallbeck et al., 1993; Emerson et al., 2007; Krepski et al., 2012). FeOB communities are typically found in isolated freshwater settings, such as tunnels and mine-drainages, and marine low-temperature hydrothermal environments, where they facilitate the formation of Fe-oxyhydroxide deposits (e.g. Hanert, 1973; Hallbeck et al., 1993; Emerson et al., 2007; Chan et al 2011). Despite much study on Fe mat community composition (e.g., McAllister et al., 2011; Baskar et al., 2012; Hegler et al., 2012; Scott et al., 2015; Chan et al., 2016) and mat-derived FeOB cultures (e.g., Hanert, 1973; Hallbeck et al., 1993; Emerson et al., 2007), we still lack basic information about Fe-deposit's architecture and how cells grow and develop microstructures in Fe-deposits located in natural, deep-marine hydrothermal settings (Chan et al., 2016; Johannessen et al., 2017).

Another area of interest regarding the formation of Fe-deposits are the deciphering of the paleo-environmental conditions that led to the formation of ancient seafloor iron formations, which has been the focus of numerous studies over the past decades (e.g. Grenne and Slack, 2003a; Beukes, 2004; Klein, 2005; Grenne, 2005; Beukes and Gutzmer, 2008; Mukhopadhyay et al., 2012). Understanding these conditions is crucial to determining the iron and oxygen cycles, as well as the development and evolution of early life. Modern hydrothermal seafloor Fe-deposits could be analogues to fossil Fe-deposits, which act as archives of ancient microbial processes (e.g. Juniper and Fouquet, 1988; Duhig et al., 1992; Ravizza et al., 1999; Davidson et al., 2001; Grenne and Slack, 2003a, 2005; Slack et al., 2007). Indeed, some jaspers have already been considered as archives for Fe-oxide biomineralization and are known to contain putative filamentous microfossils, including twisted and branching morphologies attributed to marine iron-oxidising bacteria (FeOB) (e.g. Juniper and Fouquet, 1988; Duhig et al., 1992; Little and Thorseth, 2002; Boyce et al., 2003; Little et al., 2004; Slack et al., 2007; Chan et al., 2016). Investigating metabolic and geochemical processes occurring in the modern analogues to these

1

ancient deposits is thus key to deciphering paleo-geochemical processes, Fe-oxide biomineralization, and its role in ancient deposit formation (e.g. Little and Thorseth 2002; Grenne and Slack, 2003a Grenne and Slack 2005, and references therein). Si-rich Fe-oxyhydroxide deposits, which are considered modern precursors to jaspers (e.g. Grenne and Slack, 2003a, Grenne and Slack 2005; Johannessen et al., 2017), form from relatively low-temperature diffuse hydrothermal fluids. Occurring globally, in different hydrothermal settings, these deposits cover extensive areas of the seafloor. (e.g. Hekinian et al., 1993; Slack, 1993; Boyd and Scott, 2001; Scholten et al., 2004; Mosier, 2009; Dekov et al., 2010; Edwards et al., 2011; Sun et al., 2015).

The venting of diffuse fluid from which the Fe-deposits form has lately been suggested to be much more abundant than previously anticipated (e.g. Tagliabue et al., 2010; Bennet et al., 2011; Resing et al., 2015), suggesting shallow, hydrothermal circulation have a significant role in the global Fe-cycling. Indeed, recent studies have suggested that the fluxes from low-temperature venting, rather than from high-temperature black smoker venting, dominate the supply of dissolved Fe derived from hydrothermal systems to the deep ocean (e.g. Elderfield and Schultz, 1996; Bemis et al., 2012; German et al. 2015).

1.2 Hydrothermal circulation, fluid modification, and mineral deposition

The main requirements for initiation of hydrothermal circulation are the presence of water, an underlying heat source, and a means of permeability for the water to circulate through the rock (Tivey, 2007). As such, hydrothermal fields are commonly associated with mid-ocean spreading ridges and hotspots where heat is provided to shallower regions of basaltic crust by rising magma. Among these areas, hydrothermal systems associated with the 60, 000 km long, global mid-ocean spreading ridge system are the most widespread. In such hydrothermally active regions, cold seawater intrudes deep into the crust through faults, brecciated rock, and sediments in areas called recharge zones (Stein and Stein, 1994; 1995) (Fig. 1.1A). Low-temperature oxidation reactions typically occur in the top of the recharge zones, as the seawater provides ample oxygen to the system. The oxidation reactions result in deposition of nontronite and celadonite, along with secondary pyrite. Deeper in the system where the temperature exceeds 150°C, anhydrite typically forms (Alt, 1995).

Some of the fluid may eventually seep down to the heated rock located close to underlying magma, as illustrated in Fig. 1.1A. The addition of heat to the seawater facilitates chemical interactions between the basaltic crust and the fluid. This area is commonly referred to as the reaction zone, and is generally found at a depth of 1.5-2km in the crust, where fluid temperatures exceed 350 °C. At this depth, most seawater oxygen has reacted with the crust, resulting in a mostly anoxic, reducing hydrothermal fluid composition (e.g. Fehn et al., 1983; Alt, 1988; Sleep, 1991; Alt, 1995 and references therein). Until eventual seawater mixing occurs closer to or at the seafloor, the fluid's chemical composition remains anoxic.

Additionally, the solubility of several elements (S, Eu, Fe, Mn, Zn, and Cu) significantly increases in the reaction zone, due to elevated ambient temperatures which allow the elements to enter the fluid phase from surrounding basalts (e.g. Sverjensky, 1984; Wood, 1990). The higher temperatures also increase Si-solubility in water, enriching the fluid in dissolved silica. As the temperature rises further, the fluid eventually becomes buoyant and begin migrating towards the surface through cracks, faults and sediments.

As the modified hydrothermal fluid rises, it subsequently cools. This results in a decrease in solubility and subsequent deposition of minerals (Alt, 1995). At high-temperature discharge sites, seafloor pyrite and other volcanogenic massive sulphide mineral deposits (VMS deposits) form, whilst areas dominated by diffuse low-temperature venting, are often characterized by iron and silica-rich oxyhydroxide mound deposit formations, (e.g. Slack, 1993; Mosier, 2009; Pedersen et al., 2010) and broad spatial distributions (e.g. Bemis et al., 2012).

Formation of low-temperature hydrothermal fluids and associated mound deposits

Low-temperature, diffuse hydrothermal fluid may be generated as a result of several subsurface interactions. Low-temperature hydrothermal fluids may be the result of seawater recharge never reaching sufficient depths to become anoxic or modified. Instead it may circulate in shallow, conductively heated hydrothermal convection systems which do not extend down to the reaction zone (Alt, 1995; Cooper et al., 2000), as portrayed in Fig. 1.1B. Diffuse, low-temperature hydrothermal fluids may also form if seawater recharge is insufficiently channelled towards the seafloor, and subsequent mixing between high-temperature hydrothermal fluid and seawater occurs , as illustrated in Fig. 1.1A).The seawater/hydrothermal fluid mixing process is often considered the most important factor in forming low-temperature hydrothermal fluids. (e.g. Alt, 1995; Cooper et al., 2000; Johannessen et al., 2017)

Such mixing results in reoxidation and rapid cooling of the modified hydrothermal fluid to a temperature of 2-50 °C (e.g. Alt, 1995; Nakamura and Takai, 2014), which are much cooler than temperatures associated with black smoker venting. As hydrothermal fluid eventually reaches the seafloor and oxygenated seawater, the remaining oxidative elements in the fluid precipitate, forming deposits such as VMS, and Fe-or Mn oxyhydroxide mounds, depending on the final chemistry of the vented fluids (e.g. Edmond et al., 1979; Alt et al., 1988; Kendall et al., 2012). The final chemistry of the venting fluid depends on fluid/seawater mixing or cooling processes, which typically occur in highly brecciated crust or in thick sediments, an example of the latter being the Troll Wall, one of the Jan Mayen vent fields (JMVF) (e.g. Pedersen et al., 2010a; Johannessen et al., 2017). In similar low-temperature hydrothermal circulation systems, massive pyrites and oxyhydroxides may rapidly precipitate in the subsurface. Precipitation occurs because temperature, and subsequently solubility becomes too low to sustain elements such as Sulphur compounds in the fluid (e.g. Hannington et al., 1995).

Iron contents must exceed sulphide contents in the hydrothermal fluid before Fe- rich deposits such as those found at the JMVF can form on the seafloor, as Iron will elsewise precipitate with

sulphur to form pyrites in the subsurface (Edmond et al., 1979; Alt et al., 1988). Thus, fluids enriched in Fe are also depleted in Sulphur and sulphur-compounds. Moreover, Fe-rich low-temperature fluids are known to form Fe- and Mn – oxyhydroxide deposits on the seafloor (e.g. Chan et al., 2007; Emerson and Moyer 2011; Johannessen et al., 2017). At ambient bottom water pH and oxygen levels, iron oxyhydroxides form much more readily than manganese oxyhydroxides (Stumm and Morgan, 1998). As a result, Fe-oxyhydroxides generally precipitate closer to the source vent, separating Fe from Mn that either disperses into the water column or accumulates further from the vent (Fig. 1.1). Consequently, distribution of iron and manganese-oxyhydroxides acts as a useful indicator when searching for local variations in redox state in hydrothermal fields.

A

Seawater

He, Mn, FeOOH, MnO_2, CH_4, H_2S,

Plume Fallout

3 – Focused, high-temperature discharge

5 – Diffuse, low-temperature discharge

1 – «Recharge Zone»

Fe/H2S>1

H^+, Ca^{2+}, Na^+

4 - Fluid mixing

«Reaction Zone»

2 - High-temperature fluid alteration, becomes boyant

MORB

Fe(II), Mn(II), H^+, Cl^-, H_4, SiO_2, H_2S, He, CH_4, Ca, CO_2, Li, K, Cu, Zn, Pb

Heat source
(heated rock or magma)

B

High-temperature venting

Low-temperature venting

Diffuse flow + low – T fluid alteration

Conductive seawater heating

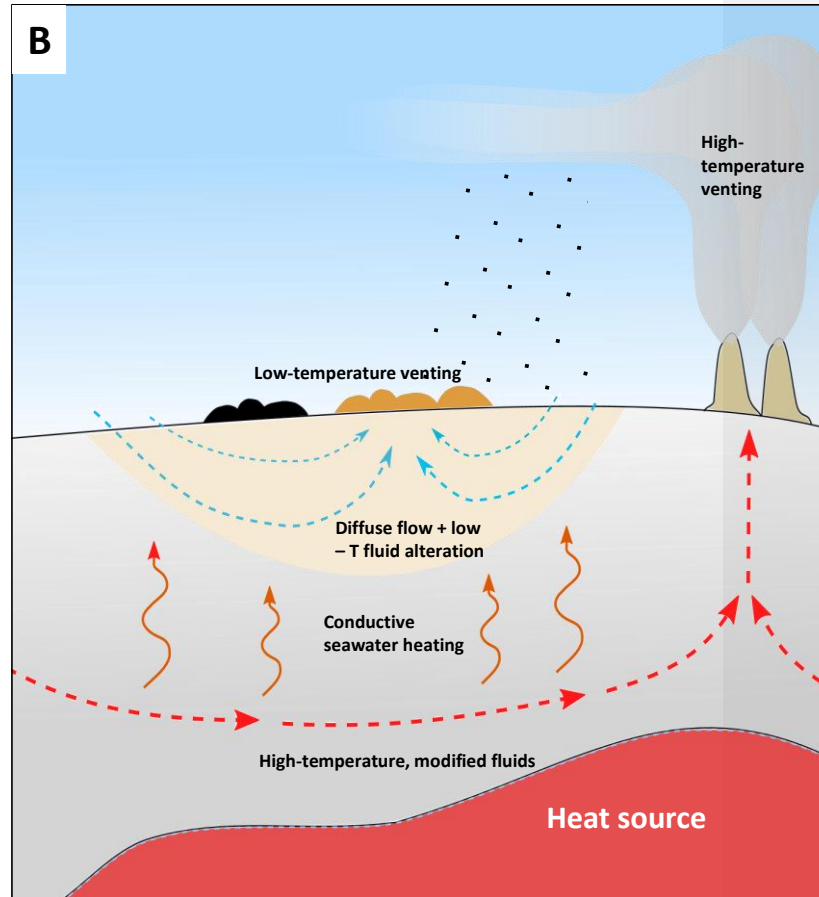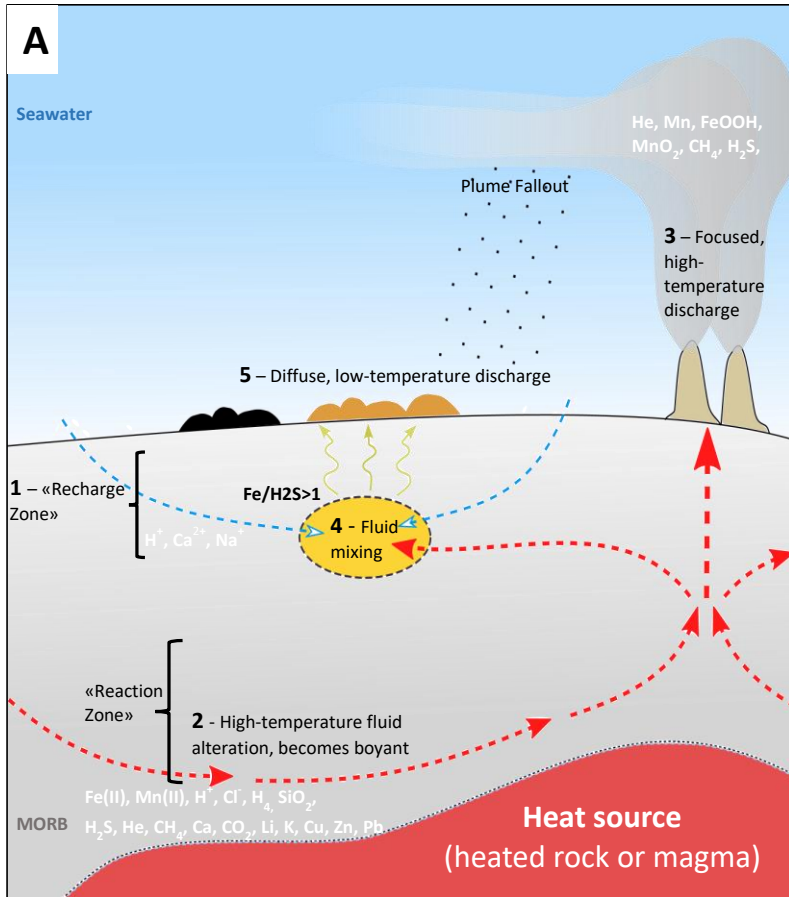High-temperature, modified fluids

Heat source

5

Figure 1.1 (above).

A) Schematic overview of a generic mid ocean ridge- hydrothermal system, modified from Tivey, 2007. The recharge zone (1) is situated off-axis, where Mg, Ca and most of the sulphate are consumed to form smectite, chlorite and nontronite. 2) Reduced metals and sulphur are enriched in the reaction zone, along with ^{3}He, CO_2, CH_4, and H_2 from magma leaching. Temperatures >200-250°C result in leaching of Eu from basalt to the fluid. 3) Hot, modified fluid with low density ascends to the surface in the discharge zone, depositing chimneys. 4) Precipitation of metals such as pyrites occurs where modified hydrothermal fluid and seawater mix close to the surface. 5) Low-temperature hydrothermal, diffuse discharge occurs off-axis (e.g. Fehn and Cathles, 1986), forming hydrothermal Fe (brown) mound deposits if all sulphur has precipitated in the subsurface. Mn-oxide deposits (black) form further from the vent.

B) Schematic overview of a conductively heated circulation system, modified from Cooper et al., 2000. In conductively heated systems, the heat source is likely a high-temperature fluid component circulating beneath the conductively heated system, which in turn has been heated at depth (Cooper et al., 2000). Therefore, no direct mixing of hydrothermal fluids and seawater occurs in these systems.

1.3 Microbiology in hydrothermal environments

The redox and temperature gradients between discharging hydrothermal fluids and seawater can potentially be utilized by extremophilic organisms to gain energy and run metabolic reactions (e.g. Henri et al., 2016). Low-temperature diffuse venting areas (≤110 °C) in hydrothermal systems are thus promising target sites for exploring the impact of extremophilic, biogenic processes, such as microbial Fe-oxidation and dissimilatory iron reduction (DIR). Many metabolic processes involving Fe oxidation and DIR have been found occuring in and leave distinct microstructural, architectural and chemical imprints on marine hydrothermal iron oxyhydroxide deposits (e.g. Alt, 1988; Juniper and Fouquet, 1988; Lizasa et al., 1998; Boyd and Scott, 2001; Emerson and Moyer, 2002; Toner et al., 2009; Dekov et al., 2010; Li et al., 2012; Chan et al., 2016; Johannessen et al., 2017). Lately, such imprints have been studied in Fe-mounds associated with low-temperature diffuse venting in the JMVF to determine prevailing paleo-environmental conditions and mound development (Thorseth et al., 2007; Pedersen et al., 2010; Möller et al., 2014; Johannessen et al., 2017).

Hydrothermal microbial Fe(II) Oxidation

Many diverse types of microorganisms can grow in hydrothermal environments by oxidizing reduced elements like H_2, or Fe(II), which are readily available in hydrothermal fluids. These include bacteria and archaea that couple Fe(II)-oxidation to the reduction of oxygen at either low (e.g. Blake et al., 1993; Edwards et al., 2000) or neutral pH (Emerson and Moyer, 1997), and bacteria that couple Fe(II)-oxidation to the reduction of nitrate at neutral pH (e.g. Benz et al., 1998; Straub and Buchholz-Cleven, 1998). These organisms can significantly affect the geochemistry of the Earth's seafloor environments.

Iron-oxidizing, chemolithoautotrophic Zetaproteobacteria have been detected in diffuse flow systems in the JMVF, where the microorganisms utilize the redox gradient between mixing seawater and hydrothermal discharge to oxidize reduced Fe(II) into Fe(III) oxyhydroxides

Johannessen et al., 2017; Vander Roost et al., 2017, submitted). Inside hydrothermal Fe-mounds, redox gradients may be even more pronounced, allowing certain FeOB to exist inside suboxic regions of the mounds (Johannessen et al., 2017). Suboxic conditions are ideal habitats for microorganisms depending on oxidation reactions. Excessive oxygen concentrations or otherwise unfavourable physiochemical conditions for FeOB could lead to FeOB being outcompeted by abiotic oxidation, resulting in encrustation of the microorganisms by iron oxide precipitates, and domination of non-biotic Fe-oxyhydroxide microtextures and precipitates such as aggregates of globules and nodules, and clusters of non-specific, spherical precipitates (e.g. Chan et al., 2016; Johannessen et al., 2017). Conversely, an inadequate oxygen supply would be insufficient for FeOB to oxidize the minimal amounts of Fe(II) required for cell metabolism. Therefore, subsurface or seafloor Fe mound deposits hosts optimal suboxic habitats for FeOB.

Subsurface Fe(III) Reduction

Dissimilatory iron reduction (DIR) is a metabolic process commonly associated with oxidation of organic matter in deeply buried sediments. DIR is responsible for reducing Fe(III)-rich oxyhydroxide minerals generated through mixing between hydrothermal fluids and seawater in low-temperature subsurface habitats. This process releases Fe(II), along with other elements previously adsorbed to Fe(III)-oxyhydroxides (e.g. Lovely et al., 1990; Emerson, 2007; Johannessen et al., 2017). DIR is believed to take place in the subsurface of most magmatically active regions in the world (Emerson 2007), and has been suggested to take place in the subsurface at the JMVF (Möller et al., 2014; Johannessen et al., 2017).

Biomineralization

The metabolic processes occurring in hydrothermal systems influence the chemistry and distribution of a wide range of elements, as they affect the redox and saturation states of the fluid in the immediate environment surrounding living cells (e.g. Stumm and Morgan, 1996; Chan et al., 2007; Dekov et al., 2010; Li et al., 2012; Chan et al., 2016). Thus, a significant contrast exists between the microenvironment surrounding cells, and the ambient aqueous environment. Consequently, mineral phases may form that would not normally be precipitated at the geochemical and environmental conditions of the ambient fluid.

Despite indirect mediation of this process by biologic activity, precipitation occurs without direct involvement from the microorganisms (Konhauser, 2012). This process is called microbial induced biomineralization, and may occur on the cell surface as products or by-products of cell metabolism, on extracellular polymeric substances (EPS) such as slimes surrounding the cell, or it may occur inside the cell (Konhauser, 2012).

The amount of mineral precipitate depends on the concentration of anions and the timeframe in which the reactions occur. Given sufficient time, the outcome of biomineralization could be a bacterial wall, sheath, or stalk containing copious amounts of mineral precipitate exceeding the mass of the microorganism responsible for the process (e.g. Beveridge, 1984; Chan et al.,

2011; Li et al., 2012; Konhauser, 2012). A typical example of such a biomineralizing bacterium is the iron oxidizer *Mariprofundus ferrooxydans* (e.g. Ishihara et al., 2014).

Biomineralization by iron-oxidizing bacteria typically occurs in two stages. Firstly, electrostatic interactions between metal cations and anionic ligands in the cell wall or EPS induce the formation of small nucleation sites of metal precipitates. The concentration of ions in solution must exceed the solubility product of the mineral phase to reach supersaturation (Stumm and Morgan, 1996). Secondly, additional precipitation at the nucleation sites results in formation of larger biomineral structures such as sub-spherical and filamentous encrustations, preceded by exopolymeric substance (EPS) excretion (e.g. Scolten et al., 2004; Konhauser, 2012; Chan et al., 2011). This process is illustrated in three steps in Fig. 1.2.
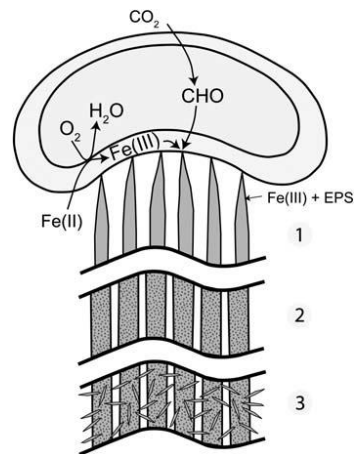
Figure 1.2 Model of stalk formation and mineralization process by iron-oxidizing bacteria, modified from Chan et al., 2011.

1) Fe(III)-polysaccharide (EPS) is excreted from the cell as fibrils.

2) Over time, Fe(III) precipitates as Fe oxyhydroxides.

3) As stalks age, lepidocrocite nucleates on fibril surface.

Biosignatures

Indicating the presence of microbial life, biosignatures are unique mineral structures that may only be generated by biological interference. Biosignatures generated by microbes like FeOB are often invisible to the naked eye, and microscopes are commonly utilized to observe and confirm such structures. Biomineralized microtextures include cell sheaths and filaments, bifurcation areas marking cell division, twisted stalks made of Fe-oxides, and $CaCO_3$ skeletal remains (e.g. Grenne and Slack, 2003a, 2005; 2007; Emmerson et al., 2007; Chan et al., 2007, Chan et al., 2016). An image of the characteristic twisted stalk biosignature produced by *M. ferrooxidans* is illustrated in Fig. 1.3.
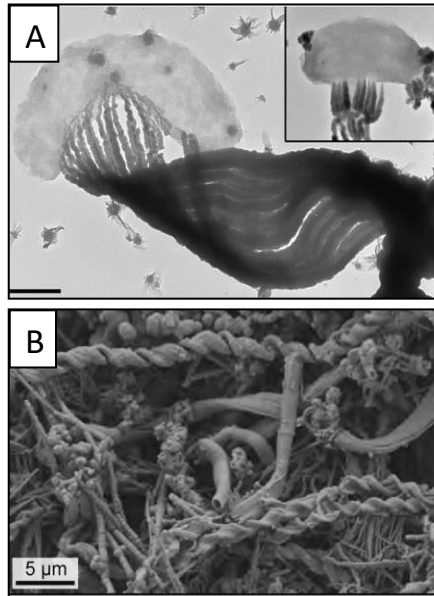
Figure 1.3
A) Recently produced twisted Fe-oxyhydroxide stalk associated with the FeOB M. Ferrooxydans, modified from Chan et al., 2011. The microorganism moves around its axis as it excretes EPS as described in Fig. 1.2, which results in the development of the characteristic, twisted structure (Chan et al., 2011).
B) Older, twisted, ribbon-like stalks occurring together with non-branching, hollow sheaths and clusters of thin fibres, in a hydrothermal mound from the Troll Wall at the JMVF. Modified from Johannessen et al., 2017.

Additionally, Fleming et al., 2014 and Chan et al., 2016 suggested certain biosignatures such as twisted, helical stalks and hollow, branching Y-guys are unique to specific niches, and may be used to infer different Fe-oxidizing communities and paleo-redox conditions prevailing within specific laminae in Fe-mounds.

1.4 Biological activity within hydrothermal Fe oxyhydroxide mound deposits

Zetaproteobacteria and related biosignatures have been discovered in vent deposits worldwide (e.g., Kato et al., 2009a; Forget et al., 2010; Li et al., 2012; Scott et al., 2015), indicating that FeOB play an essential role in facilitating the formation of Fe-oxyhydroxides in modern marine low-temperature hydrothermal environments.

Indeed, one of the most striking examples of ferric oxyhydroxide biomineralization is found in marine hydrothermal settings, where ferric iron minerals precipitate directly from 2-50°C low-temperature hydrothermal fluids on the seafloor as centimetre-metre scale Fe-rich coatings and mounds (Juniper and Tebo, 1995). Often characterised by the occurrence of micro-structures and morphologies connected to the presence of FeOB, these deposits include twisted spirals connected to *Leptospirillum ferrooxydans*, nest-like structures connected to marine *Siderocapsa,* twisted helical stalks connected to the marine species *Mariprofundus*

ferrooxydans, along with a multitude of structures associated with as-of yet unknown FeOB species (e.g. Chan et al., 2007; Chan et al., 2011; Krepski et al., 2013; Chan et al., 2016; Johannessen et al., 2017).

M. Ferrooxidans are highly redox sensitive, requiring strongly opposing redox gradients of Fe(II) and O_2 (e.g. Krepski et al., 2013). Extracellular stalks allow the bacteria to retain their position in the redox gradient and simultaneously avoid encrustation by Fe-precipitates (Chan et al., 2011). As a result of the gradual decrease in Fe(II) concentration and increase in O_2-concentration across the subsurface-seawater interface, iron-oxidizers such as *M.Ferrooxydans* show directional growth, forming organized microbial mats and mounds composed of the characteristic twisted stalks (Fig.4.3)(Chan et al., 2016; Johannessen et al., 2017 and references therein). These structures are an excellent way to investigate crustal circulation patterns, as they retain both a morphological and chemical fingerprint of the evolution of hydrothermal fluid from which they formed, which in turn may provide information on the geology, depth and chemistry of the hydrothermal circulation cell (e.g. Chan et al., 2016; Johannessen et al., 2017). For this reason, mound structures are generally studied through suitable chemical element analysis and microscopy techniques.

1.5 Investigating scavenging characteristics of hydrothermal Fe-deposits

Evidence has been found for fractionation of the elements La, Ce, Gd, Y, and Lu during partitioning between coexisting hydrous Fe oxides and Mn oxides in ferromanganese crusts and seawater (e.g. Byrne and Kim; 1990; Bau, 1999; Bau et al., 1996; Bau and Koschinsky, 2008). The decoupling is due to the properties of Fe- and Mn– complexes to scavenge, or adsorb, dissolved REE's and other trace elements efficiently from seawater and hydrothermal fluids (e.g. German et al., 1990; Sherrell et al., 1999; Baruah et al., 2014). As such, the chemical compositions of the fluid will remain detectable in the deposits as a paleo-signature long after the scavenged fluid is gone (e.g. Grenne and Slack; 2003a; 2005; Chan et al., 2016; Johannessen et al., 2017).

Scavenging properties therefore make Fe-oxyhydroxide rich deposits such as the relatively young Si-Fe oxyhydroxide mounds at the JMVF valuable modern analogues to archives of paleo-geologic and paleoenvironmental information (Johannessen et al., 2017).

An essential element reflecting redox conditions on hydrothermal systems is Ce, which is easily scavenged by Fe-oxyhydroxides. In reducing conditions, Ce is in its soluble form (Ce^{3+}), while in oxidizing conditions, Ce in the form of Ce^{4+} precipitates as CeO_2 onto Mn-oxides and Fe-oxyhydroxides (Bau, 1999; Bau and Koschinsky, 2009), depleting Ce in the oxidative environment. Indeed, the negative Ce-anomaly of seawater has been attributed to oxidative scavenging of Ce on Mn-oxides and Fe-oxyhydroxides (Bau, 1999; Bau and Koschinsky, 2009). As such, high Ce and Ce/Ce* values in Fe-oxyhydroxides often translate to a more anoxic depositional environment (e.g. Koschinsky 2009).

Rare earth element (REE) distributions in submarine hydrothermal fluids have been used extensively as an indicator of sub-seafloor processes associated with hydrothermal activity,

including crustal alteration by hydrothermal fluids. Other elements such as phosphorous, aluminium, titanium, and trace elements like Ba, Zn, Cu and Pb may also be analysed to investigate processes occurring in hydrothermal systems. Such processes include detrital sedimentation, plume fallout and subseafloor diagenesis (e.g. MacLeand and Kranidiotis, 1987; Johannessen et al., 2017 and references therein).

When investigating the origins of source fluids of Fe-oxyhydroxides, careful examination and comparison of REE patterns and values has recently been suggested to be a good approach (Johannessen et al., 2017). Indeed, the origin of low-temperature hydrothermal source fluid which formed Fe-deposits has been determined by analysing LREE/HREE ratios and Eu-anomalies in the deposits (e.g. Alt 1988; Michard et al., 1993; Craddock et al., 2010; Johannessen et al., 2017). For example, positive chondrite-normalised anomalies of Eu imply source fluid to hydrothermal deposits originate at a depth which translates to a temperature of 200-250C, enabling Eu to enter the fluid phase (Sverjensky, 1984; Wood, 1990).

A positive correlation generally exists between LREE enrichment and temperature for hydrothermal source fluids in basalt-hosted vent systems (e.g. Bao et al, 2008). Indeed, LREE enrichment is evident in high-temperature venting fluids when compared to diffuse, low-temperature fluids in the Troll Wall area (Johannessen et al., 2017). However, fluid speciation effects and secondary mineral formation processes should be considered when using REE in hydrothermal vent fluids to infer REE sources in subseafloor reaction zones from which the fluids are derived (Allen and Seyfried, 2005).

1.6 Objectives

Located at the Arctic Mid-Ocean Ridge (AMOR) in the Norwegian-Greenland Sea, the JMVF consist of three hydrothermal sites containing numerous low-temperature Fe-deposits. Thus far, only samples from one Fe-mound in the low-temperature area of the Troll Wall field have been subjected to detailed investigations (Johannessen et al., 2017). In this study, another Fe-deposit in the Troll Wall field, together with a Fe-deposit in the latest discovered vent field in the JMVF area, Perle & Bruse, have been investigated. The aim of the study is to reveal possible variations of textural and geochemical characteristics of the deposits, and their formation mechanisms. The study includes detailed textural and geochemical analyses of the sample material from both sites.

The results show that the Perle & Bruse mounds are precipitated from hydrothermal fluid strongly influenced by basalts, while Troll Wall hydrothermal fluid seem more affected by sediments in the subsurface. Although the mounds at both sites are derived from low-temperature fluids, geochemical and morphological signatures indicate the hydrothermal fluid that formed the Perle & Bruse seem to have been more anoxic, hotter, and stem from a deeper circulation cell than the Troll Wall source fluids.

2. Geological Setting

The section of the Mid-Atlantic Ridge north of 66 °N, the Arctic Mid-Ocean Ridge (AMOR), is one of the slowest spreading ridges in the world, with spreading rates of < 20 mm/year. The AMOR extends from the shelf of Iceland to the Laptev Sea in Siberia and is subdivided into 6 sections: the Kolbeinsey Ridge, the Mohns Ridge, the Knipovich Ridge, The Molly Ridge, the Lena Trough and the Gakkel Ridge (Pedersen et al, 2010) (Fig. 2.1A). The southern section of the Mohns ridge is strongly influenced by magmatic activity from the Jan Mayen hotspots, uplifting a section of the ridge to a depth of only 700-550 m below sea level (mbsl), a shallow depth compared to other sections of the Mohn's Ridge (Kelley et al., 2002; Pedersen et al., 2010).

2.1 The Jan Mayen Vent Fields

At this comparatively shallow and active section of the Mohns ridge, the Jan Mayen Vent Fields are situated at a depth of 550-700 mbsl, located at 71°N and 6°W (Fig. 2.1A). Two active, basalt–hosted hydrothermal vent fields located 5 km apart, the Troll Wall and Soria Moria, were discovered in this area in 2005 (Pedersen et al., 2005). A third field, Perle & Bruse, was discovered more recently in 2013 (Olsen et al., 2016), and is located approximately 2.5 km east of The Troll Wall (Fig. 2.1B).

The Troll Wall vent field

The Troll Wall field is situated within a 150m deep and 2km wide NE-SW-trending rift graben containing copious amounts of siliciclastic sediments, which transects the large central volcano Frøya (Fig. 2.1B). Vigorous high-temperature (270 °C) venting takes place at a relatively shallow depth of approximately 550 m and gives rise to numerous active white smoker chimneys composed mainly of anhydrite, barite, sphalerite and pyrite. The venting occurs through talus deposits at the base of the wall of a rift-bounding normal fault (Pedersen et al., 2010).

Diffuse low-temperature hydrothermal fluids emanate from ridge-parallel faults and fissures along the central rift 500 m west of the active high-temperature venting area, at a depth of approximately 600 mbsl. The low-temperature fluids are associated with extensive reddish-brown flat mats to meter high mounds of siliceous Fe-deposits, which rest on a substrate composed primarily of silicified hyaloclastite and basaltic debris (Pedersen et al., 2010). All sharing a circular and often elongated appearance, more than 150 of these Fe-mounds have been mapped in this area (Johannessen et al., 2017). The mound deposits are comprised of stratified, millimetre- to centimetre-thick layers of siliceous ferrihydrite of low-temperature hydrothermal origin, separated by fluid-filled voids. Fluid between layers within the mounds has been measured 2–7 °C above the ambient seawater temperature (–0.4 °C) (Johannessen et al., 2017). Scanning electron microscopy (SEM) investigation has revealed that the Fe oxyhydroxide layers largely consist of microbial filaments coated by siliceous iron

oxyhydroxides and abiotically formed massive Fe-oxyhydroxide precipitates. DNA analysis has confirmed the occurrence of microorganisms closely related to the Fe-oxidizing bacteria *Mariprofundus Ferrooxidans* (Johannessen et al., 2017). The internal structures and architecture together with the chemical composition of the mounds reflect periodic changes in the local hydrothermal activity (Johannessen et al., 2017).

The Perle & Bruse vent field

The Perle & Bruse field is located on the eastern flank of Frøya, a large central volcano that is undergoing rifting (Fig. 2.1B). Previous mapping of this area by AUV carrying a synthetic aperture sonar system (SAS) has revealed both active and extinct vent sites, along with large areas covered by yellow to rust-coloured hydrothermal deposits (Olsen et al., 2016; Johannessen et al., 2017). The active venting occurs along rift-parallel faults, and is primarily located at two hydrothermal mounds. These are the Perle mound and the Bruse mound, which are separated by 300 m. Vent fluid temperature and composition are thought to be comparable to that of the nearby Troll Wall and Soria Moria vent fields (Thorseth, personal communication, 2017), however no fluid has been measured or sampled from the vents at Perle & Bruse at the time of writing.
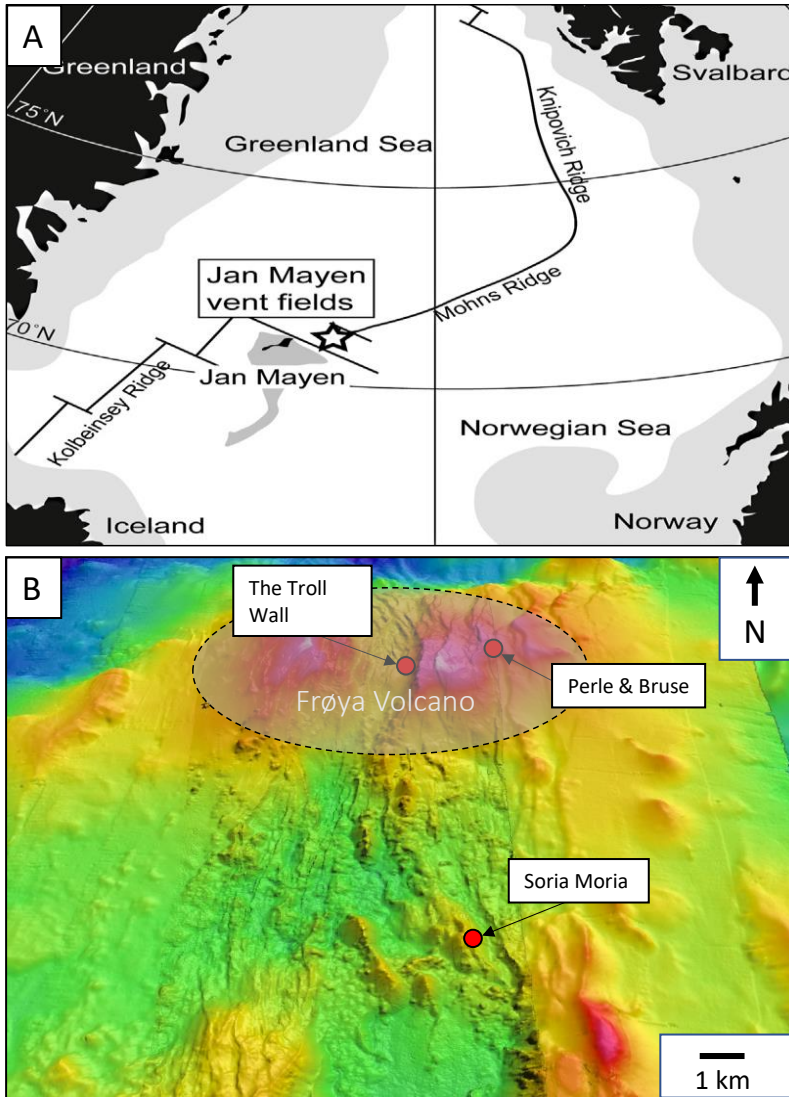
Figure 2.1. A) Map showing the location of the spreading ridges in the Norwegian-Greenland Sea (modified from Pedersen et al., 2010). B) Bathymetric map of the Jan Mayen vent field area at the southern part of the Mohn's ridge. The Troll Wall field is located along a normal fault that defines the eastern margin of a small rift transecting the shallowest part of the ridge segment (the Frøya volcano). Perle & Bruse is located approximately 2.5 km to the east of The Troll Wall.

3. Materials and Methods

3.1 Sample material

Samples from the Troll Wall and the Perle & Bruse vent fields were collected during the Centre for Geobiology cruise summer 2014 to the Norwegian-Greenland Sea with the R/V G.O. SARS. The samples were collected with a Bathysaurus Xl remotely operated vehicle (ROV) (Argus Remote Systems). The ROV was equipped with an advanced high-resolution digital video camera and a 60x60 cm aluminium sampling box with a shovel front, which was used to collect Fe-oxyhydroxide mound fragments by shuffling.

The sample from the Troll Wall was taken from a deposit formed along a fracture in the western wall of the rift valley at 71°17.99'N and 05°46.84'W, at a depth of 556 m. A site with light yellow surface was targeted, as this was assumed to represent active diffuse flow (Fig. 3.1A) (Pedersen et al., 2010; Johannessen et al., 2017). The sample (GS14-ROV12) disintegrated into several fragments of approximately 5x5 cm to 12x10 cm in size (Figs. 3.1B-3.1E).

The sample from the Perle & Bruse vent field was taken from a mound located at 71°17.84'N 05°42.10'W, at a depth of 614 mbsl, between the Perle and the Bruse vent. The targeted mound had a darker surface than those at the Troll Wall, displaying a reddish-brown coloration (Fig. 3.2A). This sample (GS14-ROV13) disintegrated into several fragments of approximately 5x5cm to 9x8cm in size (Fig. 3.2B).

All samples were air dried and stored in plastic containers until further analysed. The samples were examined texturally by optical microscopy and SEM, and geochemically by major element analysis by X-Ray Fluorescence (XRF) and Inductively Coupled Plasma Optical Emission Spectrometry (ICP-OES), and trace and rare earth element analysis by Inductively Coupled Plasma Mass Spectrometry (ICP-MS).
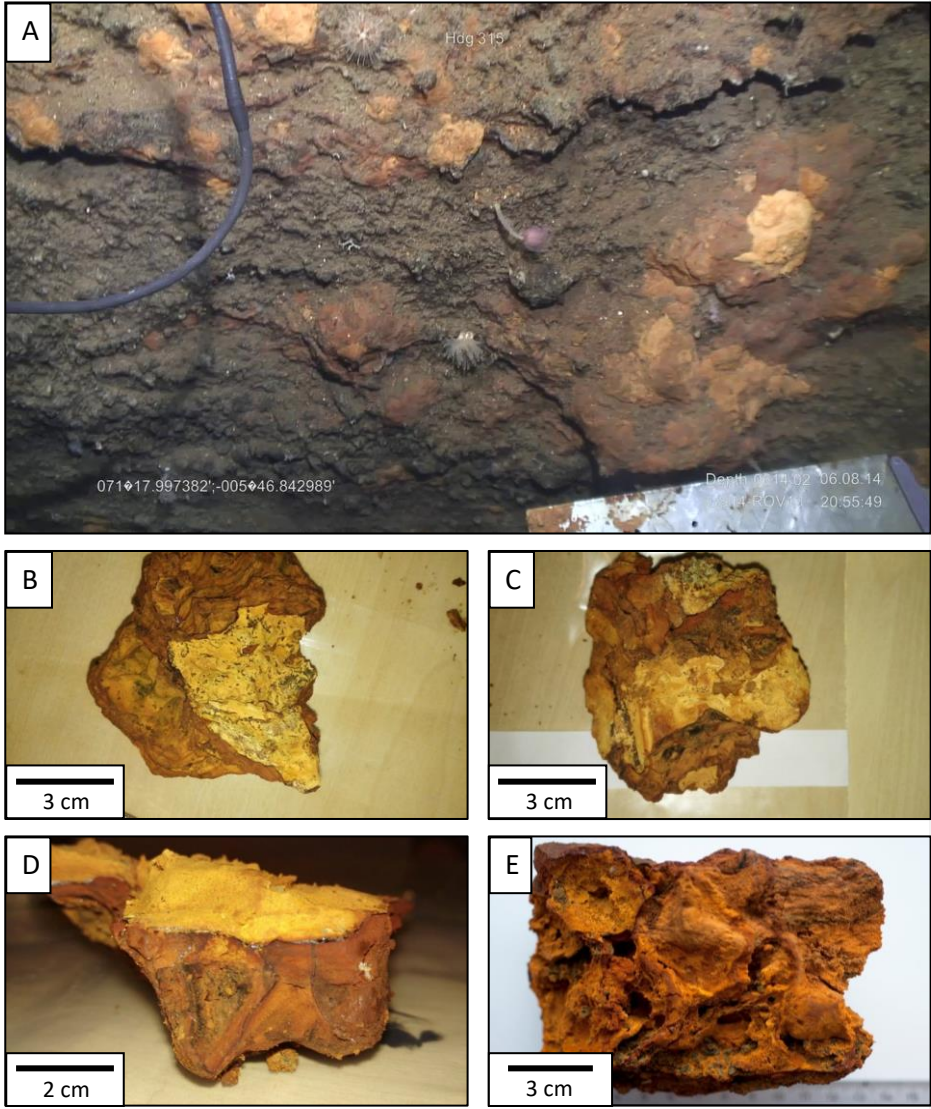
Figure 3.1. Low–temperature Fe-mound deposits at the Troll Wall field. (A) Surface of the Fe-mound occurring along a fracture in the western rift valley wall before sampling. The yellow surface area is indicative of active venting and Fe-precipitation (Johannessen et al., 2017). (B-E) Air-dried mound fragments displaying macroscopic internal cavities and yellow, brown and glass-like laminae. The view is upside-down with respect to seafloor orientation for D. For B, C, and E, images are taken facing the underside of the mound samples.
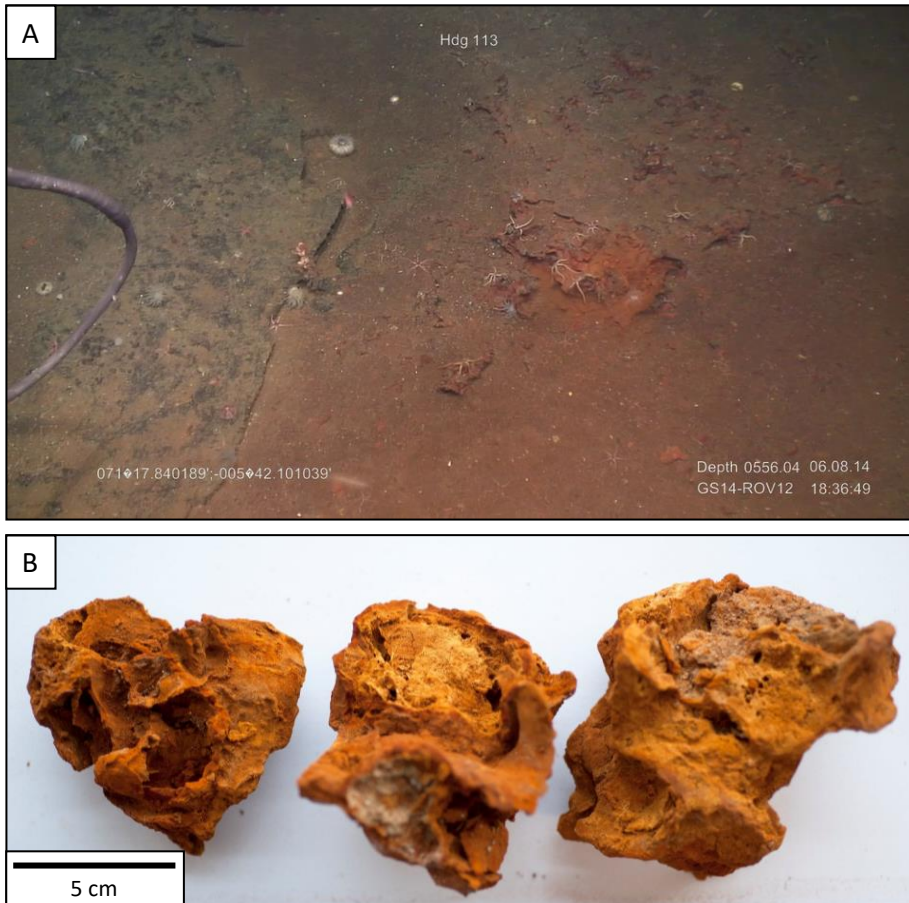
Figure 3.2. Perle & Bruse samples. All mound surfaces look darker than in the Troll Wall sample site. A) Fresh mound before sampling at dive GS14-ROV 12. B) Air-dried mound sample fragments.

3.2 Microscopy

Optical Microscopy

Thin sections were made of selected parts of the Troll Wall and Perle & Bruse samples showing distinct characteristics such as complex patterns and textures. Fragments of the air-dried samples were gently sliced and impregnated with epoxy resin before polished petrographic thin sections were made. A Nikon Eclipse Lv100 Polarizing optical microscope using a DS-Fi1 Nikon Digital sight for photo capture was used for optical photography. The data was then processed using NIS-Elements BR software.

SEM

Smaller fragments were gently removed from the main samples with scalpel and tweezers, and glued onto aluminium stubs with carbon glue. The samples were then coated with iridium (Ir) in a Gatan 682 Presicion etching coating system. Many of the fragments were extremely fragile and thus difficult to glue onto the stubs without damaging their structure.

Microtextures and microscale chemical variations were investigated using a Zeiss Supra 55VP Field Emission SEM equipped with a Thermo Noran Six Energy Dispersive Spectrometer (EDS) system.

3.3 Geochemical analysis

Samples from distinct laminae and laminated layers in the material from both the Troll Wall and Perle & Bruse vent fields were subjected to geochemical analysis by XRF, ICP-OES and ICP-MS. The laminae were distinguished based on macroscale properties such as colour, texture and degree of consolidation, and were carefully separated with a scalpel. Particularly, the thin laminae were difficult to detach, possibly resulting in some contamination from adjacent laminae.

To avoid an apparent mass deficiency in some of the samples ascribed to the unquantified contents of chlorine derived from seawater, and sulphur derived from hydrothermal minerals, the obtained oxide data for all analyses were normalized to 100 wt% without including the LOI. The presence of detrital hydrothermal minerals such as Cu, Zn and Pb might give some samples an artificially low total oxide wt%.

For the samples of insufficient mass for Si analysis, the SiO_2 content was calculated as the difference between 100 wt% and the amount of all other major elements by subtracting the concentration of all other oxides. Obtained calculated values are within the range of the SiO_2 values obtained for most of the analysed samples (Table 1).

Major Element Analysis

Analysis of SiO_2 content was performed with X-Ray Fluorescence (XRF) spectroscopy. Each sample was finely ground in agate mortars, before being ignited at 1000°C. Loss on ignition (LOI) was measured by the difference in weight before and after 1, 3 and 20 hours of heating. Masses of 0.96g of sample material were mixed with 6.72g lithium borate ($Li_2B_4O_7$). The mixtures were subsequently melted at 1200°C into a glass bead in a Classie Flux platina diegel. XRF major element analysis on the glass bead was performed by a S4 PIONER X-Ray spectrometer. Samples PB-p2-CH-GUL, PB-p1- CH1, Tp1-2a, Tp1-3-Glass, Tp1-4, and Tp1GUL had insufficient mass required for SiO_2 XRF analysis.

Repeated measurements on the International standards BCR-2 and BHVO-2 gave analytical precisions better than 2.5% for all elements.

Analysis for all other major elements were performed by a Thermo Elemental iCap ICP-OES. 100g of the grinded and ignited sample material was weighted in a savillex cup, and dissolved in 3ml of hydrofluoric acid (HF). The cup with the dissolved material was dried at 135 $^{\circ}$C for 48 hours. The HF was then fully evaporated before the sample was subsequently converted to nitrate through addition of 20-25ml 2N HNO_3. As a last step, this solution was evaporated before 1-2ml 2% HNO_3 was added, and the solution was heated until the precipitate was either dissolved or accumulated. This last step was repeated until all precipitate was dissolved. Finally, the sample was transferred to a volumetric flask and diluted before being analysed, using ^{45}Sc as an internal standard. Repeated measurements on the international standard BCR-2 gave analytical precisions better than 2.5% for all elements.

Trace and Rare Earth Element analysis

Trace element and rare earth element (REE) compositions were measured on a Thermo Finnigan Element 2 high-resolution ICP mass spectrometer (HR-ICP-MS). Sample preparation was similar to that of the ICP-OES (see section above). 1 ppb ^{115}In was added as an internal standard. Accuracy was determined through measurements on BCR-2 reference samples and was within ±10% for all remaining REEs with respect to the reference values (USGS). For all trace elements accuracy was within ±13%.

The obtained REE data was normalized to the chondrite composition reported by Boynton, 1984. Anomalies were calculated using the formula $\mathbf{Ce_N/Ce_N}^* = \sqrt{LaN * PrN}$ for Ce and $\mathbf{Eu_N/Eu_N}^* = \sqrt{GdN * SmN}$ for Eu, taken from Rollinson, 1993.

4. Results

4.1 Architecture

The samples of Fe-mounds from the Troll Wall and Perle & Bruse vent fields generally display a complex architecture of domelike structures composed of repeatedly stacked sequences of <1mm to 1cm thick laminae and laminated layers of distinct coloration, porosities, textures, and brittleness. Each sequence range in thickness from approximately 1-3cm, is locally interlaid by central cavities. The cavities have a maximum height and width of approximately 1x1 cm.

A full sequence consists of five laminae or laminated layers (Fig. 4.1). Some sequences are incomplete, and lack certain units and/or an internal cavity. Fig 4.3A shows an example of a sequence, where a yellow lamina separating the light brown and glass-like lamina is missing.

The first, innermost layer (layer 1 in Fig. 4.1) in a sequence is usually a light brown layer. The light brown layer often has a highly porous texture consisting of filamentous structures that are connected to a compact, semi-continuous glass-like lamina (layer 3, Fig. 4.1), as depicted in macroscale in a sample fragment from the Troll Wall (Fig. 4.2), and in microscale from Perle & Bruse (Figs. 4.3 A and 4.3B). A yellow <1mm thick lamina (layer 2, Fig. 4.1) is evident in between the glass-like lamina and the light brown layer in some of the samples. The glass-like lamina is usually anchored in a 5-15mm thick overlying brown layer (layer 4 in Fig. 4.1). This brown layer has lower porosity than the light brown and yellow laminas, and contains varying, laminated internal structures. The top layer of a sequence comprises the crustal, outer section of most of the samples, and is dark brown to black in colour and is around 0.5-1 mm thick (layer 5 in Fig. 4.1).

Even in macroscale, there are some obvious differences between the mound samples from the Troll Wall and the Perle & Bruse vent fields. The yellow laminae are generally found in greater abundance in the Troll Wall sample than in the Perle & Bruse sample. The material from Perle & Bruse was generally less consolidated and more brittle than the Troll Wall sample. The Perle & Bruse sample was also generally darker rust-coloured, while the Troll Wall sample displayed a lighter coloration. However, it is only through micro-textural SEM investigation and geochemical analyses that many of the characteristics and distinct differences between the Perle & Bruse and the Troll Wall material become truly evident.
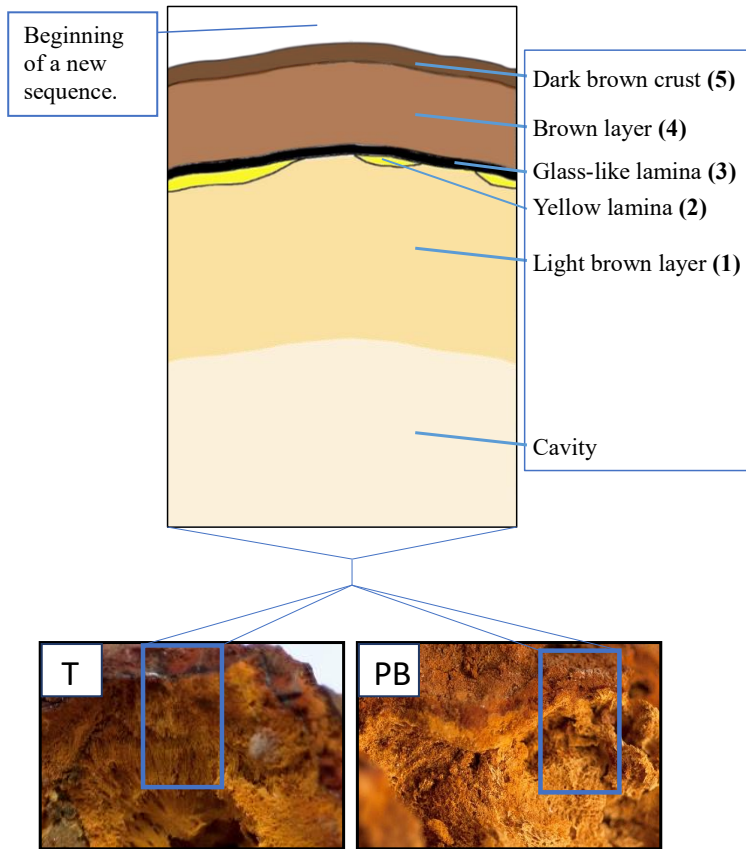
Figure 4.1. Architecture of a fully developed layered sequence in the Troll Wall (T) and Perle & Bruse (PB) mound samples. Note that not all layers and laminae were continuous or present in every sequence that were sampled.
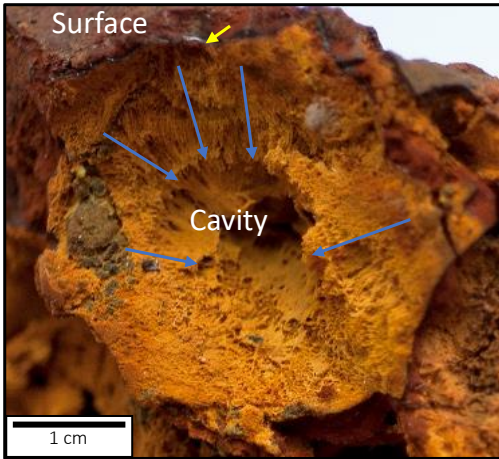
Figure 4.2. Photograph of a fragment of the Troll Wall sample displaying a dome-like structure with distinct lamination. The fragment is seen from below. The blue arrows indicate a direction of the structures comprising the light brown layer, which seem to propagate from the glass-like lamina (marked with a yellow arrow) and inwards to the central cavity, away from the mound surface. Propagation is displayed with blue arrows.
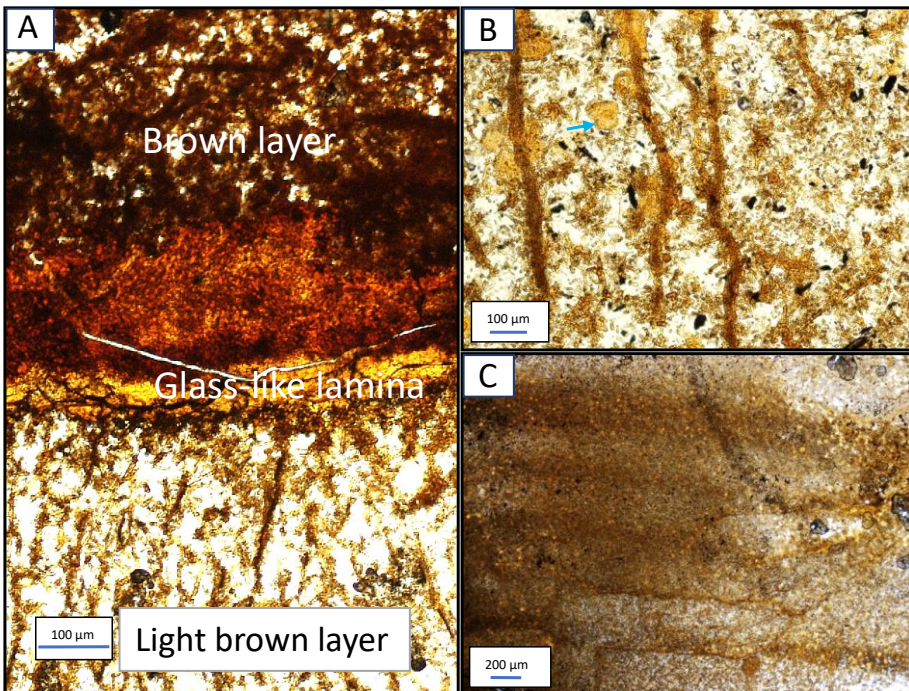
Figure 4.3. Microphotographs of thin sections. A) A sequence of layers in the Perle & Bruse sample material. The glass-like lamina and light brown layer show different porosities and textures. A yellow lamina separating the light brown and glass-like laminae are missing in this sequence. A dark brown, crustal layer covering the top of the

22

brown layer is difficult to discern in this microphotograph. B) Higher magnification of the light brown layer in A displaying nodules (blue arrow) and long structures or veins C) Internal lamination distinguished as zones of variable porosity within a brown layer in the Troll Wall material.

4.2 Microtextures

Distinct layers and laminae and laminated layers within the mounds contain several unique microtextures. Figs. 4.4 and 4.6 depict overviews of the most distinct structural features found in each unit in the samples from the Troll Wall and Perle & Bruse field, respectively. Some of these textures were unique to each field, while others show striking similarities between the two fields.

The Troll Wall

Light brown innermost layer (1)

The innermost part of a layered sequence in the Troll Wall sample consists of a very porous and fragile material consisting of numerous 300- 1000 nm thick, straight or gently curved fibres of Si-rich iron oxyhydroxide (Fig. 11D). The fibres form a network consisting of 5-20 μm wide bundles (Figs. 4.4C, 4.5B and 4.5G). The bundles propagate outward from the glass-like lamina (Fig. 4.5A) and their far ends typically mark the beginning of central cavities. This can be seen in macroscale in Fig. 4.2, and in microscale in Fig. 4.4C. Attached to the bundles are 1-2 μm thick twisted filaments reminiscent of extracellular stalks of iron-oxidizing bacteria. Smaller nodules of Si-Fe oxyhydroxide, as well as distinct honeycomb-structured material displaying a composition similar to nontronite (11D), were found covering the surface of all microstructures in this layer (Figs. 4.5B, and 4.5G)

Yellow lamina (2)

The 1mm thick, yellow lamina consists of straight and gently curved 200nm-300 nm thick fibres (Fig. 4.4A), rich in phosphorous (Fig. 11A), which form a loose, irregular network of 2-4 μm wide bundles. Unlike the bundled structures in the light brown layer, the bundled fibres in the yellow laminae do not contain mineral any mineral cover. Nodes consisting of 50-100 nm wide string-like textures reminiscent of clay were also observed within this lamina.

Glass-like lamina (3)

An approximately 1μm thick, semi-continuous, massive, glass-like lamina was found separating the outer brown and crustal layer from the interior yellow lamina or light brown layer in all the Troll Wall samples (Figs. 4.5C and 4.3). The lamina appears dark in colour in macroscale, as seen in Fig. 4.1. The glass-like lamina crosscut the brown layer in some cases (see sketch 1 in Fig. 4.4), but rarely enters underlying layers or the dark surface layer of the mound. SEM images show that on a microscale, interior parts of the glass-like lamina contain distinct crystals about 10-15 μm in diameter (Fig. 4.5D). In certain areas, the glass-like matrix thinned out or disappeared, creating small gaps in the lamina (Fig. 4.4B). Abundant 2 μm wide, branching

twisted hollow stalks were observed in the immediate vicinity of the gaps (Figs. 4.4F and 4.5E). Some bundled fibres usually common in the light brown layer were observed near the gaps. These were covered by twisted stalks, which did not show any honeycomb-structured coverage, but a smooth surface as seen in Fig. 4.4F.

Brown layer (4)

In microphotographs, the layer is observed to have an internal lamination distinguished as zones of variable porosity (Fig. 4.3 C). The most common microtextures are 5-15 µm wide, 50-100 µm long filamentous structures, often with small nodules of clay minerals, calcium carbonate shells, and basaltic detrital fragments in located between the structures. Some of the filaments show a partly unidirectional pattern (Fig. 4.5F), roughly perpendicular to the underlying glass-like lamina. Globular precipitates rich in iron and silica (Fig. 11C) were also prevalent throughout the layer. Additionally, hollow approximately 10 µm wide and 20 µm long cylindrical tubes (Figs. 4.4E, and 4.5C) were found concentrated in certain regions throughout the layer. The number of detrital fragments and nodules is highest in the outermost section of the layer, which borders the dark brown layer. All the above-mentioned structures in the brown layer are covered in a thick honeycomb coating (Fig. 4.8).

Dark brown crustal layer (5)

Detritus and NaCl crystals were observed covering the dark brown deposit surfaces, along with abundant slime-like material (see Fig. 4.4D), and oxyhydroxide nodules rich in Mn (Fig. 11B). The layer is periodically penetrated by underlying Si-Fe oxyhydroxide filamentous structures, which are more commonly found in the brown layer (not depicted). Filamentous, 500 nm thick structures reminiscent of microbial sheaths (Fig. 4.4D), and threads reminiscent of exopolymeric substances (EPS) (Fig. 4.5I) were observed on top of the slime like material.
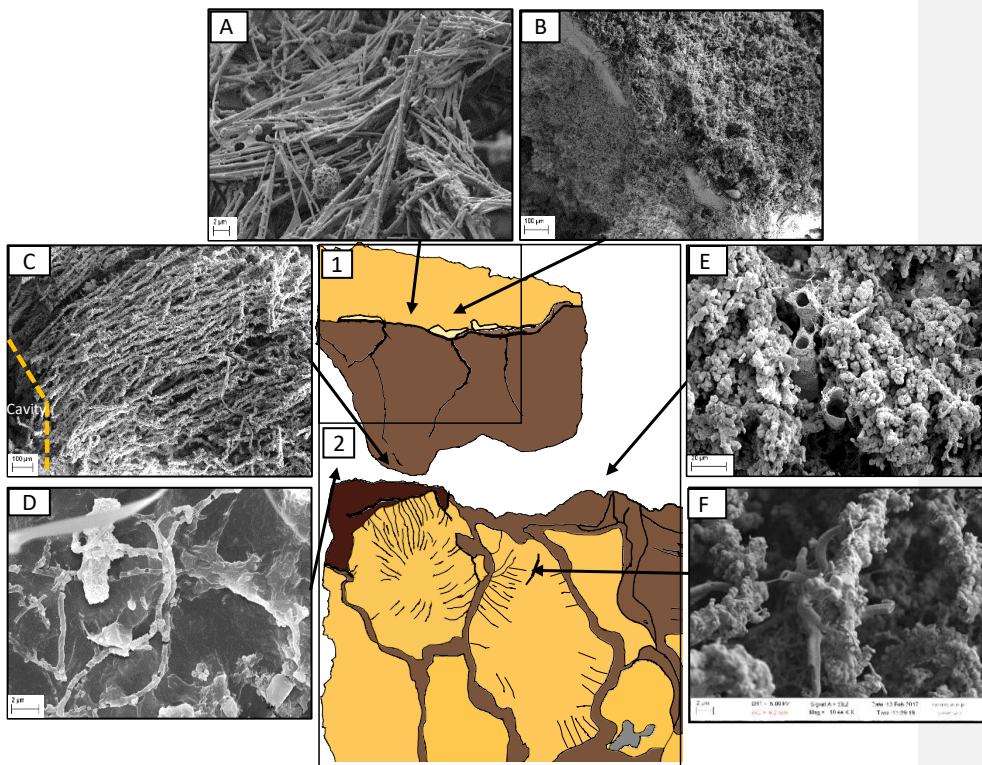
Figure 4.4. Overview of variations in architecture (sketch of fragment 1 and 2) and microtextures observed by SEM in different laminae and layers in a Troll Wall sample. Dark brown areas represent the darkest mound surface not containing detrital fragments, while the grey area represent surface areas covered by sediments. The lightest, yellow area in fragment 1 represents the yellow lamina. The light brown areas represent the light brown layer with interior cavities (not depicted, see Fig. 4.2) and bundled fibre structures in the light brown layer. A) Network of 200-300nm thick, bundled fibres. The yellow arrow shows a node consisting of 50-100 nm wide string-like textures. B) Dense, mineralized glass-like lamina. A channel in the lamina connects the overlying brown and underlying light brown layers. See Fig. 4.5E for a closeup of a zone of transition between the layers. C) 20 μm thick and >1000μm long bundles of fibres displaying growth orientation towards the cavity. D) Mound surface covered in detritus and branching microtextures similar to colonies of elongated sheaths, located on top of a slime-like substrate. E) Section of the brown layer composed primarily of bulbous filaments and some 10μm wide, hollow tubes. F) Hollow, twisted sheaths or stalks growing out from a bundle of fibres found in the light brown layer, close to a channel in the glass-like lamina. The bundle is covered in nodules; however, the twisted stalks reveal a smooth surface unaffected by nodule growth or mineral coatings.
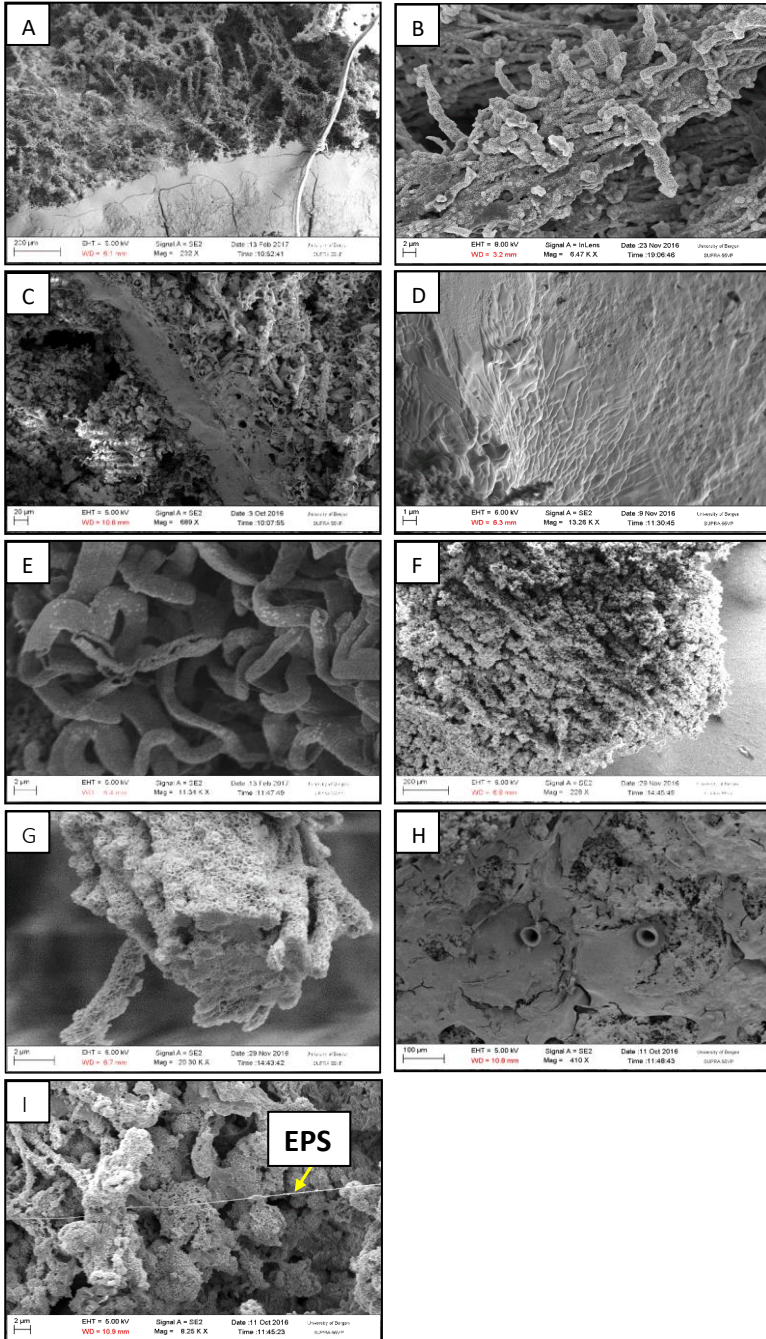
Figure 4.5. (Above): Additional SEM photos from the Troll Wall samples. A) Bundled stalks in the light brown layer propagating out from the glass-like lamina towards the mound cavity. The bundles are directly attached to the glass-like lamina. B) Bundled fibres discovered in the light brown layer. Twisted Si-Fe-oxyhydroxide stalk-like structures seem to grow out from the bundles. A honeycomb structure covers the bundles. C) Glass – like vein with distinct layers on each side. The light brown layer to the right of the vein is dominated by 10μm wide and 20 μm long tube-like precipitates, while the brown layer to the left mainly consists of globular structures and massive fibres. D) Crystallized precipitate on the glass-like lamina. E) High density of hollow, 2μm wide weakly branching twisted stalks. The picture is taken inside an opening in the glass-like lamina, creating a direct transition between the light brown and brown layers. F) Partly orientated filamentous structures in the brown layer covered in nodules of precipitate. G) Cross section of a bundle comprising the network in the light brown layer. Honeycomb structure coats the bundles, which are made up of 500nm-1μm wide fibres. H) Cylindrical tubes penetrating slime or crust on the mound surface. I) Distinct extrapolymeric substance (EPS) located on top of the crustal, dark brown (5) layer.

Perle & Bruse

Light Brown innermost layer (1)

The light brown layer is mainly composed of a very porous framework of bundled 300-500 nm thick gently curved fibres. Like similar structures in the Troll Wall samples, these structures display a unidirectional orientation (see Fig. 4.6E) which is perpendicular to the glass-like lamina, and extend from the glass-like laminae towards the central mound cavity (Fig. 4.7H). The length and extent of bundled fibres were smaller for the Perle & Bruse samples than those found in the Troll Wall samples, however. The bundles were often found covered in twisted or braided Fe-Si stalks displaying similarities to morphologies connected to biomineralization processes involving the Fe-oxidizing bacteria *Mariprofundus ferrooxidans*, shown in Fig. 4.7A), although exact morphologies are difficult to discern due to the amount of mineral cover. The twisted stalk-like morphologies observed here were generally smaller and less abundant than those found in the Troll Wall Samples. Much like the light brown layer in the Troll Wall, a honeycomb structure covers the surface of the bundles. The twisted morphologies and bundles are covered in globular textures and mineral cover, making primary structures largely unrecognizable.

Yellow Lamina (2)

An approximately 1mm thick, yellow lamina consisting of 200-300nm thick massive, gently curved bundled fibres forming a randomly oriented network were located underneath the glass-like laminae in some of the Perle & Bruse samples (Fig. 4.6A). This lamina is generally absent however. Instead, the glass-like lamina typically connects directly to the light brown layer. Like the yellow lamina in the Troll Wall, considerable amounts of phosphorous have been observed in this lamina (see Table 1 and Fig. 12A). Like the yellow lamina in the Troll Wall, this lamina contains no distinct honeycomb cover on its structures. However, high-magnification SEM photos show that nodules tend to cover the filaments (see Fig. 4.7B).

Glass-like massive lamina (3)

Like in the Troll Wall samples, a 1mm thick, glass-like, massive lamina was observed in all Perle & Bruse samples. Figure 4.7F shows that this lamina contains distinct internal, relatively unidirectional 2 μm wide hollow tube-like structures perpendicular to the length of the lamina

which display branching features. Progressive encrustation of these structures by globular precipitates is evident at the interface between the stacked structures and the massive part of the lamina, where no structures remain visible. The tube-like structures generally show a growth orientation out from the central part of the massive glass-like lamina towards the mound cavity, thus appearing at the interface between the glass-like and the yellow or light brown layers (Figs. 4.6C and 4.7F). Like in the glass-like lamina in the Troll Wall samples, crystals of a distinct size and shape were observed inside some parts of the glass-like laminae (Fig. 4.6B). EDS confirmed these crystals were primarily composed of calcium, oxygen, and sulphur (Fig. 12B). Similar crystals of the same composition were also found inside some areas of the brown and light brown layers close to the glass-like lamina, although the majority of all crystals were large and distinct crystals confined to the glass-like lamina. In certain areas, the glass-like matrix thinned out or disappeared, creating small gaps in the lamina with some twisted stalks in the immediate vicinity of the gaps, much like the gaps found in the Troll Wall samples (not depicted). These gaps were rare in the Perle & Bruse samples however, and twisted stalks growing near the gaps (Fig. 4.7H) were less abundant.

Brown Layer (4)

The brown layer mainly consists of distinct massive, cylindrical unidirectional Si-Fe oxyhydroxide filamentous structures, with lengths varying between of approximately 50-300 µm, and a width of 5-15 µm. These structures are much more prevalent here than in the Troll Wall samples (Figs. 4.6 G, 4.7D, and 4,7E). The fibres seem to bend, alternating between exposing the length and orientation of the tubes and the cross-sectional area of the tubes. Larger, 3-5 µm wide hollow tube-like structures similar to those described in the Troll Wall samples are found concentrated near massive, glass-like laminated structures as well as near the main glass-like (3) layer, displayed in Figs. 4.7C and 4.7I. Like in the Troll Wall, basaltic detritus fragments and calcium carbonate shells are evident in the outermost section of this layer, and clay minerals fill up pore spaces between fibres in some areas. Parts of the layer found near, or directly in contact with the glass-like lamina is composed of abundant clusters of hollow, branching tubes, and 1-3 µm wide, braid-like twisted stalks in the brown layer, which were thinning out near the termination of the structures (Figs. 4.6F and 4.7G). The hollow, branching tubes have one to several branching points and are typically 1 µm to 3 µm wide, and their tube walls are <100 nm thick. Larger, filled or partially filled cylindrical tubes were also observed within this layer. All the above-mentioned structures in the brown layer are covered in a honeycomb coating, although the coating is not as pronounced here as in the Troll Wall samples (see Fig. 4.10 for a comparison).

Straight, 1,5 µm thick fibres were on rare occasions observed within the layer. However, these fibres seem loose as they do not anchor anywhere. Additionally, small sections of several massive 40-50 µm thick, glass-like laminae consisting of matrixes of Fe-Si oxyhydroxide globules were found dispersed throughout the layer. The lamina depicted in Fig. 4.7C is an example of such a section. These sections are both thinner and less continuous than the main glass-like (3) layer, but usually separate texturally distinct areas within the brown layer, as illustrated in Fig. 4.7C.

Dark brown crustal layer (5)

The dark brown, crustal layer in the Perle & Bruse mound samples are less pronounced and extensive than the crustal layers observed in similar fragments taken from the Troll Wall. The layer consists of basaltic detritus and calcium carbonate shells, as well as crystals rich in Silica and Titanium (Figs. 12C and 4.6 D). NaCl crystals and organic slime partly cover areas of the surface, with Si-rich filamentous structures covered in globular nodules comprising most of the immediate underlying framework. Like in the Troll Wall, the filamentous structures penetrate the slime surface in certain places (not depicted).
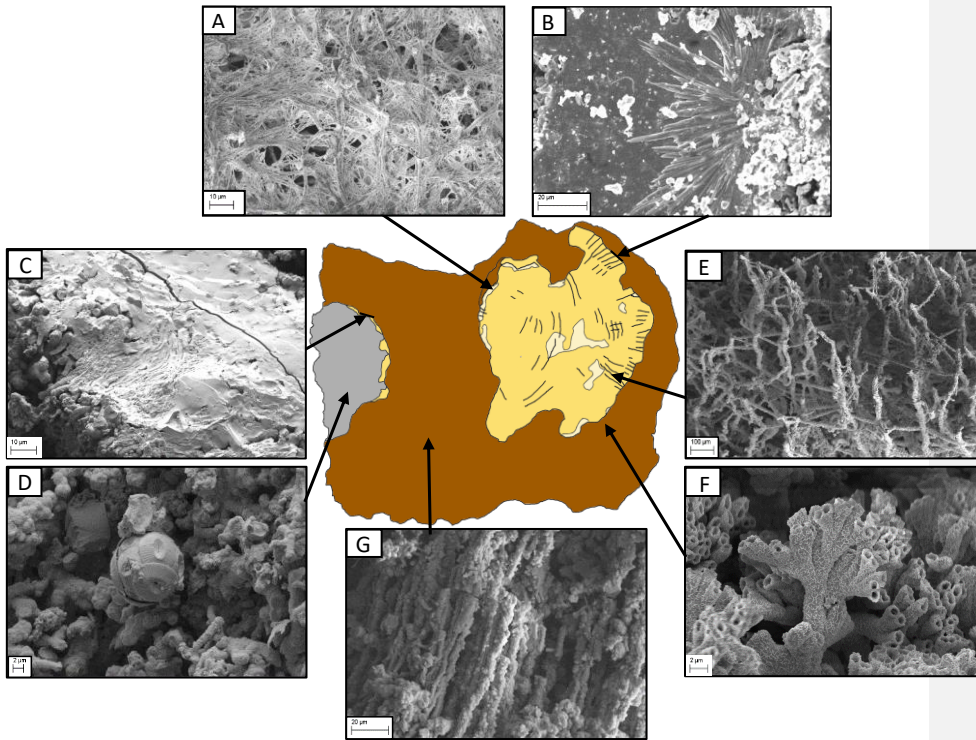
Figure 4.6. Overview of SEM images demonstrating variations in architecture and micro textures in different laminae in the Perle & Bruse samples. The grey area represents mound surface areas covered in sediments. The lightest areas represent the yellow lamina. The light brown areas represent the light brown layer with interior cavities (not depicted) and growth orientations. A) 200nm wide gently curved fibres and Si-Fe nodules occurring in the yellow lamina. B) Crystals growing on the surface of the massive glass-like lamina. C) Branching, tube-like structures with an orientation perpendicular to the glass-like lamina. Both hollow and massive tubes are observed. The structures originate in the middle of the glass-like lamina. The structures are more prevalent closer to the edge of the layer which lies next to the yellow or light brown layer, while they disappear completely at the edge of the glass-like lamina which borders the brown layer. D) Basaltic detrital fragments and calcium carbonate shells covering the mound surface. E) Bundled filaments in the light brown layer showing a uniform growth orientation. F) Clusters of hollow, branching tubes in the brown layer close to an opening in the glass-like lamina. G) Parallel filaments in the brown layer. The filaments are covered in nodules and show a uniform orientation. This microtexture disappears and reappears throughout the brown layer.
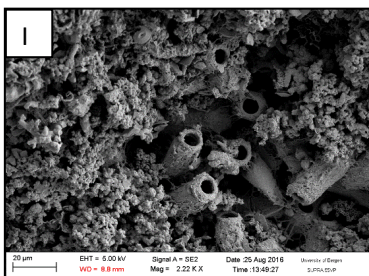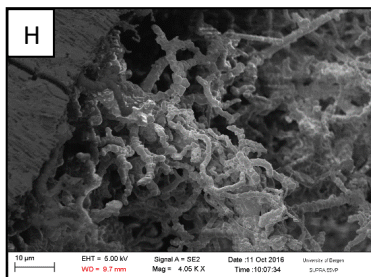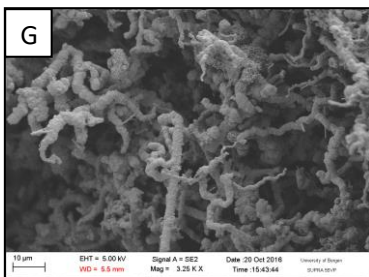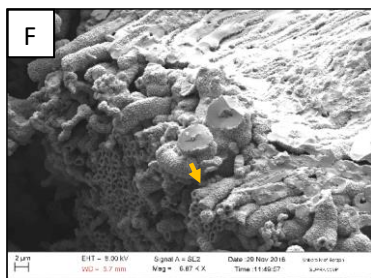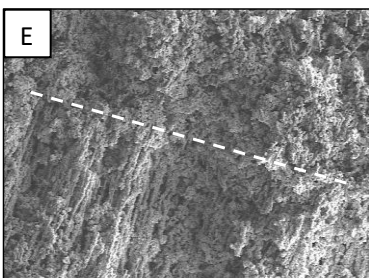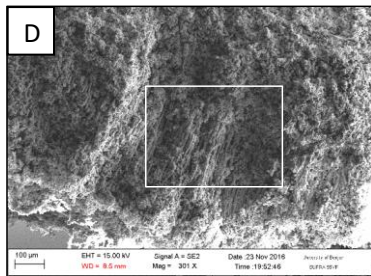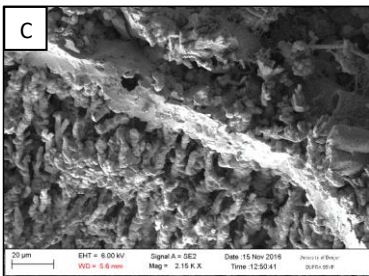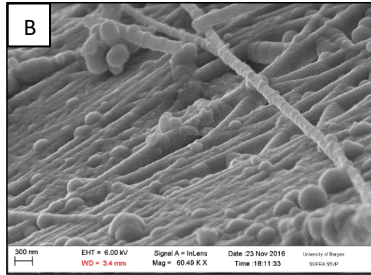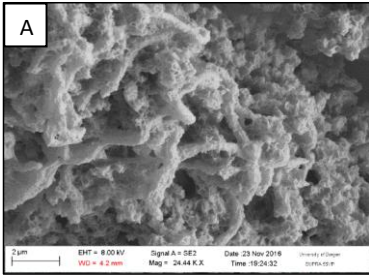
Fig 4.7. (above): Additional SEM photos of the Perle & Bruse samples. A) Twisted stalks seen growing on the side of a bundle of gently curved stalks in the light brown layer. B) 200-300nm thick fibres and nodules from the yellow lamina. No evidence of a honeycomb structure. C) Glass-like vein separating two texturally distinct parts of the brown layer. The lower brown layer consists of distinct hollow or precipitate-filled unidirectional filamentous structures, while the upper brown layer consists of bundled hollow stalks and 10 µm wide, 20 µm wide hollow tubes. D) Precipitate-filled, cylindrical unidirectional fibres with an orientation perpendicular to the glass-like laminae. E) Magnified section (white rectangle) of Fig. 4.7D. The dashed line represents an area within the brown layer where the length of the unidirectional fibres begins to appear. F) Branching, 2 µm wide tube-like unidirectional structures with an orientation perpendicular to the glass-like lamina. Both hollow and massive tubes are observed. The structures originate in the middle of the glass-like lamina. The structures are more prevalent closer to the edge of the layer which lies next to the yellow or light brown layer, while they disappear completely at the edge of the glass-like lamina which borders the brown layer. The branching, Y-shaped structure is marked with a yellow arrow. G) 1-3 µm wide, braid-like twisted stalks in the brown layer, thinning out near the termination of the structures. H) Bundled fibres containing braid like stalks. These structures are located in the light brown layer, and are anchored in the glass like lamina to the left in the image. The structures were located near a gap in the overlying glass-like lamina. I) Closeup of the 10 µm wide, 20 µm long hollow tube-like structures located in the brown layer and described in Fig. 4.7C.

Honeycomb cover thickness comparison
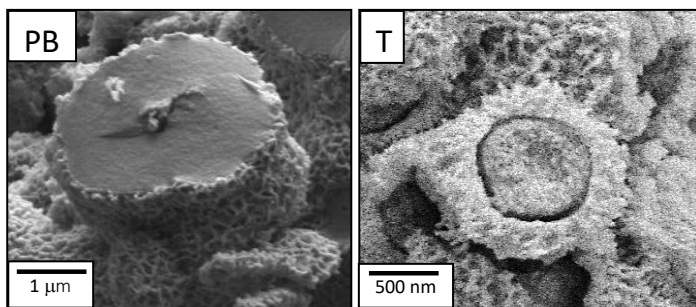
Fig. 4.8. Honeycomb cover thickness comparison between unidirectional massive, fibre-like structures in the Brown layer in Perle & Bruse and Troll Wall samples. The honeycomb cover is distinctly thicker in the Troll Wall (T) samples.

4.3 Geochemistry

Major element composition

The analysed layers were primarily composed of Fe_2O_3 and SiO_2 (Table 1). The LOI ranged between 21- 50 wt% (Table 1). The average total amount of oxides in the fully analysed samples was close to 100 wt%, except for the sample from the outermost layer (Tp1-2b), which displayed high concentrations of Cu, Zn, and Pb (Fig. 4.9B).

The analyses reveal high P_2O_5 content in the yellow laminae (4.71-5.34 wt%) and the light brown layers (2.84-2.90 wt%) for both the Troll Wall and the Perle & Bruse samples relative to the glass-like (3), brown (4), and dark brown surface (5) layers, which all display values in the range of 0.56-2.22 wt% (Table 1).

In the Troll Wall sample, the MnO concentrations were highest in the brown (4) and dark brown (5) layers (1 wt%-1.6 wt%). Consistently low MnO concentrations of <0.15 wt% were evident for all analysed laminae and layers from Perle & Bruse, with the notable exception of the grey crustal layer that displayed MnO values of 0.39 wt%. All MnO values are displayed in Table 1.

Al_2O_3 and TiO_2 concentrations were highest in the light brown (1) and yellow (2) layers relative to the other layers for both the Troll Wall and the Perle & Bruse samples (Table 1), although the highest concentrations are evident in the Troll Wall samples. A notable exception is the high TiO_2 concentration in the grey, crustal layer from Perle & Bruse. The light brown layer in the Troll Wall sample shows significantly higher Al values than any other layer (2,37 wt% Al_2O_3). TiO_2 and Al_2O_3 concentrations are also positively correlated ($R^2 = 0.9961$), as displayed in Fig. 4.9C. The concentration of TiO_2 also correlates with the concentration of Zr ($R^2=0.9563$).
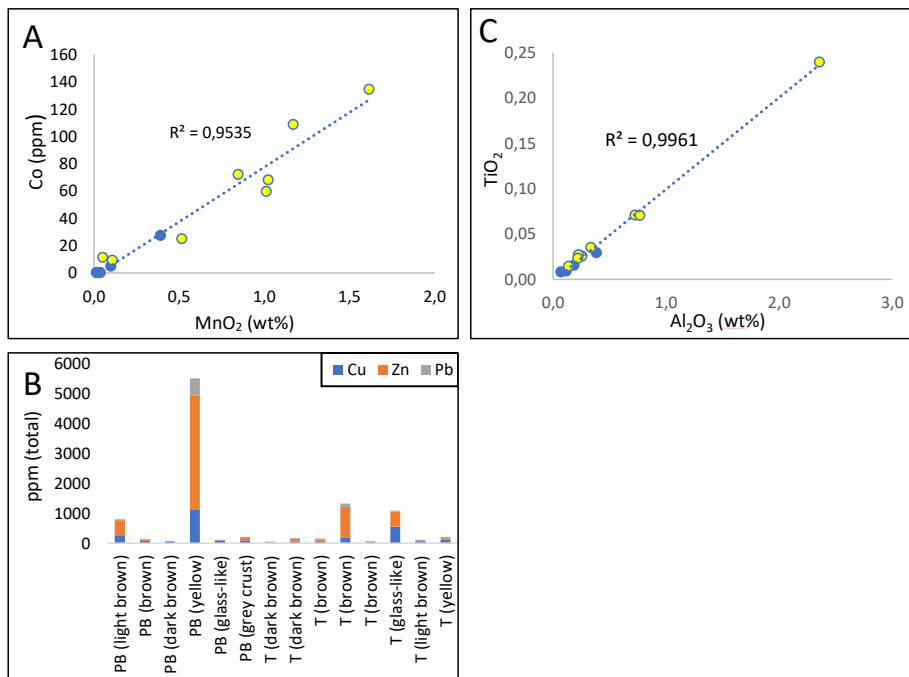
Fig. 4.9. Relationships between a selection of major and trace element data from the sampled Jan Mayen Fe-mounds. A) TiO$_2$ and Al$_2$O$_3$ correlations in the Troll Wall (yellow dots) and Perle&Bruse (blue dots). B) Diagram displaying the total concentrations of Cu, Zn and Pb in certain layers. C) Zr and TiO$_2$ correlations in the Troll Wall (yellow dots) and Perle&Bruse (blue dots).

Trace element composition

High Co concentrations of >100ppm were obtained for dark brown laminae from the Troll Wall sample, while Co was low (<72 ppm) or below the detection limit in the Perle & Bruse samples, and in the other the Troll Wall laminae (See Table 2). Co displays a strong correlation with MnO in both mound fragments (R^2 = 0.9535) (Fig. 4.9A), and are enriched in all crustal layers relative to other layers or laminae from the same sample sites. Trace elements except Li and Sr were slightly depleted both in the Troll Wall and Perle & Bruse samples relative to basalts from nearby JMVF ridge segments (Svellingen, 2004, Table 4).

Cu, Zn, Pb concentrations were significantly higher in the light brown (1) and yellow (2) layers in the Perle & Bruse samples, and the glass-like laminae and brown layer (sample Tp1-2b) in the Troll Wall samples (Table 2, Fig. 4.9B). The yellow lamina from Perle & Bruse displays significantly higher concentrations of these elements relative to any other sample (1105 ppm Cu, 3836 ppm Zn, and 567 ppm Pb).

Excluding La and Ce, the Troll Wall sample was strongly depleted in all light REE (LREE) and slightly depleted in most heavy REE (HREE), while the Perle & Bruse sample was only slightly depleted in LREE but more strongly depleted in HREE compared to basalt from the same area (Table 3,4,5 and Fig. 4.10). The darker layers in both samples generally display stronger depletion in all REE's relative to JM basalts than the lighter (yellow and light brown) layers. The glass-like laminae show intermediate REE values compared to JM basalts.

Most chondrite normalized REE concentrations yielded similar distribution patterns for laminae with distinct colours and textures (Fig.4.10). The light brown (2), yellow (5), and glass-like (3) layers display REE enrichment relative to the brown (4) and dark brown (5) layers for samples from both the Troll Wall and the Perle & Bruse sample sites. An exception is a brown (4) layer (sample Tp-2/3) from the Troll Wall (see Fig 4.10B), which show REE enrichment relative to most other layers and laminae from the Troll Wall. A major difference between the two sample sites (the Troll Wall and Perle & Bruse) is the general REE distribution patterns. All Perle & Bruse samples display significant Light Rare earth element (LREE) enrichment, and Heavy rare earth element (HREE) depletion when compared to the Troll Wall mound samples (see Table 3 and Fig. 4.10). The samples from Perle& Bruse (see Fig. 4.10A) displays REE values notably similar to the REE compositions of Jan Mayen basalts collected by Svellingen (2004), (Fig. 4.10C) while the Troll Wall sample REE distribution patterns (Fig. 4.10B) are similar to that of Troll Wall low-temperature fluids taken by Johannessen et al., 2017 (Fig. 4.10 D).

Light Rare Earth Element (LREE) enrichment and negative Eu-anomalies (Eu/Eu*< 1) are evident throughout all sampled layers (Figs. 4.10A, 4.10B, and Table 3), indicating lower concentrations than expected from extrapolation of neighbouring elements. Samples from the yellow (2) and dark brown (5) crustal layers from the Troll Wall, and samples from the crust and glass-like laminae of Perle & Bruse samples display a positive Eu-anomaly when run in standard definition mode. These samples also contain high concentrations of Ba, however (~680-6362 ppm BaO, see Table 2). Eu-anomalies has been assumed to be attributed to interferences between the peaks of ^{153}Eu and BaO (Johannessen 2017, and references therein). Therefore, to counter potential interference, an average of the concentrations for the Eu isotopes Eu151 and Eu 153 were run in High Resolution (HR) mode for all samples. All positive Eu anomalies were removed

once run at high resolution in the ICP-Mass Spectrometer, and therefore only HR-ICP concentrations are used. All chondrite-normalized REE values are presented in Table 3.
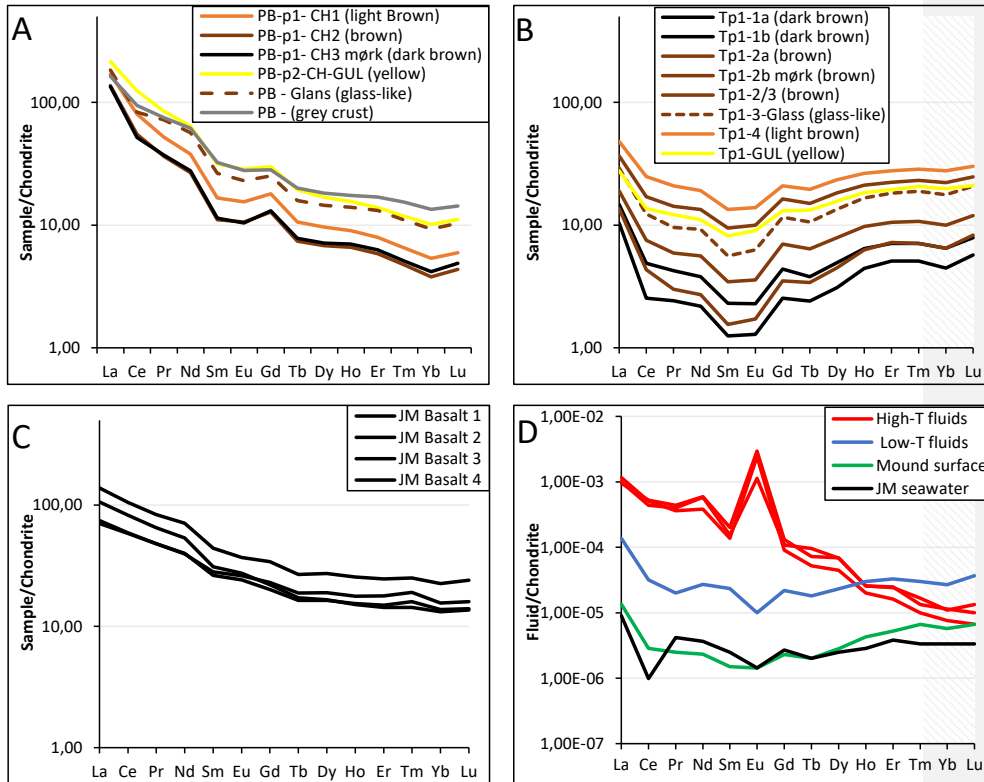
Figure 4.10. A) REE concentrations for Perle & Bruse samples normalized to chondrite. B) REE concentrations for the Troll Wall samples normalized to chondrite. C) Chondrite normalized REE values from basalt samples from the Jan Mayen Platform area taken from Svellingen, 2004, represented in Table 4.D) Jan Mayen deep seawater and hydrothermal fluid REE compositions taken from Johannessen et al., 2017, normalized to chondrite. All Chondrite values are taken from Boynton, 1984. Values displayed in A and B are taken from Table 3, while values displayed in C and D are taken from Table 4.

In addition to low (<1) Eu/Eu* values, Ce/Ce* values of < 1 was detected in all samples from both the Troll Wall and Perle & Bruse. There is generally a correlation between Ce/Ce* and Eu/Eu* values within the same sample, as seen in Table 3. The dark brown, crustal layers in the Troll Wall samples has both notably lower Ce/Ce* and Eu/Eu* values relative to other all other layers in all samples (see Table 3). Moreover, both the Eu/Eu* and Ce/Ce* values were somewhat lower in the dark brown (5) layer compared to the other layers sampled from Perle & Bruse. La/Yb values were high (La/Yb >10) for all Perle & Bruse samples relative to the samples from the Troll Wall, which all displayed relatively flat REE curves, reflected by low La/Yb values of < 2 (Table 3). Y/Ho values are significantly higher than the Y/Ho values for local basalts, although depleted compared to previously analysed Troll Wall low-temperature hydrothermal

fluids (See Table 4 and Table 5). Additionally, the Y/Ho values of all Perle & Bruse samples are generally somewhat higher than both values from the Troll Wall reported in this thesis, and Y/Ho values reported by Johannessen et al., 2017 from similar Fe-mound deposits from the Troll Wall.
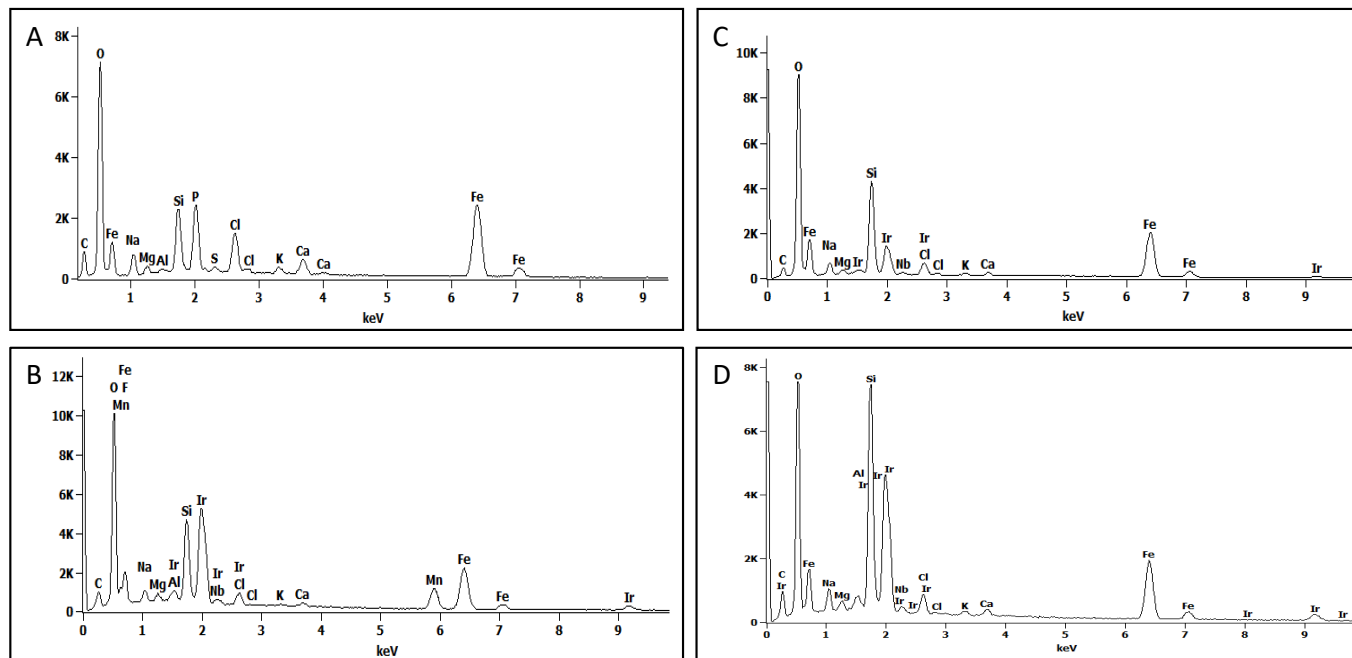
EDS - Troll Wall

Figure. 11. The Troll Wall. A) Phosphorous-rich yellow lamina. B) Mn-rich oxyhydroxide nodule from the dark brown layer. C) Si-Fe globular precipitates in the brown layers. D) Composition of the bundled fibres in the light brown layer. The bundled fibres contain a high amount of Silica.
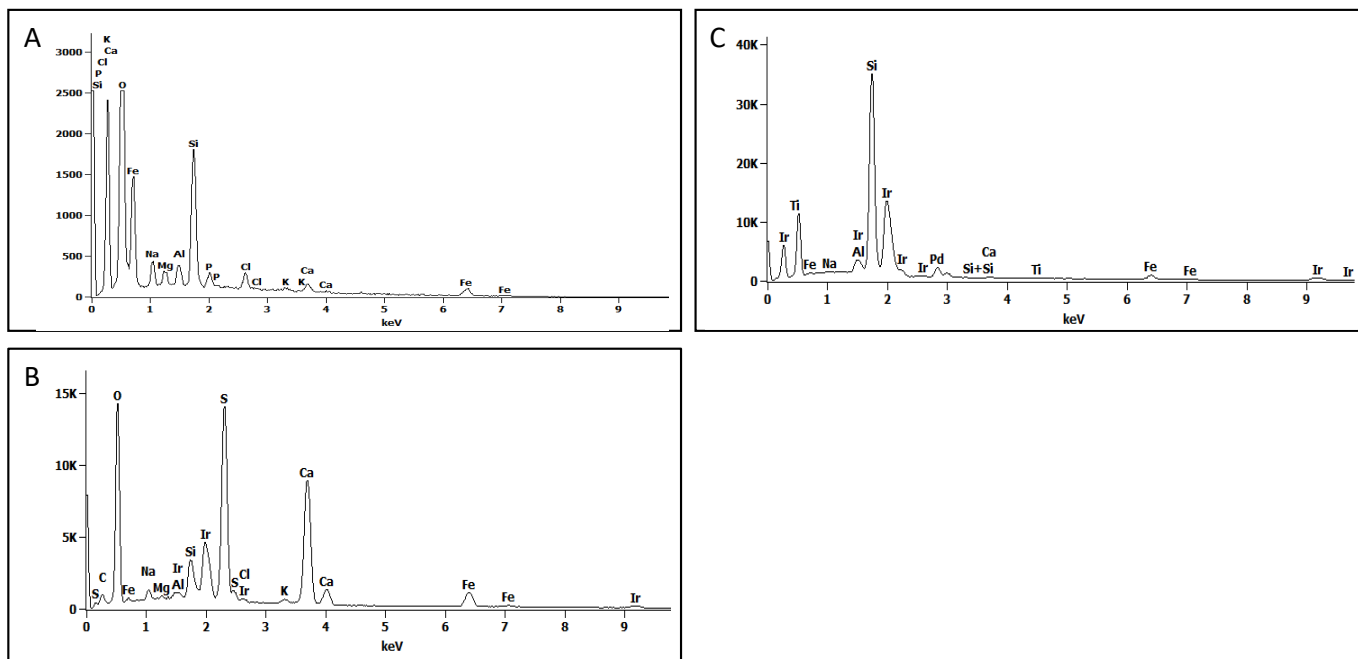
Figure. 12. Perle & Bruse. A) Composition of the yellow lamina, which display phosphorous enrichment. B) Composition of the crystallized precipitate found in the glass-like lamina. The precipitate contains mostly sulphur, oxygen, and calcium. C) Composition of crystals located in the dark, crustal layer. The crystals display large amounts of Si and Titanium.

ICP analysis – Tables

Table 1

Major element composition of layers and laminae in samples from the Troll Wall and Perle & Bruse. Estimated SiO2 values are in red. Some data was below the detection limit or could otherwise not be detected by the instrument.

	MgO	Al$_2$O$_3$	SiO$_2$	P$_2$O$_5$	K$_2$O	CaO	TiO$_2$	MnO$_2$	Fe$_2$O$_3$	LOI
	wt%	wt%	wt%	wt%	wt%	wt%	wt%	wt%	wt%	wt%
Perle & Bruse										
PB-p1- CH1 (light brown)	1.84	0.19	23.32	2.9	1.00	3.02	0.02	0.04	67.69	26.92
PB-p1- CH2 (brown)	-	0.07	25.23	2.07	0.68	2.87	0.01	0.01	69.77	26.33
PB-p1- CH3 mørk (dark brown)	1.81	0.12	22.03	2.06	0.67	2.79	0.01	0.02	69.24	28.04
PB-p2-CH-GUL (yellow)	-	0.38	28.66	4.71	1.45	2.54	0.03	0.11	62.11	28.79
PB – Glans (glass-like)	-	-	-	-	-	-	0.02	0.1	-	26.27
PB (grey crust)	-	-	-	-	-	-	0.72	0.39	-	21.27
Troll Wall										
Tp1-1a (dark brown)	1.68	0.14	14.04	1.64	-	2.44	0.01	1.17	79.36	26.37
Tp1-1b (dark brown)	-	0.34	22.81	2.22	0.78	2.38	0.04	1.62	71.4	50.05
Tp1-2a (brown)	1.68	0.26	17.62	0.56	0.75	2.09	0.03	1.02	76	27.49
Tp1-2b mørk (brown)	-	0.23	28.96	1.84	1.48	1.71	0.03	1.01	58.27	44.58
Tp1-2/3 (brown)	-	0.73	33.2	2.14	0.94	1.47	0.07	0.02	58.59	24.82
Tp1-3-Glass (glass-like)	-	0.22	23.07	2.19	0.77	1.53	0.02	0.52	71.68	24.19
Tp1-4 (light brown)	1.92	2.36	37.23	2.84	1.28	2.66	0.24	0.05	51.41	23.08
Tp1-GUL (yellow)	-	0.77	24.46	5.34	1.52	2.47	0.07	0.85	64.52	27.66

Table 2

Trace element composition of layers and laminae in samples from the Troll Wall and Perle & Bruse (ppm). Some data was below the detection limit or could otherwise not be detected by the instrument.

	Li	V	Sr	Ba	Y	Zr	Cr	Co	Ni	Cu	Zn	Pb
Perle&Bruse												
PB-p1- CH1 (light brown)	67.47	346.18	1019.02	1086.42	29.94	12.13	-	-	-	265.91	498.64	39.79
PB-p1- CH2 (brown)	68.04	281.29	955.71	204.89	23.61	12.11	11.61	-	-	77.05	38.14	28.19
PB-p1- CH3 mørk (dark brown)	48.40	324.79	899.97	106.89	25.23	11.43	-	-	-	58.90	-	-
PB-p2-CH-GUL (yellow)	116.82	969.12	921.32	417.21	44.99	15.12	46.40	9.10	-	1105.36	3836.52	567.21
PB – Glans (glass-like)	-	863.10	705.10	338.30	34.40	3.39	8.29	4.69	7.25	91.09	14.55	1.43
PB (grey crust)	-	1091.00	1154.00	6362.00	39.09	64.89	41.88	27.21	23.81	97.06	98.06	2.60
Troll Wall												
Tp1-1a (dark brown)	75.32	413.53	762.49	684.69	19.15	14.45	10.65	108.62	37.72	24.49	22.29	-
Tp1-1b (dark brown)	61.66	338.86	706.71	810.67	20.33	13.50	11.43	134.45	38.59	54.84	76.36	36.94
Tp1-2a (brown)	109.92	42.18	611.28	299.02	24.20	13.50	16.51	68.02	36.13	56.96	53.37	46.94
Tp1-2b mørk (brown)	145.59	-	501.98	130.79	25.11	9.45	-	59.61	20.15	174.15	1039.12	106.73
Tp1-2/3 (brown)	50.99	50.94	388.86	711.56	47.00	15.90	-	-	-	21.80	23.72	25.70
Tp1-3-Glass (glass-like)	73.99	45.46	507.12	334.51	38.57	14.39	10.62	24.97	-	550.70	501.48	34.22
Tp1-4 (light brown)	84.52	79.05	496.28	1424.09	54.99	26.86	26.79	11.20	-	41.99	32.58	44.26
Tp1-GUL (yellow)	157.46	113.03	819.47	4619.82	38.39	11.73	27.42	72.00	28.95	114.79	51.53	41.54

Rare earth element (REE) composition of layers and laminae in samples from the Troll Wall and Perle & Bruse (ppm). Normalized to the chondrite composition presented by Boynton (1984). (Non-normalized values in Table 5).

	La	Ce	Pr	Nd	Sm	Eu	Gd	Tb	Dy	Ho	Er	Tm	Yb	Lu	La/Yb	Eu/Eu*	Ce/Ce*
Perle & Bruse																	
PB-p1- CH1 (light Brown)	169.65	80.36	51.92	37.88	16.65	15.43	17.96	10.60	9.59	9.00	7.95	6.50	5.36	5.93	28.59	0.89	0.86
PB-p1- CH2 (brown)	136.81	54.90	36.33	26.78	11.05	10.57	12.77	7.40	6.78	6.57	5.86	4.73	3.79	4.37	31.33	0.89	0.78
PB-p1- CH3 mørk (dark brown)	134.39	51.77	37.17	27.65	11.35	10.43	13.08	7.80	7.13	7.00	6.29	5.10	4.17	4.87	27.61	0.86	0.73
PB-p2-CH-GUL (yellow)	214.74	124.57	84.42	64.08	31.35	28.57	29.92	19.40	16.81	15.57	13.86	11.77	10.13	11.13	19.29	0.93	0.93
PB - Glans (glass-like)	183.03	83.15	71.75	56.73	26.35	23.00	25.08	15.80	14.47	14.00	13.14	11.00	9.29	10.33	17.71	0.89	0.73
PB - (grey crust)	163.29	94.05	75.08	61.43	32.35	27.86	28.27	20.00	18.16	17.43	16.90	15.33	13.43	14.33	11.39	0.92	0.85
Troll Wall																	
Tp1-1a (dark brown)	10.39	2.54	2.42	2.18	1.25	1.29	2.54	2.40	3.09	4.43	5.10	5.10	4.45	5.70	1.82	0.72	0.51
Tp1-1b (dark brown)	14.71	4.89	4.25	3.78	2.30	2.29	4.38	3.80	4.94	6.43	7.10	7.07	6.48	7.90	1.86	0.72	0.62
Tp1-2a (brown)	13.58	4.32	3.00	2.72	1.55	1.71	3.50	3.40	4.50	6.29	7.19	7.10	6.49	8.27	1.64	0.74	0.68
Tp1-2b mørk (brown)	18.97	7.52	5.92	5.60	3.45	3.57	7.00	6.40	7.88	9.71	10.52	10.70	9.96	11.93	1.59	0.73	0.71
Tp1-2/3 (brown)	36.61	17.06	14.25	13.42	9.45	10.00	16.35	15.00	18.34	21.14	22.29	23.10	22.16	24.63	1.49	0.80	0.75
Tp1-3-Glass (glass-like)	29.19	12.27	9.58	9.23	5.60	6.29	11.62	10.60	13.44	16.57	18.14	18.80	17.66	20.73	1.41	0.78	0.73
Tp1-4 (light brown)	48.00	24.81	20.83	19.13	13.40	13.86	20.92	19.60	23.44	26.43	27.62	28.57	27.75	30.20	1.59	0.83	0.78
Tp1-GUL (yellow)	27.61	13.60	12.17	11.03	8.15	9.00	13.04	13.20	15.69	18.43	19.48	20.67	19.81	21.03	1.31	0.87	0.74

Table 4

Low and High-temperature hydrothermal fluids from the Jan Mayen Vent Fields (ppt), and Jan Mayen Deep seawater REE concentrations (ppt) as presented by Johannessen et al., 2017. The table also show Mayen basalt compositions taken from Svellingen, 2004 (ppm).

	Y	La	Ce	Pr	Nd	Sm	Eu	Gd	Tb	Dy	Ho	Er	Tm	Yb	Lu	La/Yb	Y/Ho	Eu/Eu*	Ce/Ce*
Jan Mayen Basalts																			
DR 90-2 (JM Basalt 1)	45.25	138.32	105.12	83.5	70.73	44.05	37	34.08	26.8	27.22	25.57	24.57	25	22.52	24	6.14	1.77	0.95	0.98
DR 70-1 (JM Basalt 2)	27.03	106.1	82.47	64.92	53.65	30.95	27.43	22	17.2	16.53	15.14	14.29	14.33	13.19	13.67	8.04	1.79	1.05	0.99
DR 91-1 (JM Basalt 3)	32.79	70.45	58.33	47.92	39.58	28.1	26.14	23.04	18.8	18.97	17.71	17.81	19	15.57	16	4.52	1.85	1.03	1.00
DR 120-7 (JM Basalt 4)	27.37	74.55	59.05	48.08	40.12	26.25	24.14	20.15	16.4	16.34	15.43	14.95	16	13.76	14	5.42	1.77	1.05	0.99
High-temperature fluids																			
12B-2-B1	64.8	309.3	353	48.1	350.1	30.8	79.2	28.2	4.8	21.8	1.8	5.1	0.5	2.3	0.4	136.7	35.1	8.76	0.69
12B-14-B2	63.1	361.7	408.7	43.6	229.5	27.4	170.7	23.5	2.6	14.2	1.4	3.4	0.3	1.6	0.2	224.1	45.8	21.94	0.78
12B-6-B2	68.7	294.2	423.1	52.5	355.6	40.1	206.7	34	3.6	22.2	1.8	5.2	0.4	2.4	0.3	124.6	37.6	18.22	0.81
Low-temperature fluids																			
11-6-B2	152.1	42.5	25.7	2.4	16.2	4.7	0.7	5.7	0.9	7.4	2.1	6.9	0.9	5.6	1.1	7.6	71.3	0.45	0.6
11-6-BS	25.6	4.2	2.3	0.3	1.4	0.3	0.1	0.6	0.1	0.9	5.6	1.1	0.2	1.2	0.2	3.5	83.1	0.66	0.52
JM mean deep seawater	11.5	2.8	0.8	0.5	2.2	0.5	0.1	0.7	0.1	0.8	0.3	0.8	0.1	0.7	0.1	3.8	50.5	0.74	0.16

Table 5

Rare earth element and Yttrium composition for the Troll Wall and Perle & Bruse samples (ppm). Non-normalized values.

	Y	La	Ce	Pr	Nd	Sm	Eu	Gd	Tb	Dy	Ho	Er	Tm	Yb	Lu	Y/Ho	La/Yb
Perle & Bruse																	
PB-p1- CH1 (light brown)	33.81	52.59	65.09	6.23	22.73	3.33	1.08	4.67	0.53	3.07	0.63	1.67	0.20	1.13	0.18	53.67	46.75
PB-p1- CH2 (brown)	25.95	42.41	44.47	4.36	16.07	2.21	0.74	3.32	0.37	2.17	0.46	1.23	0.14	0.80	0.13	56.41	53.35
PB-p1- CH3 mørk (dark brown)	26.95	41.66	41.93	4.46	16.59	2.27	0.73	3.40	0.39	2.28	0.49	1.32	0.15	0.88	0.15	55.00	47.56
PB-p2-CH-GUL (yellow)	48.60	66.57	100.90	10.13	38.45	6.27	2.00	7.78	0.97	5.38	1.09	2.91	0.35	2.13	0.33	44.59	31.30
PB – Glans (glass-like)	39.50	56.74	67.35	8.61	34.04	5.27	1.61	6.52	0.79	4.63	0.98	2.76	0.33	1.95	0.31	40.31	29.10
PB (grey crust)	39.95	50.62	76.18	9.01	36.86	6.47	1.95	7.35	1.00	5.81	1.22	3.55	0.46	2.82	0.43	32.75	17.95
Troll Wall																	
Tp1-1a (dark brown)	21.35	3.22	2.06	0.29	1.31	0.25	0.09	0.66	0.12	0.99	0.31	1.07	0.15	0.93	0.17	68.87	3.45
Tp1-1b (dark brown)	22.16	4.56	3.96	0.51	2.27	0.46	0.16	1.14	0.19	1.58	0.45	1.49	0.21	1.36	0.24	49.24	3.35
Tp1-2a (brown)	25.78	4.21	3.50	0.36	1.63	0.31	0.12	0.91	0.17	1.44	0.44	1.51	0.21	1.36	0.25	58.59	3.09
Tp1-2b mørk (brown)	25.61	5.88	6.09	0.71	3.36	0.69	0.25	1.82	0.32	2.52	0.68	2.21	0.32	2.09	0.36	37.66	2.81
Tp1-2/3 (brown)	48.49	11.35	13.82	1.71	8.05	1.89	0.70	4.25	0.75	5.87	1.48	4.68	0.69	4.65	0.74	32.76	2.44
Tp1-3-Glass (glass-like)	40.14	9.05	9.94	1.15	5.54	1.12	0.44	3.02	0.53	4.30	1.16	3.81	0.56	3.71	0.62	34.60	2.44
Tp1-4 (light brown)	58.16	14.88	20.10	2.50	11.48	2.68	0.97	5.44	0.98	7.50	1.85	5.80	0.86	5.83	0.91	31.44	2.55
Tp1-GUL (yellow)	39.37	8.56	11.02	1.46	6.62	1.63	0.63	3.39	0.66	5.02	1.29	4.09	0.62	4.16	0.63	30.52	2.06

5. Discussion

5.1 Microtexture formation

Formation of Fe-oxyhydroxide deposits in modern low-temperature hydrothermal environments may be attributed to both microbial mediated Fe-oxidation and abiotic auto oxidisation (e.g. Emerson and Moyer, 2011; Chan et al., 2016; Johannessen et al., 2017). These processes may result in a complex array of microstructures, which reflect the prevailing environmental conditions at the time of deposition (e.g. Emerson and Moyer, 2002; Emerson et al., 2007; Kennedy et al., 2003a, 2003b; Edwards et al., 2011; Chan et al., 2016; Johannessen et al., 2017). Twisted, helical stalks produced by *Mariprofundus ferrooxydans,* which is considered the most characteristic morphological trace of microbial Fe-oxidizing metabolism in marine habitats (e.g. Emerson et al., 2010; Krepski et al., 2013), were not observed in the studied samples from Perle & Bruse and the Troll Wall. Instead, other similar morphologies associated with uncultured strains were dominating. Some of the morphologies can be linked to metabolism by FeOB, such as Y-guys and braided, twisted stalks (e.g. Emerson et al., 2007; Chan et al., 2011, 2016). However, the formation mechanisms of bundled fibres (Figs. 4.4F, 4.5 B, 4.6E, and 4.7A), unidirectional filamentous structures (Figs. 4.5F, 4.6G, 4.7D, and 4.7E), and large cylindrical tubes (Figs. 4.4E and 4.7I) are more ambiguous. The diversity of microstructures observed in the distinct layers and laminae (Fig. 4.1) of the samples from both vent fields are discussed in detail below.

Microtextures in the light brown (1) layers

The distinct, bundled fibres (Figs. 4.4F, 4,5B, 4.7A) comprising the light brown layer in both the Troll Wall and the Perle & Bruse samples form a loose and highly porous 3D network, where fluids may have migrated relatively freely (Figs. 4.4C and 4.6E). This texture has not been reported previously from any other modern Fe-deposits. Unlike the fibres and bundles of fibres in the yellow laminae reported by Johannessen et al., 2017 and observed in this study (Figs. 4.4A, 4,6A, 4.7B), the bundles of fibres found in the light brown layers in both samples were covered by honeycomb-shaped minerals, and globular and nodular Fe-oxyhydroxide precipitates. Such structures are generally formed through passive, abiotic nucleation from hydrothermal fluids (e.g. Jones et al., 2004; Chan et al., 2016; Johannessen et al., 2017), and filaments are known to serve as templates for mineral precipitation (Fortin et al., 1998; Phoenix et al., 2003). This passive mineralization process must have occurred over some time in order to form the thick coatings observed. The fibres lacking such coating in the yellow (2) laminae are therefore likely precursors to the bundled fibre structures comprising most of the light brown (1) layer. The light brown layer would form from nucleation of mineral coatings and amorphous precipitates to pre-existing bundles of fibres seen in the yellow laminae. These structures probably precipitated from the mound cavity hydrothermal fluid over time, slowly building up the amorphous coatings and nodular structures covering the bundled fibres in the light brown layer. Since the bundled fibres are anchored to the outer massive, glass-like lamina

45

(3) (Figs. 4.3A, 4.5 A, and 4.7H), but are not anchored in the opposite end, they have likely grown inwards, towards the centre of the cavity. The cavity itself likely formed as a product of hydrothermal pressure building up in hydrothermal fluids trapped by overlying laminae, and subsequent bulging of these laminae, a process that is discussed further in section 5.4, and depicted in Fig. 5.4A-D. Indeed, Johannessen et al., 2017 suggested that mound cavities in similar Fe-mound deposits form gradually, as hydrothermal fluids are blocked from escaping the mound by a mineralized horizon similar to the glass-like (3) laminae.

The bundled fibres could either have formed sometime after the mound cavity had fully developed, or developed in synergy with cavity development. In the latter case, more space would be made available for bundle growth as the cavities grew. In both cases, the light brown layer would grow inwards toward the centre of the cavities, where space was still available. This growth direction is clearly visible, even in macroscopic scales (See fig. 4.2). The bundles likely keep growing until the cavities are filled, or until changes in environmental conditions prevents further structure formation.

The twisted, braid-like structures which are attached to the bundled fibres (Figs. 4.5B, 4.6F 4.7A) display signs of microbial origin, although the thick, secondary mineral encrustation partially mask the primary structures. The hollow, twisted tabular stalks attached to a strongly mineralized bundle of fibres in the Troll Wall sample (Fig. 4.4F), provides a notable exception. These stalks have no mineral crust, indicating that they were formed after the bundled structures, possibly at microaerophilic conditions, where FeOB may catalyse oxidation of Fe(II) while rapid abiotic autoxidation is prevented due to low oxygen availability. Structures similar to the twisted stalks in Fig. 4.6F have recently been connected to an uncultured marine FeOB species, which are a secondary colonizer that has adapted to the low oxygen conditions found deep inside microbial mats (Chan et al., 2016). It is thus likely the twisted stalks formed by similar secondary colonizing FeOB, after the interior oxygen conditions changed to a level acceptable for microbial life to flourish. For example, the initial influx of hydrothermal fluid to the mound and cavity may have been too anoxic for the growth of FeOB, but later diffusion of oxygen into the mound cavity would give rise to acceptable physiochemical conditions for microbial growth in the mound cavities, resulting in the formation of the twisted stalks covering the bundled fibres. The bundles of fibres could potentially grow inwards towards the centre of the mound cavities via abiotic nucleation to EPS generated by microorganisms living in the mound cavities. Further, microbial EPS are effective nucleation sites for iron oxyhydroxides (e.g. Chan et al., 2009), and similar structures in Fe-deposits from the JMVF have been suggested to form by mineral nucleation to EPS (Johannessen et al., 2017). This EPS is likely generated by microorganisms that utilize compounds in the hydrothermal fluid for sustenance. Ammonia and nitrite has recently been reported interior mound fluids from Fe-deposits at the Troll Wall (Johannessen et al., 2017), and provide ample sustenance for ammonium oxidizing bacteria such as Nitrosopumilus. Indeed, co-occurrence of Nitrosopumilus and Fe-oxidizing Zetaproteobacteria has previously been reported in Fe-mats in active hydrothermal areas in the Mariana Trough (Kato et al., 2009b, 2015). Moreover, several studies have suggested a

metabolic connection between Fe-oxidizing Zetaproteobacteria and autotrophic ammonium oxidizers in Fe deposits and in low-temperature hydrothermal settings (e.g. Kilias et al., 2013; Johannessen et al., 2017). Given the right conditions, coexisting ammonia oxidizers and FeOB could potentially form a similar synergetic community inside the Fe-deposit's isolated cavities, where nitrite is produced by Nitrosopumilus and used by Zetaproteobacteria during oxidation of Fe(II), resulting in the growth of EPS and the bundled stalks observed (Figs. 4.5B, 4.6F, and 4.7A). However, fluid samples from the mound interiors need to be performed in order to determine which microbial processes occur there, and what microorganisms could be responsible for producing the EPS required for initial bundle growth.

Microtextures in the yellow (2) laminae

The fibres comprising the yellow laminae in Fe-deposits from the Perle & Bruse and the Troll Wall fields show striking similarities both to each other and to the bundled structures in the underlying, light brown layer. They are usually found in bundles, making up a highly porous 3D network with high permeability, but they lack the characteristic twisted morphology of biogenic FeOB stalks discussed above. Johannessen et al., 2017 suggested that yellow laminae in Fe-deposits at the JMVF form during initialization of new hydrothermal pulses, where Fe-oxyhydroxides would nucleate abiotically onto pre-existing EPS which cover the deposit's surfaces. No distinct biosignatures were found in the yellow laminae, further suggesting that they formed abiotically in environmental conditions not suitable for FeOB growth, such as almost anoxic conditions. Such conditions would be typical for hydrothermal fluids where most oxygen has been lost due to diagenetic reactions in the subsurface (e.g. Sleep, 1991; Tivey, 2007). This process would have taken a very long time however, as oxygen is required to form oxyhydroxides (hence the name). It is therefore more likely that the precipitation occurred too quickly for biosignatures to develop. Intense redox gradients would develop at the hydrothermal fluid/seawater interface, amplifying the process of Fe-oxyhydroxide nucleation onto pre-existing EPS. Requiring oxygen to precipitate as amorphous Fe-oxyhydroxides, the lack of any mineral cover and other amorphous structures in the yellow laminae does however suggest anoxic or suboxic conditions prevailed for some time after the laminae's initial formation. The structures comprising the yellow laminae thus probably developed in intense redox gradients during initial hydrothermal activity, followed by a period of oxygen-poor (suboxic) conditions. Such suboxic conditions could have developed if an overlying impermeable lamina formed rapidly, preventing mixing between hydrothermal fluids and oxygen-rich seawater inside the mound. This scenario is depicted in fig. 5.3 B. Further, such laminae were observed in all samples, depicted in Figs. 4.5C and 4.6C.

Microtextures in the glass-like (3) laminae

The absence of distinct microtextures in most of the massive glass-like laminae in the Troll Wall and Perle & Bruse samples (Figs. 4.5C and 4.6C) suggests that these laminae formed during rapid precipitation. The globules comprising most of the matrix in the laminae probably formed abiotically through rapid oxidation of hydrothermal fluid, a process which would have

outcompeted the formation of any biotically mediated mineralization, or at least enveloped any pre-existing biosignatures. Johannessen et al., 2017 report of similar glass-like laminae in Fe-deposits from the Troll Wall field, and suggest that they co-develop with yellow laminae through rapid oxidation of hydrothermal fluid at the seafloor, marking the beginning of a new pulse of hydrothermal influx to the mound. This would mean the yellow and glass-like laminae were the first to develop during each new hydrothermal pulse, following periods of hydrothermal quiescence.

Containing no distinct biosignatures, the outermost part of the glass-like laminae likely formed through rapid abiotic oxidation, the same way as the glass-like laminae reported by Johannessen et al., 2017. However, the presence of certain structures in the investigated samples suggest that the formation process of these laminae is more complex than Johannessen et al. 2017 proposed. Firstly, the crystalline structures (Figs. 4.5D, 4.6B) and geochemical composition (Fig. 2B) of the outermost part of the layers from both vent sites indicate co-precipitation of a mineral such as gypsum or anhydrite with Fe-oxyhydroxide globules (see also section 5.2). The fact that most of the crystalline structures were observed in the outermost rim of the glass-like laminae imply that the earliest, outermost section of the laminae formed under different conditions than the innermost part of the laminae, where such structures are relatively absent. Secondly, the innermost part of glass-like laminae in the Perle & Bruse sample contain abundant clusters of hollow, branching structures (Figs. 4.6C and 4.7F), indicating that the depositional environment was different there, allowing preservation of these structures.

The clusters of hollow, branching structures display bifurcation, indicating cell division has taken place. Development of similar structures in Fe-deposits has been connected to a species of uncultured marine microaerophilic FeOB (Y-guys), which form small clusters in Fe-mats at the Loihi seamount (Chan et al., 2016), and in Fe-deposits at the Troll Wall (Johannessen et al., 2017). It is possible the glass-like laminae developed in two stages, beginning with initial abiotic precipitation of the outermost part in the strong redox gradients associated with an initial hydrothermal pulse and seawater mixing. This first stage was then followed by a period of biotically mediated formation of the inner part of the layer, perpetrated by a change in physiochemical environmental conditions, which allowed communities of FeOB to thrive. A change in the physiochemical conditions may also explain the abundant hollow, branching structures in gaps in the glass-like laminae in the Troll Wall sample (Figs. 4.6C and 4.7F). In these gaps, oxygen-rich seawater and interior, oxygen-poor hydrothermal fluid would mix, generating the conditions suitable for the growth of Y-guys. Optimal growth conditions for FeOB producing Y-guys in marine Fe-deposits are typically stable, suboxic redox conditions, good nutrient and Fe(II) availability, and moderate temperature and pH levels (e.g. Emerson and Moyer, 1997; Emmerson et al., 2007; Chan et al., 2007; Chan et al., 2011; Chan et al., 2016; Johannessen et al., 2017), although these conditions may vary within distinct species of FeOB.

Growth conditions were probably better in the Perle & Bruse Fe-deposits and therefore cells would divide faster, resulting in a high density of strongly branching Y-guys (Fig. 4.6F). Conversely, non-optimal growth conditions would explain the hollow, weakly branching stalks observed in the gaps of the glass-like laminae in the Troll Wall samples (Fig. 4.5E). Similar gaps in the laminae probably sporadically opened and closed in response to underlying fluid pressure from hydrothermal influx into the mounds. Visible gaps in the laminae were rare in the Perle & Bruse deposits relative to Troll Wall sample, suggesting these structures were rarely preserved in the Perle & Bruse Fe-deposits. An explanation could be that hydrothermal influx to the deposits was more continuous in the Perle & Bruse mounds, and more sporadic, violent, and short lived in the Troll Wall mounds. This would result in few, but very distinct ruptures in the glass-like laminae in the Troll Wall mounds, while in the Perle & Bruse mounds, smaller hydrothermal pathways through the glass-like lamina would develop and be cemented continuously.

Microtextures in the brown (4) layers

The extent of variations in microstructures between the brown layers of the two samples indicate extensive variations in physicochemical growth conditions between Perle & Bruse and the Troll Wall hydrothermal deposits. For example, the brown layers in the Troll Wall sample generally exhibit few distinct morphologies; mainly localized clusters of 10μm wide, 20μm long, hollow tubes (Fig. 4.4E), whilst the brown layer in the Perle & Bruse sample hosts similar structures, but also clusters of Y-guys (Fig. 4.6F), and braid-like twisted stalks (Fig. 4.7G). All these structures are geometrically consistent with the size, form, and aggregation of microorganisms, suggesting the structures are products of microbial mediated biomineralization. The Y-guys and twisted, ribbon-like structures were only observed in brown layer in the sample from the Perle & Bruse field, indicating that physiochemical growth conditions for FeOB were best there. Although these structures are likely of biogenic origin; their formation processes and related microorganisms remain ambiguous.

The cylindrical, hollow tubes located in the brown layers of both the Troll Wall and Perle & Bruse samples (Figs. 4.4E, 4.4C, and 4.7I) are too large to suggest they were formed by prokaryotes. The large size of the tubes could likely rather be attributed to eukaryotes (Thorseth, per.com 2017).

The microorganisms responsible for the formation of the ribbon-like, twisted stalks (Fig. 4.7G) observed exclusively in the Perle & Bruse sample are quite ambiguous. The stalks seem to thin out close to the terminations. This is a characteristic biosignature which show that the area closest to the cell had less time for mineralization to occur than the thick, older part of the stalk. The characteristic twisted structure has been attributed to cells coordinating their movement and growth in the redox-gradient within microbial mats (Chan et al., 2016). Although the twisted morphology of the stalks is similar to that of the twisted stalks produced by *M. ferrooxydans* (e.g. Emerson et al., 2007; Chan et al., 2011), the lack of a characteristic helical structure indicates these structures are not produced by *M. ferrooxydans*. Johannessen et al.,

2017 suggested that Fe-oxidizing Zetaproteobacteria at the Troll Wall may produce a range of stalk morphologies other than the characteristic twisted ribbons of *M. ferrooxydans*, including branching, flattened tubes. The similarities between the observed structures (Fig.4.7G) to the helical stalks of *M. ferrooxydans* (Fig. 1.3B) should not be ignored however. The twisted, ribbon-like morphology in the brown layer is likely produced by a close relative of *M. Ferrooxydans*, or other FeOB producing twisted stalks, such as the betaproteobacteria *Gallionellacea*, that are typical for fresh water habitats (Hallbeck and Pedersen, 2005), but which recently has been detected in marine Fe-oxyhydroxide deposits (e.g. Kato et al., 2009; Li et al., 2012; Chan et al., 2016; Johannessen et al., 2017).

The clusters of Y-guys located close to the glass-like lamina in the Perle & Bruse deposit (Fig. 4.6F) are strongly bifurcated, suggesting the growth conditions likely were optimal for microaerophilic FeOB. Strongly branching Y-guys related to biomineralization by FeOB have also been detected in Fe-deposits at other vent fields (e.g. Boyd and Scott, 2001; Emerson et al., 2010; Edwards et al., 2011; Breier et al., 2012; Scott et al., 2015; Peng et al., 2015; Chan et al., 2016), and was a dominant microbial morphotype observed in mound samples from the Troll Wall field (Johannessen et al., 2017), indicating that this feature is common to hydrothermal Fe-oxyhydroxide deposits worldwide. However, to the authors understanding, no Y-guys have been described with such an extreme degree of branching as the Y guys in the Perle & Bruse Fe-deposits, depicted in Fig. 4.6F. Perhaps the Y-guys in the Perle & Bruse Fe-deposits formed as a result of hydrothermal fluids continually seeping through the glass-like laminae (see "Microtextures in the glass-like (3) laminae"), providing pockets of localized optimal conditions for microbial growth. Conversely, the more extreme sporadic influxes of hydrothermal fluids to the brown layers of Troll Wall deposits were likely not enough to sustain colonies of FeOB producing abundant Y-guys, confining the colonies of FeOB to more isolated gaps in the glass-like laminae, as seen in Fig 4.5 E.

The unidirectional filamentous structures at both sample sites (Figs. 4.5F, 4.6G, 4.7D, and 4.7E), likely represent areas where abiotic precipitation dominates. There are several reasons why this may be so. Firstly, these structures rarely occur in conjunction with the abovementioned structures of likely biological origin, instead occurring in conjunction with abiotic precipitates, clays, and CaC0$_3$ shells (not depicted). Secondly, the filamentous structures are massive and covered in precipitates such as Fe-nodules and globules which display no biosignatures. These structures could perhaps develop when hydrothermal influx rates were too low to sustain communities of FeOB, and abiotic precipitation of Fe-oxyhydroxides thus outcompeted the formation of biotically mediated Fe-oxyhydroxide morphologies. The uniform direction of the filamentous structures would correspond to flow direction during the mounds development. These structures were more prevalent, and had much less mineral cover in the Perle & Bruse samples (see Fig. 4.8). This may infer shorter periods of hydrothermal quiescence at the Perle & Bruse vent sites relative to the Troll Wall. If hydrothermal influx resumed shortly at Perle & Bruse after being cut off, biological activity would again dominate microtexture formation in

the Fe-deposits, and the filaments would have had less time for abiotic nucleation of nodules and mineral cover to occur, giving smooth surfaces. However, the continuous influx of Fe(II) would still cause these structures to form, even during periods of abundant microbial growth, explaining why the unidirectional filaments are longer and more abundant in Perle & Bruse samples. Thus, a more continuous hydrothermal input and abundant biological activity explains the smoother surfaces of microtextures, general lack of Fe-nodules and thick mineral coatings, and the higher content of microbial mediated morphologies observed in the Perle & Bruse mound samples.

Microtextures in the crustal (5) layers

The observation of microbial filaments and slimy EPS on the surface of the Mn-rich crustal layer of the Troll Wall sample (Figs. 4.4D and 4.5I), indicate biofilm formation (see also section 5.4). Examples of microorganisms responsible for producing the biofilms could be heterotrophic Mn-oxidizing bacteria metabolizing organic matter that accumulate on the mound surface in periods of hydrothermal quiescence, as has been demonstrated in umber deposits at the Southern Mid-Atlantic Ridge (Peng et al., 2015). Such microorganisms have already been suggested to cover the surfaces of Fe-deposits in the JMVF (Johannessen et al., 2017), and have been associated with Mn-oxidation occurring on the surfaces of Fe-deposits and ridge flank basalts in deep-sea environments (Tebo et al., 2005; Templeton et al., 2005; Peng et al., 2015). Morgan, 2005 demonstrated how oxidation of Mn(II) is kinetically unfavourable and sluggish even in environments with abundant oxygen, particularly in the absence of biological catalysts. This suggests that Mn-oxidizers were present and active during periods of hydrothermal quiescence when oxygen were plentiful, and that at least some of the Mn-oxides observed in the crustal layer at the seawater interface formed as by-products of biologically mediated Mn-oxidation.

Biofilms and EPS are known to act as excellent nucleation sites for Fe-oxyhydroxides and other minerals (e.g. Scolten et al., 2004; Chan et al., 2009; Toner et al., 2009; Barge et al., 2011). EPS and biofilms forming on the mound surfaces could thus catalyse the formation of abiotically precipitated oxyhydroxide filaments when exposed to a mix of hydrothermal fluids rich in Fe(II) and oxygen-rich seawater, resulting in the formation of the yellow lamina. This process is depicted in Fig. 5.3A. This theory is further supported by Johannessen et al., 2017, which suggested Fe-precipitation and fibrous encrustation of extracellular polymeric substances occur at the sediment–seawater interface of similar oxyhydroxide mounds at the Troll Wall.

5.2 Geochemistry

Hydrothermal fluids have a characteristic geochemical signature that reflects the source, redox state and temperature of the fluids (Alt, 1995 and references therein), and this signature is retained in Fe-oxyhydroxide deposits which form from hydrothermal fluids (e.g. MacLean and Kranidiotis, 1987; Alt, 1988; Chan et al., 2016; Johannessen et al., 2017). Hydrothermal circulation depth, flow rate, temperature and subsurface fluid-rock interactions, seawater mixing and certain microbial processes may consequently be inferred by analysing the

geochemical composition of the sampled Fe-oxyhydroxide deposits. Sedimentation events may also be revealed from the element composition by reflecting detrital components in the deposits (MacLean and Kranidiotis, 1987).

Records on mineralization and diagenetic processes

Chemical investigation shows that the samples are largely composed of iron and silica (50-80 wt% Fe_2O_3 and 20-35 wt% SiO_2) (Table 1), which is consistent with the chemical composition reported by Johannessen et al., 2017 for Fe-mounds of low-temperature hydrothermal origin at the Troll Wall field. The high LOI measured for all samples (20-50%) (See Table 1), indicates one of the most prominent Fe-oxyhydroxides in the samples are Ferrihydrite ($5Fe_2O_3 \bullet 9H_2O$), as the mineral contain large amounts of water. The high Fe content of the mounds imply that Fe exceeded sulphur (H_2S) in the fluids that formed the deposits (see also Introduction, section 1.2). Excess iron must have been left in the hydrothermal fluid after all sulphur (H_2S) reacted with iron in the subsurface to form sulphides, with the remaining iron forming the investigated Fe-deposits. As high-temperature hydrothermal fluids are generally enriched in sulphur (H_2S) and depleted in Fe (e.g. Edmond et al., 1979; Alt, 1988; Alt, 1995), a low-temperature hydrothermal origin of the investigated Fe-deposits seem most likely.

Element scavenging from hydrothermal fluids onto oxyhydroxides in ferromanganese crusts is a process that continue until the oxyhydroxides are saturated (e.g. German et al., 1990; Sherrell et al., 1999; Baruah et al., 2011). This process likely accounts for the high amounts of P, and REE observed in the deposits. The element scavenging likely continued as long as hydrothermal influx to the mound remained active. Thus, a higher REE content may correspond to a longer influx duration.

EDS analyses confirmed high S and Ca contents in the crystalline material in the glass-like lamina of the Perle & Bruse sample (Fig. 4.6B and Fig. 12 B), indicating that this is gypsum or anhydrite. As the source low-temperature fluids were enriched in Fe and thus devoid of Sulphur, the sulphur in the crystalline material cannot have originated from the hydrothermal fluid. Indeed, no other mound structures contained sulphur in any form when EDS analysis was performed. Consequently, the source of sulphur must have been something else, such as sulphate, which is readily available in seawater, and also make up both gypsum ($CaSO_4 \cdot 2H_2O$) and anhydrite ($CaSO_4$). Gypsum and anhydrite may form when hydrothermal fluids react with seawater sulphate and Calcium, resulting in oversaturation due to changes in redox conditions, temperature, and pH (Johnston and Williamson, 1916; Alt, 1995).

CaO values of 1,5-3 wt% (Table 1) in all analysed layers suggest calcium was present in the hydrothermal fluids. Jan Mayen seawater also contain dissolved Ca, which may have contributed to mineral formation. However, low-temperature fluids from the Troll Wall are slightly enriched in Calcium relative to seawater (see Johannessen et al., 2017), suggesting that most of the Calcium in the gypsum or anhydrite derived from hydrothermal fluids during mixing with seawater.

Biosignatures were discovered in the glass-like lamina in the Perle&Bruse samples, close to the crystals. Hydrothermal derived anhydrite usually forms at 150°C (Alt, 1995), which far exceeds the highest temperature (122°C) any microorganism has been proven to survive (Takai et al., 2008). Anhydrite would likely have formed if an initial pulse exceeding 150°C generated the outermost part of the glass-like laminae, which were later colonized by FeOB as the temperature cooled. This is unlikely however, as crystalline material rich in Ca and S was observed covering Y-guys in the glass-like lamina, and in in the brown layer (not depicted). Consequently, the crystalline mineral is most likely gypsum, which can form at lower (<60C) temperatures.

Johannessen et al., 2017 proposed that the glass-like lamina is among the first layer to form during initial hydrothermal influx to hydrothermal Fe-deposits. Perhaps the plume-head of this initial fluid were enriched in Ca, allowing co-precipitation of gypsum and the initial, first part of the glass-like laminae. What could have caused this plume-head enrichment is difficult to determine from the data available in this study, although some diagenetic process would likely be involved for Ca subsurface enrichment. However, the slight Ca-enrichment of low-temperature hydrothermal fluids at the Troll Wall relative to ambient seawater measured by Johannessen et al., 2017 indicate some alteration and enrichment of Ca did occur in the subsurface, likely through leaching from local basalts, which are known to contain relatively high amounts of Ca (Svellingen, 2004). If hydrothermal fluid were trapped in the subsurface by cemented sediments, as was suggested by Johannessen et al., 2017, this process may have enriched the fluid further, leading to Ca-enrichment of the trapped hydrothermal fluid comprising the pulse head generated from new hydrothermal influx to the Fe-deposits. The glass-like laminae do not display significant enrichment in Ca compared to other layers however, indicating contamination from surrounding layers occurred during the challenging process of isolation of the very thin laminae.

As similar crystalline structures were observed in the Troll Wall sample, formation of gypsum from similar processes is a possibility in the Troll Wall deposits as well, although EDS analysis of the crystalline structures (Fig. 4.5D) in the Troll Wall samples was not performed and is needed to confirm these structure's composition.

Another major element in the mounds is phosphorous (P_2O_5). The highest P_2O_5 values for both the Toll Wall sample (4.71 wt%) and the Perle & Bruse sample (5.34 wt%) were obtained from yellow laminae, which is consistent with, but somewhat lower than the P_2O_5 values reported from yellow laminae in similar deposits by Johannessen et al., 2017. However, phosphorous is still strongly enriched in the sample material relative to local basalts (Svellingen, 2004, Tables 1 and 4). Phosphorous scavenged by Fe-oxyhydroxides in the subsurface were likely released to the fluids through subsurface dissolution of these oxyhydroxides, enriching all trapped fluids in phosphorous, and in other scavenged elements such as REE's. Indeed, Johannessen et al., 2017 suggested that phosphorous enrichment in similar Fe-deposits was facilitated by diagenetic processes releasing phosphorous scavenged by Fe-oxyhydroxides in the subsurface. Diagenetic release of elements scavenged by oxyhydroxides could either occur through phase

transformation from ferrihydrite to goethite (e.g. Poulton and Canfield, 2006) or through dissimilatory iron reduction (DIR) (e.g. Lovely et al., 1990; Jensen et al., 1995; Emerson et al., 2007) in underlying Fe-deposits (Johannessen et al., 2017), or as a combination of these two processes. To reveal which process that likely dominate at the sample sites, analyses of DNA and vent fluids would be required.

As phosphorous-enriched fibres in the yellow laminae likely precipitate from initial hydrothermal pulses (See section 5.1), the beginning of new phases of hydrothermal activity at the JMVF may be inferred by the presence of yellow laminae in local Fe-deposits. Phosphorous concentrations were significantly higher in the yellow laminae relative to all other layers and laminae in both the Troll Wall and Perle & Bruse samples (Fig. 4.10, Tables 1 and 3), and REE concentrations were among the highest in the yellow laminae. This indicates that the initial pulse head of a hydrothermal influx cycle does indeed contain the most enriched fluids, followed by a relatively continuous flow of hydrothermal fluid with lower P_2O_5 and REE concentrations. However, some phosphorous enrichment must occur in the subsurface even during active hydrothermal venting, as all layers and laminae are enriched in phosphorous relative to local basalts (Tables 1 and 4).

Co and MnO_2 record hydrothermal quiescence and hydrothermal flow

Elevated Mn concentrations were discovered in the brown and crustal sample layers (Table 1). The high MnO_2 content indicates slow growth of the crustal layers, as Mn-oxidation rates are several orders of magnitude slower than Fe-oxidation in the deep ocean (Stumm and Morgan., 1998), meaning that for Mn to be concentrated in the samples, the growth of Fe-oxyhydroxides would have to cease. This indicates that the Mn-rich crustal layers did not precipitate alongside Fe(II) oxyhydroxides, but rather as a product of periods of interaction with oxygenated seawater during dormancy of hydrothermal activity and subsequently low input of Fe and mound growth. Conversely, the elevated presence of Mn oxides in all layers in the Troll Wall mound sample relative to the Perle & Bruse mound sample (See Table 1) indicate that flow rates and mound growth were slower at the Troll Wall than at the Perle & Bruse site. Mn oxides at the Perle & Bruse site must have had less time to accumulate at the seawater interface before hydrothermal activity and mound growth resumed, resulting in comparatively low MnO levels in these samples.

Co concentrations show a strong positive correlation with Mn in all samples (Fig. 4,9A). This is to be expected, as dissolved Co(II) experience rapid oxidation to Co(III) by MnO_2 particles on the surface of ferromanganese crusts at neutral pH (e.g., Murray and Dillard, 1979). The microenvironment at the mound surfaces thus likely had a neutral pH, and were oxidative during periods of hydrothermal quiescence, meaning aerobic, neutrophilic microorganisms would likely have been dominating in periods of low or no hydrothermal influx. Oxidative scavenging of Mn-oxides from seawater to Fe-oxyhydroxide complexes on the mound surface would explain the generally darker coloration of the brown and dark brown layers relative to other layers and laminae in the samples. Due to seawater contact, the depositional

microenvironment of the crustal layers rich in Mn oxides must have been oxidative. These dark layers were generally located at the seawater interface during sampling of the mounds (Figs. 3.1A, and 3.2A), and are thus probably the layers which interacts with seawater the longest, resulting in a higher Mn content than other layers (Table 4).

Additionally, high amounts of detrital fragments were found in the crustal layers (Figs. 4.4D and 4.6D). These fragments likely accumulated on the mound surfaces during periods of hydrothermal quiescence and low mound growth, further indicating that the dark, crustal layers of Fe-deposits mark periods of hydrothermal inactivity.

Detrital components record hydrothermal activity

The amount of detritus deposited on a oxyhydroxide mound surface is reflected by the elements Al and Ti, as they are considered immobile in hydrothermal fluids and seawater (MacLean and Kranidiotis, 1987). Data obtained from detrital components in the Fe-deposits show that these elements are strongly correlated (Fig. 4.9). The chalcophile trace elements Pb, Cu, and Zn, which normally are associated with high-temperature hydrothermal structures like chimneys or VMS deposits, can also indicate hydrothermal plume fallout (Baruah et al., 2014). The presence of Cu, Pb, and Zn in the Troll Wall and Perle & Bruse Fe-deposits thus reflects the nearby hydrothermal plume or fragments of high-temperature deposits. Johannessen et al., 2017 suggested that the development of Si-Fe mound deposits at the JMVF was connected to pulses of hydrothermal activity, perpetrated by intervals of high regional tectonic activity connected to the nearby volcanism. The high concentration of detrital components (Cu, Zn, and Pb, Fig. 4.9B) in layers of the Perle & Bruse mound may be explained by this regional tectonic activity, and nearby plume activity from the two high-temperature vents (the Perle and the Bruse sites). Nearby vent activity was likely high at the time of tectonic activity and pulse generation. Perhaps the pulse was strong enough to disturb plume fallout covering the seafloor, trapping it inside the mound cavity as the glass-like lamina quickly sealed the mound off from the surrounding seawater environment. As the plume particles got trapped, Zn, Pb and Cu values would remain relatively high in the mound cavity, eventually becoming incorporated into the light brown layer during its formation from the cavity fluid. Only clay particles have been observed in layers beneath the glass-like lamina (Fig. 4.4A), so the high Cu, Pb and Zn values cannot be a result of avalanche sedimentation. This model also makes sense, as the Perle & Bruse field is located on a very shallow incline (Fig. 2.1B), almost on top of the large, central rifted volcano. Here, plume fallout would be likely, but avalanche unlikely due to the shallow incline of the sample area.

Detrital components like clay, $CaCO_3$ shells and basaltic debris found within the brown and dark brown layers at both sample sites (see Figs. 4.4D and 4.6D) indicate that these layers were deposited during periods of relative hydrothermal quiescence. During such a period, the detrital deposits would have had time to slowly accumulate in or on the brown or dark brown layers (Figs. 4.4D and 4.6D). Of th

ese layers, the highest amounts of detrital components were observed in the dark brown layer. Thus, slow mound growth would correspond to detritus becoming incorporated into the brown deposit layers as they slowly grew, while sediments would accumulate on top of the dark brown, crustal layer in periods of total or near-total hydrothermal quiescence where no growth occurred. As such, the accumulation of relatively large amounts of detrital sediments on the mound surfaces (dark brown and brown layers) at the Troll Wall and Perle & Bruse is not necessarily an indication of complete cessation of hydrothermal discharge, but it confirms that the flux of reduced hydrothermal species is intermittently too low to permit rapid mound growth through the precipitation of Fe-oxyhydroxides. This is supported by the findings of Johannessen et al., 2017, which suggested that Fe-deposits at the Troll Wall grew sporadically due to changing hydrothermal influx rates.

Bau, 1993 has shown that the REE distributions of Fe-rich sediments with low total REE contents are sensitive to detrital input. The detrital influence on the REE patterns of The Troll Wall and Perle & Bruse Fe-deposits is negligible however, because of the generally high REE concentrations. This implies that the REE enrichments seen in the yellow and light brown layers of the Troll wall and Perle & Bruse samples (Figs. 4.10B and 4.10A) are not attributed to a high content of basalt fragments. An exception might be the grey, crustal layer in the Perle & Bruse sample, which consists of mostly basaltic fragments, something which is reflected in the layer's chondrite normalised REE pattern, which follows the pattern for Jan Mayen basalts (Fig. 4.10C).

REE record hydrothermal circulation characteristics

The REE content in the sampled Fe-oxyhydroxide deposits is several orders of magnitude higher than REE in diffuse, low temperature hydrothermal fluid (see Fig. 4.10 and Tables 3, 4, and 5). Fe-oxyhydroxides are excellent adsorbents for REE (e.g. German et al., 1990; Sherrell et al., 1999; Craddock et al., 2010), and element scavenging from hydrothermal fluids onto oxyhydroxides in ferromanganese crusts is a process that continue until the oxyhydroxides are saturated (e.g. German et al., 1990; Sherrell et al., 1999; Baruah et al., 2011). Therefore, a positive correlation is to be expected between the REE enrichment in oxyhydroxide deposits and the amount of time hydrothermal flow is occurring. As such, REE scavenging from fluids over time by oxyhydroxides likely accounts for the high amounts of REE observed in the deposits relative to local hydrothermal fluids (Table 4). The element scavenging at the Troll Wall and Perle & Bruse likely continued as long as hydrothermal influx to the deposits remained active. The Troll Wall sample contain less REEs (especially LREEs) than previously analysed samples from the Troll Wall site (Johannessen et al., 2017). This would imply a more rapid formation of the Troll Wall Fe-deposit investigated in this study, likely resulting from higher hydrothermal flow rates occurring over a shorter time period. During this period, less REEs would be able to accumulate in the mounds, giving the comparatively lower REE signature. This means that the intra-field hydrothermal circulation and flux controls on the formation of Fe-deposits within the Troll Wall differ. This makes sense, as the mound samples investigated in

this study and Johannessen et al 2017's study were taken from distinctly separate sections of the Troll Wall vent field.

The elevated REE content of the Perle & Bruse mound sample (See fig. 4.10 and Table 3) initially indicate a hydrothermal influx model where Fe-deposit development is a slow process, gradually enriching the Fe-deposits in REE's. A rapid but also relatively continuous hydrothermal discharge of hydrothermal fluids already enriched in REE's from subsurface interactions with basalts could also have formed these deposits, however. If the hydrothermal fluids supplying the Perle & Bruse sample sites are indeed enriched in REE, they likely reach relatively high subsurface temperatures before rising to the surface, as element leaching to the fluid phase from crustal basalts occurs more rapidly at higher temperatures (e.g. Sverjensky, 1984; Wood, 1990; Alt, 1995). The latter model is more likely, as the Perle & Bruse mound samples mostly show similarity in REE composition to high-temperature hydrothermal fluids and Jan Mayen basalts (Table 4), with the notable exception of Eu, which display a negative anomaly (Fig. 4.10A).

Eu(II) is soluble in hydrothermal fluids, and would therefore display a positive anomaly in the mounds if the fluid temperature reached 200-250C, which is the required temperature for leaching of Eu from basalt to the fluid phase (Sverjensky, 1984; Wood, 1990). The negative Eu anomaly (Eu/Eu* <1, see Table 4 and Figs. 4.10A and 4.10B) consequently imply that the hydrothermal fluids at The Troll Wall and Perle & Bruse did not reach sufficient temperatures for Eu(II) to enter the fluid phase in the subsurface. As such, both the Troll Wall and Perle & Bruse vent fields may be classified as low-temperature systems, even though the hydrothermal fluids supplying the Perle & Bruse Fe-deposits likely have a higher temperature than Troll Wall fluids.

Yttrium (Y) depletion in Fe-deposits has been associated with scavenging of REEs from hydrothermal fluid due to reaction with Fe-oxyhydroxides in the hydrothermal upflow zone (e.g. Bau and Dulsky; 1996 Bau, 1999; Bau and Koschinsky, 2009). Measured as Y/Ho ratios, the sampled Fe-precipitates show depletion in Y relative to low-temperature hydrothermal fluid previously reported from the Troll Wall (Johannessen et al., 2017) (see Tables 4 and 5). This enrichment thus indicates that REEs likely are scavenged by Fe-oxyhydroxides in the subsurface at both sample sites, not just at the vent sites.

Low Ce and Ce/Ce* values in Fe-oxyhydroxides often translate to a more oxic depositional environment, and high Ce/Ce* to an anoxic environment (see also section 1.5). The ambient deep seawater from the JMVF generally display a strong negative Ce-anomaly (Ce/Ce* =0.16, see Table 4), which is not surprising considering that oxygen is plentiful in seawater. Ce/Ce* values are much higher for all mound samples than for the ambient seawater, however (Table 3 and Table 4), indicating chemical subsurface alteration and subsequent depletion of oxygen occurred in the fluids circulating in both the Troll Wall and Pere & Bruse hydrothermal systems. The significantly higher REE enrichment, and Ce/Ce* values of the Perle & Bruse mound sample compared to The Troll Wall sample may imply seawater has been more strongly modified through alteration reactions with basalts in the Perle & Bruse hydrothermal system, as higher

temperatures allows for more efficient element leaching from basalts (e.g. Sverjensky, 1984; Wood, 1990; Alt, 1995; Bach, and Irber, 1998; Thorseth, per. com 2017). This may be attributed to a deeper circulation cell at Perle & Bruse, or less subsurface mixing with fresh seawater. It should be considered however, that high amounts of La in the Troll Wall sample may be at least partly responsible for the low calculated Ce/Ce* values reported when compared to the Perle & Bruse deposits, which display no such elevated La content (Table 4).

Inhibited mobilization of Eu(II) and stabilization of HREE over LREE suggest source low-temperature fluids would originate from a shallow subsurface circulation system that does not extend all the way to the high-temperature reaction zone (Johannessen et al., 2017 and references therein). Such patterns are clearly visible for The Troll Wall samples (Fig. 4.10). Further, LREE/HREE which is measured as La/Yb, is < 2 for all Troll Wall samples (Table 3), indicating the hydrothermal circulation cell at the Troll Wall sample site is shallow. In fact, the HREE patterns for the Troll Wall samples show striking similarities to the HREE patterns of the ambient Jan Mayen seawater (Fig. 4.10D). The similarities to seawater REE patterns along with the low Ce/Ce* (Table 4) of Troll Wall Fe-deposits in this and Johannessen 2017's study, strongly imply significant seawater presence in the subsurface at the Troll Wall. Indeed, the thick sediment substrates covering the rift at the Troll Wall vent field would provide an excellent, shallow path for seawater to circulate and become slightly modified, heated either conductively by circulating high-temperature fluids or heated by underlying magma (see Fig. 5.1).

The Perle & Bruse sample do not share the same compositional similarities to seawater, however. The Perle & Bruse sample instead show REE compositions that show striking similarities to compositions of local fresh basalts reported by Svellingen, 2004 (Fig. 4.10A and Table 3). The observed fractionation (Ya/Yb>10, Table 3) between heavy and light REEs can best be explained by differences in fluid–rock interactions (i.e., pH, temperature, and availability of complexing ligands), which affect the relative solubility and mobilization of REEs from rock to fluid phase (Bau, 1991; Bach and Irber, 1998; Bach et al., 2003; Allen and Seyfried, 2005; Craddock et al., 2010). An explanation for the observed fractionation of REEs in the Perle & Bruse sample might be that the Perle & Bruse Fe- deposits lies upon a relatively thin, minor substrate of sediments underlain by strongly brecciated and faulted basalts. The existence of such a substrate seems likely, considering Perle & Bruse is located on the flank of an active volcano (Fig. 2.1). The brecciated substrate would allow for a continuous and focused flow of hydrothermal fluids to the surface. This semi-continuous, focused flow would give substantially less time and room for hydrothermal fluid/seawater interactions to occur in the upwelling zone at the Perle & Bruse site than at the sediment-dominated Troll Wall site. Thus, the Perle & Bruse hydrothermal fluid would be less diluted by subsurface seawater mixing than Troll Wall fluids. Additionally, the hydrothermal Fe-deposits at Perle & Bruse reflect the chemistry of warmer, basalt-modified fluids rather than low-temperature hydrothermal fluids (Figs. 4.10A and 4.10D), indicating that the circulation cell at Perle & Bruse produce warmer, and subsequently more strongly altered hydrothermal fluids relative to the Troll Wall fluids.

5.3 Hydrothermal circulation at the Perle & Bruse and Troll Wall sample sites

The investigation of mound composition and microstructures of the samples from both the Troll Wall and Perle & Bruse vent fields has revealed intriguing similarities and differences between the respective hydrothermal circulation systems. These characteristics are assumed to reflect key factors and processes such as flow rates of hydrothermal discharge, fluid temperature, fluid oxygen availability, and likely subsurface fluid alteration. Despite the inability to determine hydrothermal circulation depth, fluid chemistry, temperature, and discharge rates without fluid samples, inferences and models may be produced based on findings from this study, supplemented by previous reported data for fluids and mounds in the Troll Wall field (Johannessen et al., 2017).

The high amounts of iron oxyhydroxides (50-80 wt%) in the deposits suggests the deposits formed from low-temperature hydrothermal fluids depleted in H_2S. The Fe-oxyhydroxides have scavenged REEs and other elements such as phosphorus from the fluid during mound formation. Phosphorous enrichment in the yellow laminae and MnO enrichment in the crustal layers relative to other layers and laminae (Table 1) suggests variation in the amount of hydrothermal discharge at both fields. In periods of low hydrothermal input, the hydrothermal fluid is likely trapped in the subsurface and become enriched in phosphorous and REEs because of diagenetic processes involving reduction and dissolution of earlier formed Fe-oxyhydroxides. These elements are later scavenged by the first Fe-oxyhydroxides precipitated at the surface during a new hydrothermal pulse forming the yellow laminae.

The diagenetic processes responsible for dissolution of subsurface Fe-oxyhydroxides could be DIR or phase transformation from ferrihydrite to goethite, as demonstrated by Poulton and Canfield, 2006. Johannessen et al., 2017 propose a similar process of subsurface diagenesis and enrichment of P and REEs at the Troll Wall field, when hydrothermal supply to seafloor Fe-deposits is blocked or partially blocked by cemented subsurface hyaloclastites. Johannessen et al., 2017 also propose that as fluid pressure builds, the blockage would eventually break from pressure cracking, and the enriched fluid would precipitate as a yellow lamina onto surface of the Fe-deposits, signalling the beginning of a new pulse of hydrothermal activity. The similarly high phosphorous and REE contents of yellow laminae relative to other layers and laminae both in the Troll Wall and the Perle & Bruse deposits indicate that this process is not exclusive to the Troll Wall systems, but also occur at Perle & Bruse and possibly at many other Fe-deposits in similar low-temperature hydrothermal settings, where intermittent hydrothermal activity occurs.

During the intervals of relative hydrothermal quiescence, sedimentation, scavenging from seawater, and likely bacterial Mn-oxidation result in accumulation of detrital components and MnO_2 on the mound surface. The lower amounts of MnO and detrital components relative to the mound composition reported by Johannessen et al., 2017 indicate that the periods of hydrothermal quiescence were shorter for the deposits investigated in this study, especially for the Perle & Bruse deposit. The low MnO_2 content in the Perle & Bruse sample suggests that

cessation or near-cessation of the hydrothermal input only occurred for brief moments before a relatively continuous hydrothermal flow was resumed. Longer periods of hydrothermal quiescence would probably have resulted in a deeper diffusion of oxygen into the mounds and therefore also of Mn-enrichment, as observed for the Troll Wall sample. More highly oxidizing conditions in the outer sections of the deposit during hydrothermal quiescence seem to have increased the abiotic oxidation and precipitation, as indicated by the brown laminae being more encrusted by abiotic precipitates than the brighter layers deeper in the deposit. Conversely, observations of fewer abiotic precipitates such as mineral cover and nodular growth, combined with more abundant morphologies from FeOB in the outermost sections of the Perle & Bruse Fe-deposits imply that the periods of hydrothermal quiescence and oxygen diffusion into the mounds were shorter at the Perle & Bruse vent site.

Shorter intervals of hydrothermal quiescence at the sample location of the Troll Wall field investigated in this study is supported by the low REE concentrations, suggesting a more rapid formation than of the mound investigated by Johannessen et al., 2017. The Perle & Bruse hydrothermal fluid was likely more enriched in REE relative to the venting fluid at the Troll Wall site, as reflected by high Ce/Ce* values, and REE distribution patterns similar to that of basalts (See Tables 3,4 and 5, and Figs. 4.10 and 5.2). This allows mound development to occur rapidly, while still enriching the deposits at Perle & Bruse in REE as they form. Alteration of the fluid in the Perle & Bruse hydrothermal system to REE patterns similar to that of Jan Mayen basalts would require the hydrothermal circulation cell at Perle & Bruse to extend deeper into the crust, where temperatures are higher, and alteration processes occur more rapidly, while depleting the fluid in oxygen and subsequently elevating the Ce/Ce* ratio of the fluid. This would explain the high Ce/Ce* values measured at the Perle & Bruse site. A proposed circulation cell for the Perle & Bruse hydrothermal circulation system is depicted in Fig. 5.2.

The Troll Wall circulation system is likely shallower, and dominated by cooler, and less modified seawater relative to the Perle & Bruse low-temperature system, as evidenced by both the low Ce/Ce* values and a REE pattern relatively similar to that of Jan Mayen seawater (see Fig. 4.10 and Tables 3 and 4). A proposed circulation cell for the Troll Wall circulation system is depicted in Fig. 5.1.

Although the hydrothermal fluid in the Perle & Bruse system likely had a higher temperature than the fluid in the Troll Wall system, the negative Eu anomalies in samples from both deposits indicate that the fluids never reached temperatures exceeding 200-250ºC, which is required for Eu to enter the fluid phase (Alt, 1995). These temperatures translate to a depth of roughly 1000m, when considering a geotherm typical for hydrothermal systems at slow-spreading mid-ocean ridges (e.g. Fehn et al., 1983; Alt, 1988; Sleep, 1991; Hannington et al., 1995; Alt, 1995; Cooper, 2000), implying that although the hydrothermal circulation systems of Perle & Bruse and the Troll Wall likely has different depths, neither circulation system would likely exceed depths of 1000m. Indeed, mainly low-temperature hydrothermal circulation has been associated with hydrothermal systems with depths of less than 1000 m in modern seafloor

hydrothermal systems at mid-ocean ridges and interoceanic arcs (e.g. Alt, 1988; Alt, 1995; Hannington et al., 1995, 2005; Slack et al., 2007).
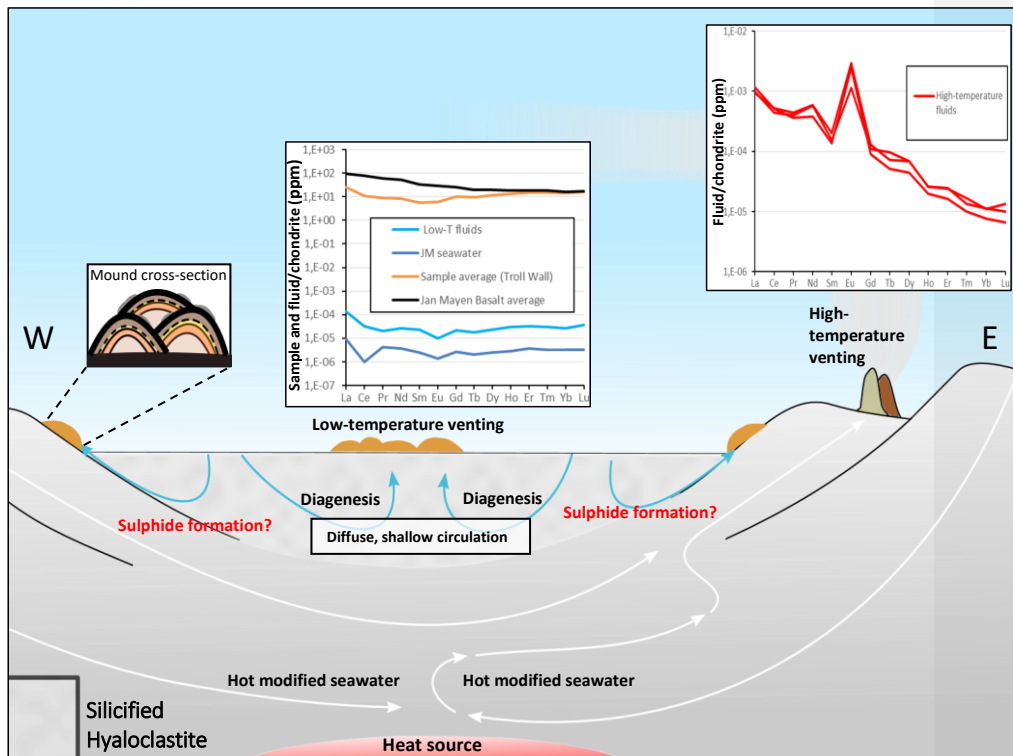
Fig 5.1 Proposed model of hydrothermal circulation at the Troll Wall field. The Troll wall mound deposit, situated in the rift valley of the Troll Wall vent field is affected by shallow hydrothermal convection of seawater. The deposit's REE composition pattern matches that of ambient seawater and of local low-temperature fluids, suggesting the fluid circulates in a shallow, low-temperature circulation cell. The local low-temperature fluids and mound samples are depleted in Eu relative to the high temperature fluid. Modified from Johannessen et al., 2017.
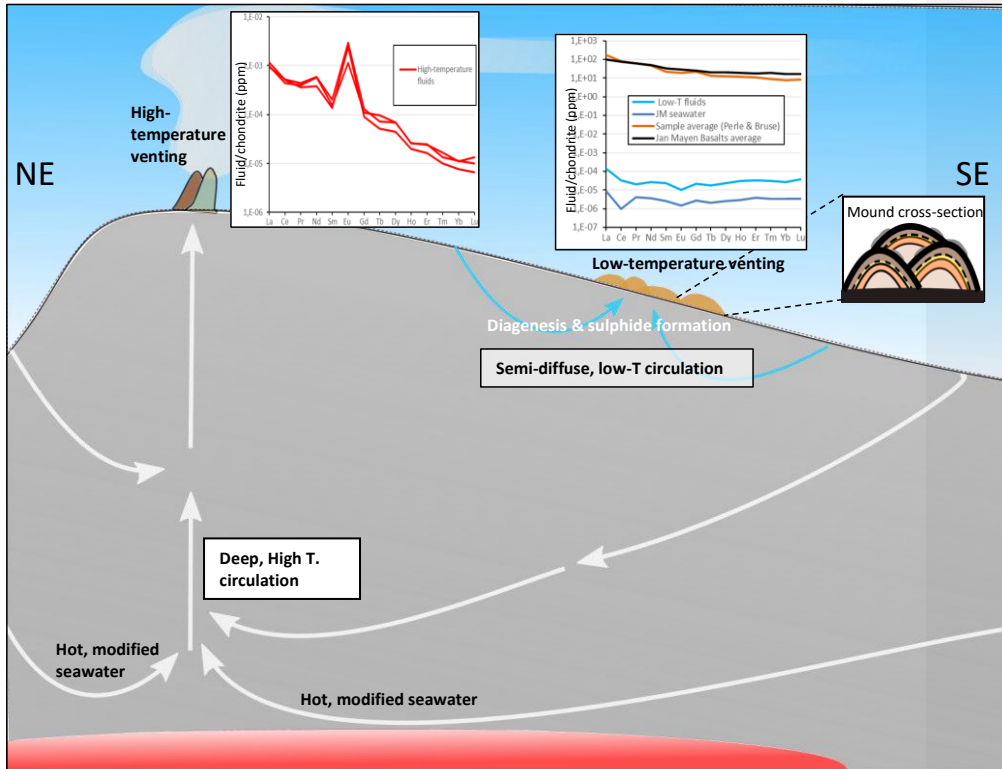
Fig 5.2 Proposed model of hydrothermal circulation at the Perle & Bruse field. The Perle & Bruse mound deposit is affected by shallow hydrothermal convection of seawater in fractured basalts. Mound REE composition pattern matches that of local basalts reported by Svellingen, 2004 rather than that of ambient seawater and of low-temperature fluids form the Troll Walla field, indicating the fluid circulates in a shallow, low-medium temperature circulation cell. The low-temperature deposit and thus also the source fluids are depleted in Eu relative to high-temperature fluids, implying a maximal fluid temperature of <200C.

5.4 Formation Model

There is a consistency in both the textural and geochemical properties between spatially separated laminae and layers of equal colour and position within each deposit, indicating that the layers formed by a repetitive sequence of processes which are depicted in Figs. 5.4A - 5.4D. Chan et al., 2016 and Johannessen et al., 2017 has described how steep redox gradients develop within Fe-deposits such as mounds and mats, and how deposit growth is governed by hydrothermal activity. Similar gradients would likely have developed in the presently studied deposits at the Troll Wall and Perle & Bruse hydrothermal fields. Changes in hydrothermal influx to the mounds would have had significant effects on redox conditions within the mounds, resulting in sudden changes in microbial habitability and subsequent mound vertical growth

rates. Hydrothermal influx rates to the mounds would therefore assert one of the main controls on the development of distinct and separate layers within the investigated Fe-mounds.

A model for Fe-mound development based on analysed geochemistry and microstructures has previously been devised by Johannessen et al 2017. The data collected in this study combined with the fluid and mound deposit data reported by Johannessen et al. (2017) allow for development of a new Fe-mound formation model, which incorporate and explain new features discovered in this study. The most noticeable of these features would be the light brown layer, and the abundant biogenic structures inside and surrounding gaps in the glass-like (3) laminae, as the development of these new features likely require unique prevailing physiochemical conditions that have not yet been fully explained. Therefore, a new model that considers these newly discovered features of Fe-oxyhydroxide deposits are presented in Figs. 5.4 and 5.5.

Formation of a sequence of distinct layers

A correlation between fluid discharge and microbial derived deposit growth is expected, as changes in flow rates would result in changes in redox conditions, influx of nutrients, and availability of Fe(II), which in turn control which microbial communities dominate in the deposit. For example, aerobic eukaryotes dominate in oxic conditions where influx is low, while suboxic conditions enhance the growth of FeOB and related biosignatures. Several studies (Chan et al., 2007; Emerson et al., 2007; Li et al., 2012; Chan et al., 2016; Johannessen et al., 2017) have suggested that abundant biosignatures are indicative of optimal conditions for microbial growth in Fe-deposits. The abundant biosignatures observed in this study were mostly concentrated around openings in the glass-like (3) laminae and certain parts of the brown (2) and light brown (3) layers. Consequently, the physiochemical growth conditions for biomineralizing FeOB were probably optimal during the development of those sections of the Fe-mounds. Conversely, abundant abiotically mediated unidirectional, massive filamentous structures (Figs. 4.5F, 4.6G, 4.7D, and 4.7E) in observed in the brown layers of all deposit samples likely record periods of inhospitable physiochemical growth conditions for FeOB.

The absence of mound cavities and distinct layers and laminae in Fe-deposits might act as indicators of continuous hydrothermal input to the mounds, periods of the deposit's development where physiochemical conditions were relatively stable. This is supported by Johannessen et al., 2017, which proposed that distinct laminae in Fe-deposits at the Troll Wall require strongly differing physiochemical conditions and distinct variations in hydrothermal influx to develop. Consequently, the variations in physiochemical growth conditions that comes with each stage of mound development would have resulted in the differing chemistry, coloration and microtextures observed between each distinct layer and laminae in the samples, which are displayed in Figs. 4.1, 4.4, 4.6 and 5.5. For example, a distinct stage of hydrothermal influx to the mounds may sustain thriving communities of FeOB, causing rapid vertical growth of the deposits through formation of biotically mediated morphologies. This growth period

would typically leave distinct textural imprints on the mound such as abundant biosignatures. When hydrothermal fluid influx diminishes however, a new, distinctly different section of the deposit develops where rapid mound growth through biomineralization are replaced with slow abiotic mineralization and accumulation of detritus. The distinct characteristics (i.e. microtextures, chemistry, and coloration) of each layer and laminae in the investigated mounds can therefore be used to indicate differing stages of mound development, and to examine and interpret the mechanics of deposit formation.

Although the textural and geochemical characteristics of the mound samples indicate that hydrothermal influx rates, hydrothermal fluid chemistry, and microtextures vary somewhat between the Troll Wall and Perle & Bruse deposits, they still display the same general characteristics such as similar types and successions of layers and laminae, coloration, and many similar microstructures, as seen in Figs. 4.1, 4.4, and 4.6. A single, three-stage development model may therefore be used to describe the general formation process of the Fe-deposits at both sites, and possibly also of any other laminated Fe deposits in similar hydrothermal settings. The various stages of the mound development process are depicted in Figs. 5.4A - 5.4D, and described below.

Stage a) Glass-like and yellow laminae, and the mound cavity

The first precipitates to form during a new stage of hydrothermal activity were likely the glass-like and the yellow laminae. Heterotrophic microbial communities which produce EPS and biofilms have been suggested to inhabit the crusts of Fe-deposits during periods of hydrothermal quiescence (e.g. Johannessen et al., 2017), indicating biofilm production during low hydrothermal activity is a relatively common phenomenon. Moreover, Toner et al., 2009 has described how mineral phases may nucleate onto such EPS to form mineralized fibres. A likely explanation for the development of the yellow laminae is that a hydrothermal pulse would have caused rapid nucleation from a Phosphorous-enriched, relatively anoxic fluid onto a biofilm (Figs. 4.4D and 4.5I), which were formed by microbes thriving on the surface during hydrothermal quiescence. Over time, bundles of fibres (Fig 5.3B) forms from nucleation of oxyhydroxides onto pre-existing EPS and biofilm. Over time, each fibre grows thicker through further nucleation from the hydrothermal fluid. The fibres probably grow in bundles because the EPS and biofilms they originally nucleated to were developed by colonies or aggregates of microorganisms living clumped together. This process is depicted in Figs. 5.3 A and 5.3 B. Together, the bundles would form the network seen comprising the yellow laminae (Figs. 4.4A and 4.6A).

The majority of the divalent iron in the pulse head of hydrothermal fluid would likely not nucleate onto EPS however, instead quickly reacting with oxygen in the strong redox gradients that develops between the oxic seawater and the reducing hydrothermal fluids to form the massive, glasslike oxyhydroxide laminae (3) observed in all samples. Johannessen et al., 2017 suggested similar, amorphous glass-like densely mineralized horizons in Fe-deposits at the Troll

Wall form abiotically at the seawater interface where the supply of oxygen is unlimited, through clogging of interstitial pores between developing fibres and extracellular stalks. Such a formation scenario seems likely for the presently investigated samples both from the Troll Wall and Perle & Bruse fields. However, this model does not explain the outer crystalline lining of the glass-like horizons (Figs. 4.5D and 4.6B). The mineralized outer lining would eventually envelop the mound surface, trapping the biofilm and hydrothermal fluids underneath.

Fluid pressure will eventually start to build as new influxes of hydrothermal fluid are trapped underneath the dense horizon, and a cavity filled with hydrothermal fluids start to form. The somewhat discontinuous character of the glass-like laminae (Figs. 3.1D, 4.2, 4.3, 4.4, 4.6) suggest that underlying fibrous and more flexible lamina eventually bulges to accommodate the fluid pressure within the mound, while the overlying more rigid crystalline and glass-like horizon is a ruptured from pressure-cracking. Some of these ruptures were likely clogged with later oxyhydroxide precipitates, while other ruptures could have remained open for longer time, resulting in the observed discontinuities (fragment 1 and 2 in Fig. 4.4) and gaps (Fig. 4.4B). As time pass, the cavity widens, and oxygen would be supplied to the cavity fluids via slow diffusion through the ruptures, generating a suboxic microenvironment. The branching, hollow tubes on the inside of the glass-like laminae of the Perle & Bruse deposits (Fig. 4.7F) display striking similarities to Y-guys that are believed to have been formed by secondary colonizers of microaerophilic FeOB (Chan et al., 2016). Such bacteria would thrive in a microaerobic environment developing in the mound cavity, indicating that the glass-like lamina was colonized shortly after the cavity's formation. The cavity development process is displayed in Figs. 5.4 B and 5.4C.

Stage b) Brown and Light brown layer

Following the initial stage of hydrothermal activity, the brown and light brown layers develop.

As time pass, more ruptures are caused by continued pressure-cracking. In these zones, mixing occurs between relatively anoxic or suboxic fluid from within the mound, and oxic fluids modified by seawater, generating multiple zones of locally increased redox potential within the mound. FeOB then colonize these ruptured zones, leading to the formation of abundant Y-guys (Fig. 4.5E) in and around the gaps in the glass-like laminae, as illustrated in Figs. 5.4B and 5.4 C. The physiochemical growth conditions for these colonizing FeOB must have been worse in the ruptured areas than in the glass-like and brown laminae however, leading to the lower amount of branching (i.e. cell division) structures. This is probably because the microenvironments of the cavity and brown laminae are more stable than the environments that rapidly form in gaps caused by pressure-cracking. The FeOB that form these structures are likely closely related to the secondary colonizing FeOB associated with the formation of very similar Y-guys at Loihi seamount (Chan et al., 2016). The formation of gaps in the glass-like laminae from pressure cracking likely continues while hydrothermal influx to the deposit persists. As old gaps clog with Fe-precipitate, new ruptures continue to open from pressure-cracking. Over time, this process slowly increases the volume of the mound and cavity from within.

Formation of the brown laminae start when hydrothermal fluid trapped in the mound cavity escapes through ruptures in the glass-like laminae and precipitate on the outside of the mineralized horizon (Fig. 5.4C). Most of the brown layer's formation occurs as the hydrothermal activity slows down after the initial phase of high hydrothermal influx. As this semi-permeable layer develops trough the abiotic precipitation of Fe-oxyhydroxides, redox gradients develop within the layer, between the reducing conditions within the mound cavity fluid and the oxidizing conditions of ambient seawater. Several species of biomineralizing FeOB likely colonize the innermost parts of the brown layer in the Perle & Bruse deposits, where biotic Fe-oxidation is not outcompeted by inorganic oxidation processes, and form the abundant clusters of Y-guys and braided, twisted stalks (Figs. 4.6F and 4.7G) observed in the immediate areas of the layer surrounding the glass-like horizon. The abundance of biosignatures and high degree of branching observed in this area in the Perle & Bruse samples suggests growth conditions for the FeOB were optimal at the time of deposition. Indeed, several species of microaerophilic FeOB associated with the production of similar morphologies have been found thriving at similar hydrothermal redox conditions (e.g. Emerson et al., 2007; Chan et al., 2011; 2016; Johannessen et al., 2017). The mentioned biosignatures are much more abundant in the Perle & Bruse mound samples, and often lacking in the brown layers of Troll Wall samples. This is likely because the higher, more continuous hydrothermal influx combined with the more strongly altered hydrothermal fluids of the Perle & Bruse circulation system allowed for a more concentrated, faster, and more steady supply of Fe(II) and other nutrients to the Perle & Bruse deposits relative to the Troll Wall deposits.

A zone devoid of morphotypes related to any known FeOB exists at the top part of the brown layers from both sampled deposits (Figs. 4.5F and 4.6G). Only abiotic structures, such as massive Fe-oxyhydroxide globules, and unidirectional filamentous structures, detrital components, and tubes likely representing aerobic eukaryotes were found in the top of the brown layers in both samples. This suggests conditions in the outermost part of the brown layer would have been too oxic for microbial Fe-oxidation. A higher oxygen content of the brown layers relative to other layers is also supported by the relatively high MnO, Co, and Ce/Ce values (Tables 1,2, and 3) in the brown layers. Thus, the outermost section of the brown layers likely forms as the hydrothermal supply slow towards the end of each hydrothermal cycle, when vertical deposit growth is mostly limited to sedimentation from the water column and abiotic mineralization processes occurring in a relatively oxic environment. The formation of the brown layer is depicted in Fig. 5.4 C.

As time pass, oxygen from the outer parts of the mound slowly diffuse into the mound interior through the ruptures in the glass-like laminae, gradually oxygenating the fluids within the deposit's relatively isolated cavity. Eventually, the conditions fall within the habitability window for microorganisms producing EPS, and the light brown (1) layer start to form. The earliest stages during the formation of the bundled stalks comprising the light brown layer are probably similar to the processes described for the yellow lamina, with the EPS acting as nucleation sites for Fe-nodules (See Fig. 5.3 A and 5.3B). As physiochemical conditions in the cavity fluids eventually fall within the habitability window for twisted stalk-forming FeOB, *Mariprofundus Ferrooxydans* or a close relative colonize these bundle surfaces, and form exterior twisted stalks (Fig. 5.3 C). The layer would continue to grow through further excretion of EPS formed by

bacteria such as FeOB or ammonia oxidizers, species which have already been suggested to coexist in cavity fluids in Fe-mounds taken from the Troll Wall (Johannessen et al., 2017). Fluid samples are needed to ascertain which exact microbial processes produce the EPS, however. As time pass, secondary oxyhydroxide minerals precipitate from the cavity fluids, creating the honeycomb coatings and Fe-nodules seen covering the bundles in Figs. 4.4F, 4.5B and 4.7 B. The bundled structures likely grow inwards, toward the centre of the mound cavity where space is still available. As the cavity keeps expanding from increasing hydrothermal fluid supply and fluid pressure, the structures will keep growing. This growth process will continue until the fluid supply gets cut off and nutrients, Fe(II), or oxygen is depleted, or the cavity is filled and stop expanding.
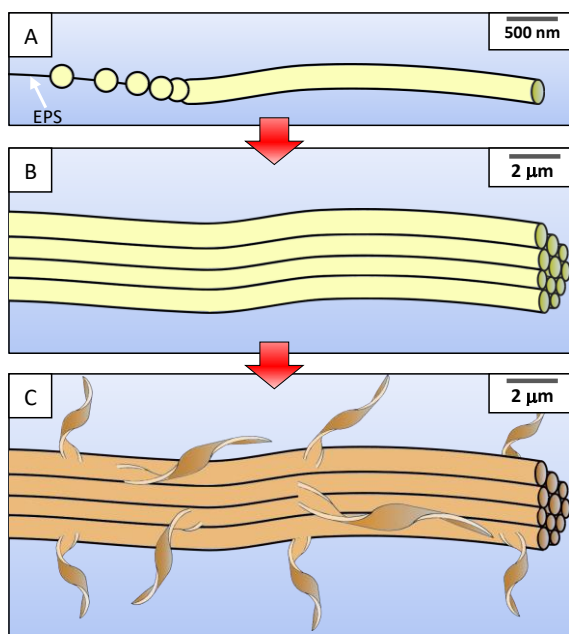
Figure 5.3. Development model of the yellow and orange layers, based on the model from Jones et al., 2004.

A) Fe-nodules nucleates from initial hydrothermal pulse onto pre-existing microbial slimes and EPS.

B) Over time, a bundle of fibres is formed, and the thickness of each fibre grow through further nucleation from hydrothermal fluid. Together, the bundles form the network seen in the yellow laminae.

C) Over time, and after new influxes of oxygen and hydrothermal fluid, secondary oxyhydroxide minerals precipitates, forming honeycomb coatings, Fe nodules, and the light brown coloration. If redox conditions eventually fall within the habitability window for FeOB, the bundle surfaces are colonized and twisted stalks are formed.

Stage c) Dark brown, crustal layer

Hydrothermal flow to the mounds is eventually redirected through a combination of fluid blockage through subsurface mineral formation, and local tectonic activity, resulting in a period of hydrothermal quiescence, depicted in Fig. 5.4 D. During periods of hydrothermal quiescence, Mn-rich crusts and biofilms like those discovered on the outer crust of both samples (Figs. 4.4D, 4.5I, and 4.6D) likely develop. Additionally, a distinct chemical fingerprint develops as chemical and biological Fe-oxidation is replaced with sedimentation, biological Mn-oxidation and sorption of Mn oxides and low contents of REEs from the water column. Thus, a crustal layer is formed which shows depletion in REE, enrichment in Mn and Co concentrations, and a more negative Ce-anomaly relative to the other internal laminae and layers (Table 3). Over time, the crust develops a distinct dark brown or black coloration, mainly as a result of the gradual accumulation of MnO, basaltic detritus, and plume fallout. Therefore, one may generally say that the darker a Fe-deposit crust is, the longer hydrothermal quiescence will have persisted. Aerobic heterotrophs such as Mn-oxidizing bacteria likely colonize the mound crust as mound growth stop and organic matter start to accumulate onto the crust. These communities of microorganisms probably generate the observed biofilms and EPS (Figs. 4.4D and 4.5I), which eventually cover the mound surface along with detrital fragments and Mn-oxides.

The comparatively low MnO values of the deposits investigated in this study relative to MnO values in the similar deposits investigated by Johannessen et al., 2017 indicates that the sampled Troll Wall and Perle & Bruse deposits likely experienced shorter periods of hydrothermal quiescence than those investigated by Johannessen et al., 2017. The quiescence periods also varied between the two sample sites.

The Troll Wall sample area likely experienced a more sporadic influx of less altered hydrothermal fluids, leading to less REE scavenging by the Fe-oxyhydroxides comprising the deposits, and more time for Mn-oxyhydroxides to accumulate onto the crustal layer. This is reflected by the low REE and high MnO contents relative to Perle & Bruse samples (Tables 1 and 3).

The Fe-deposits at the Perle & Bruse sample site likely experienced relatively continuous hydrothermal input of strongly altered and REE- enriched hydrothermal fluid accompanied by very short periods of hydrothermal quiescence. This means there were little time for accumulation of seawater MnO and development of crustal layers. However, a continuous scavenging of the REE-enriched fluid by oxyhydroxides likely occurred throughout development of the Perle & Bruse deposits, resulting in the high REE contents observed (Tables 3 and 5).

Tectonic activity is common at the JMVF, and is associated with local seafloor spreading (e.g. Pedersen et al., 2010). If hydrothermal flow is resumed through tectonic activity, a new sequence is deposited, starting again with stage a). The flow rate, lifetime, and geochemistry of each hydrothermal pulse will likely vary, and result in deposition of slightly or strongly varied sequences with certain layers or laminae being more or less pronounced (Figs. 3.1, 3.2, and 4.1). Hydrothermal flow might also be abruptly redirected and cut off as the result of tectonic activity. In such a case, the mound growth stop, and instantly resumes Stage C, where hydrothermal quiescence and MnO formation dominates.

Mound layers

🟨	Yellow lamina
🟫	Brown layer
🟧	Light Brown layer
⬛	Mn-rich Crustal layer
▬	Glass-like lamina
⬜	Sediment substrate
⬜	Fluid-filled cavity

Mound Structures

⚹⚹⚹⚹	EPS/biofilm
🟩	Active biotic growth zone
🟢	Active Microorganism
≡≡≡	Abiotic microtextures
⬇	Biotic microtextures
〰	Hyaloclastite/blockage
〰	Growth direction
→	Hydrothermal Fluid path
┅►	Fluid pressure direction
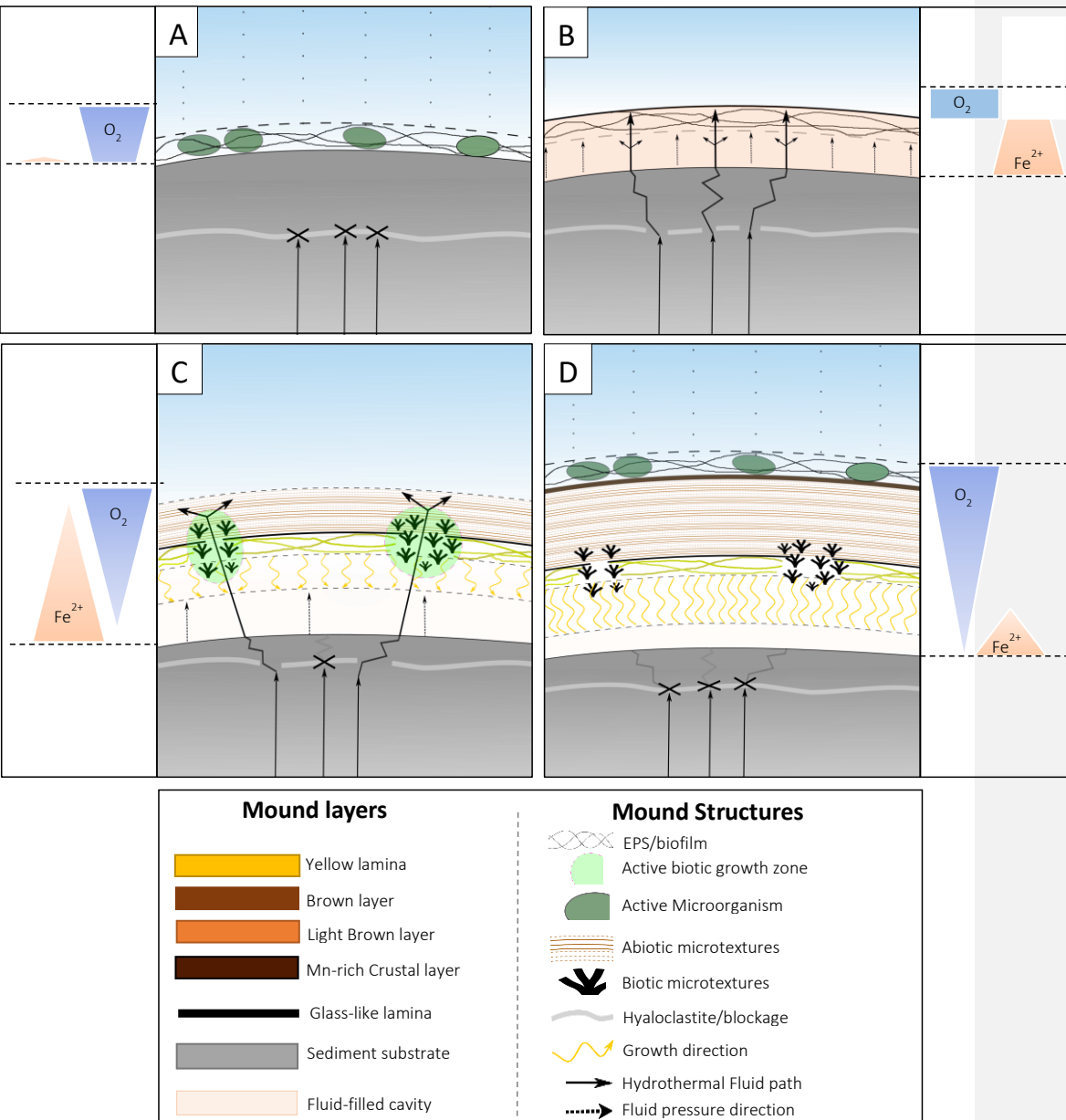
Figure 5.4 (above): Conceptual model of different hydrothermal, redox, and growth stages during the development of laminated low-temperature Fe-deposits, based on data from the investigated Troll Wall and Perle & Bruse Fe-mound deposits.

A) Relatively anoxic hydrothermal fluid builds up in subsurface sediments. A barrier prevents the fluids from reaching the deposit surface. DIR and diagenesis likely occurs in the subsurface and the fluid is enriched in

69

phosphorous and possibly other elements such as REEs and Ca. Heterotrophic microorganisms thrive on the surface, feeding on biogenic debris. These microorganisms generate a biofilm of cells and slimy EPS on the surface.

B) Tectonic activity in the area opens the barrier, and the enriched hydrothermal fluid reaches the surface. At the seawater/hydrothermal fluid interface, the glass-like lamina forms through rapid oxidation of Fe(II) from the fluid. This layer is then lifted as fluid pressure underneath builds, while the enriched fluid from the initial pulse start to nucleate on the microbial slime now trapped under the glass-like lamina.

C) The pressure eventually fractures the glass-like lamina and hydrothermal fluid seeps through, generating a redox zone where microaerophilic FeOB thrive and abundant biomineralization occur. Higher in the deposit, where oxygen levels are elevated, abiotic 50-300μm long fibre structures precipitate where the hydrotermal fluid reaches the seawater interface, forming most of the Brown layer. Iron oxides continue to nucleate on the slime layer, now forming from less phosphorous-enriched fluid. The fluid flow eventually dies off as fluid paths are blocked by precipitates and sediments, and fluids are redirected elsewhere. Meanwhile, the bundles of fibres comprising the light brown layer begins to grow via formation of, and nucleation to EPS formed by microorganisms which colonize the mound interiors as oxygen diffuses into the mounds. The bundled structures grow towards the path of least resistance, which is towards the fluid-filled cavity.

D) As the hydrothermal fluid supply end or is slowed to a minimum, dark Mn oxides scavenged from seawater, and detritus begin to cover the mound surface. Eventually heterotrophic organisms such as Mn-oxidizers return to the surface as oxic growth conditions stabilize, completing one full sequence of growth stages for the Fe-deposit. Meanwhile, the light brown layer continues to grow into the cavity until either the growing space is exhausted inside the cavity, or the Fe(II) or oxygen supply run out.
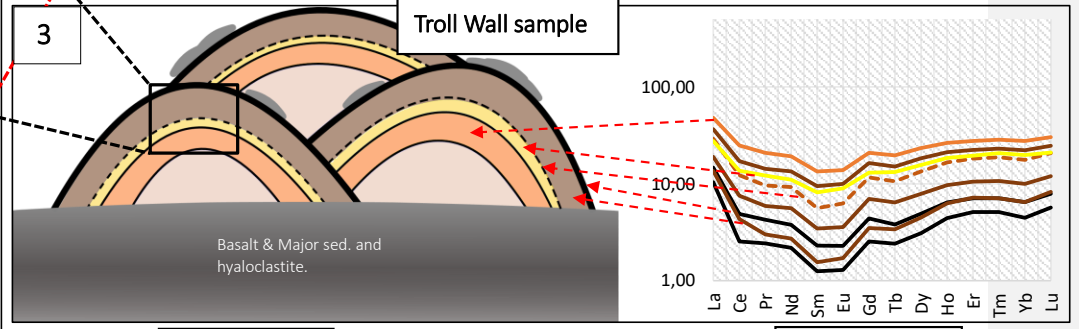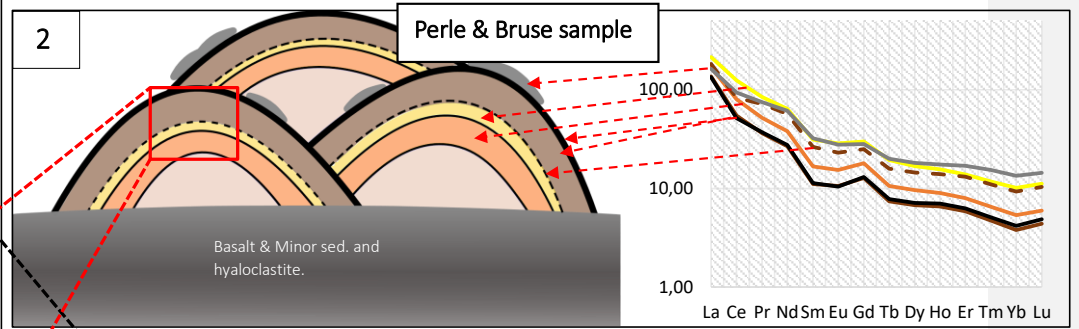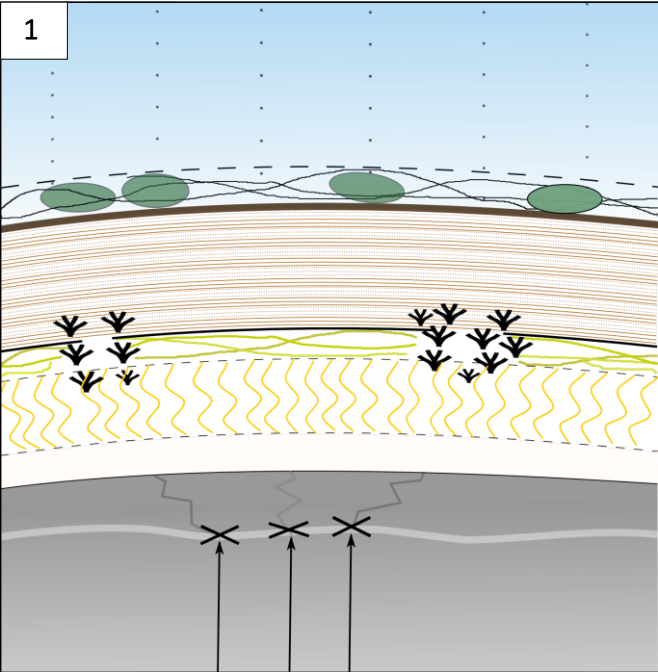
1

Mound layers

- Yellow lamina
- Brown layer
- Light Brown layer
- Mn-rich Crustal layer
- Glass-like lamina
- Sediment covered crust
- Fluid filled cavity

Mound structures

- Active Microorganism
- Abiotic microtextures
- Biotic microtextures
- Cemented Hyaloclastite
- Hydrothermal Fluid path
- Fluid pressure direction
- EPS/biofilm

2 Perle & Bruse sample

Basalt & Minor sed. and hyaloclastite.

100,00

10,00

1,00

La Ce Pr Nd Sm Eu Gd Tb Dy Ho Er Tm Yb Lu

3 Troll Wall sample

Basalt & Major sed. and hyaloclastite.

100,00

10,00

1,00

La Ce Pr Nd Sm Eu Gd Tb Dy Ho Er Tm Yb Lu

4 Troll Wall sample

W

Low – T venting

Diagenesis & shallow circulation

Sillicified hyaloclastite

High – T alteration

High – T venting

E

High-temperature venting

Perle & Bruse sample

NW

Diagenesis & low-T venting

SE

Deep, High T. circulation
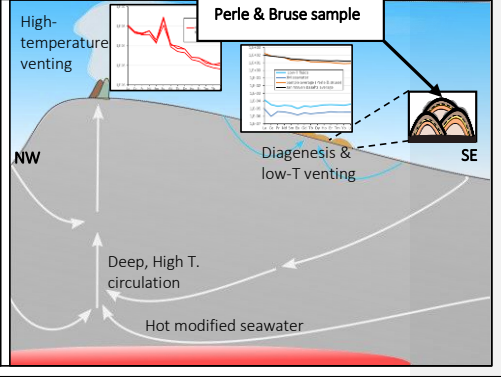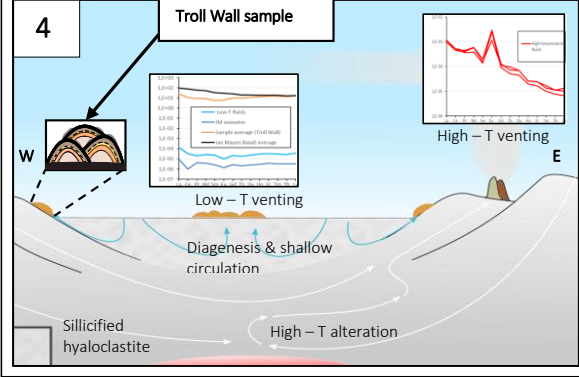
Hot modified seawater

71

Figure 5.5 (above): Overview model depicting geologic setting, and chemistry within each specific layer of the sampled Fe-deposits from Perle & Bruse and the Troll Wall 1) cross-sectional model of a stacked sequence within a mature Fe-mound (See Fig. 5.4 D). 2) Perle & Bruse Fe- mound deposit made up of stacked sequences, with REE patterns displayed for each layer. 3) Troll Wall Fe- mound deposit made up of stacked sequences, with REE patterns displayed for each layer. 4) Geologic setting of the Troll Wall and Perle & Bruse hydrothermal fields, modified from Johannessen et al., 2017. Local (Troll Wall) low and high-temperature hydrothermal fluid REE patterns are also displayed.

5.5 Implications

Implications: Modern low-temperature hydrothermal deposits and systems

This study supports the use of chondrite normalized REE patterns, and Eu- and Ce- anomalies to evaluate if Fe-deposits are derived from plume-fallout related to high-temperature venting, or if they formed through precipitation at the seafloor from low-temperature hydrothermal fluids. Use of chondrite normalized REE values has lately been suggested by Johannessen et al., 2017 to be a favourable method for evaluating fluid-rock interactions in modern and ancient hydrothermal Fe-deposits. Traditionally, shale composite normalised values were used for this purpose, but since shale is usually depleted in Eu relative to Sm and Gd (e.g. Gromet et al., 1984; Taylor and McLennan, 1985), shale-normalization may lead to misguiding, anomalously positive Eu values. Eu anomalies are a key indicator of the presence or absence of high temperature components in hydrothermal fluids (e.g. (Michard et al., 1993), and chondrite-normalized Eu values are within the range of variability of other light REEs (e.g. Hekinian et al, 1993) in chondrites. Therefore, the use of chondrite-normalized REE patterns to evaluate rock-fluid interactions should be preferred over shale compositions when evaluating hydrothermal fluids and deposits. However, it is important to note that shale-normalised REE patterns will give the best comparisons to seawater-derived precipitates (Johannessen, per.com 2017).

Microtextural details vary between and within low-temperature vent fields, as reflected by the distinct compositions and structures comprising the different laminated layers in each deposit. Due to variation in venting styles and physicochemical signatures of diffuse fluids (e.g. Bemis et al., 2012 and references therein), the architecture, microtextures, and microbial community structure of Fe-oxyhydroxide deposits will differ. The hydrothermal flow rate may therefore display a significant control on textural variability between samples. This control become evident when comparing microbial low-temperature Fe-oxyhydroxide deposits from the Loihi seamount to the investigated deposits from the JMVF.

Unlike the investigated Fe-deposits, laminated textures and internal cavities are absent in Loihi Seamount deposits. Instead, the deposits are composed of a microbial mat with internal structures inferred to be a function of the ecological succession within a bacterial community dominated by *Mariprofundus ferrooxydans* (Chan et al., 2016). Unlike the investigated Fe-deposits, the deposits at Loihi seem to have a relatively stable supply of dissolved Fe(II) (e.g. Karl et al., 1988; Chan et al., 2016, and references cited therein), providing the FeOB communities there with a continuous influx of nutrients. The lack of cavities and distinct laminae, and prevalence of FeOB and related microtextures of Loihi Fe-deposits relative to the investigated Fe-deposits may therefore be explained with differences in fluid influx. Stable

fluxes would give stable and good growth conditions for FeOB, and thus no chemically or texturally distinct laminae would develop in the Fe-deposits at Loihi. Conversely, the laminated layers of the investigated Fe-deposits reflect a sporadic hydrothermal influx, and strongly varied physiochemical conditions. Recognition of microtextures from alternate mound fragments, integrated with chemical and microbial community structural data may help resolve the difference in mechanisms behind the formation of Fe-deposits at separate sites such as the JMVF and Loihi.

As negative Eu-anomalies and LREE/HREE ratios are preserved within mounds, potential recognition of ancient Fe-deposits formed directly from low- temperature diffuse flow on the seafloor is plausible by analysing distinct REE signatures (Johannessen et al., 2017). Such conclusions are supported by the data from the Troll Wall sample investigated in this study, indicating that investigation of chondrite-normalized REE patterns and microtextures of modern Fe-oxyhydroxide mounds may help distinguish between high and low-temperature hydrothermal processes. Moreover, the data presented here supports that analysis of microtextures, REE distribution patterns, Ce and Eu anomalies, MnO, and detrital components within Fe-mounds can be used to determine variations in paleo-flow rates, paleo-physiochemical conditions, and habitability of modern hydrothermal systems. Application of similar techniques may potentially help determine a high or low-temperature origin for other Fe-oxyhydroxide deposits found in hydrothermal settings on a global and temporal scale.

Despite a short separation distance of two kilometres, the inferred relatively anoxic, basalt dominated, and REE-enriched source fluid that the sample from Perle & Bruse formed from differed significantly from previously sampled fluids from the Troll Wall (Johannessen et al., 2017), indicating differences in circulation depth, temperature, compositions, and possibly subsurface diagenetic processes exists between the two sites. The chemical differences in the hydrothermal fluids are also reflected in the varied microtextures observed in the different Fe deposits from Perle & Bruse and the Troll Wall. For example, variations in amount of mineral coatings and stalk bifurcation imply different redox and physiochemical conditions between the investigated sites. This study thus shows that variation between individual hydrothermal systems within the same geographical area could be common. This study also links mound development rate to hydrothermal influx rate and microbial habitability, supporting the suggestion made by Johannessen et al., 2017 that hydrothermal activity is the main control on habitability of FeOB in Fe-deposits. Consequently, hydrothermal influx rates are likely the main cause of textural variability between Fe-deposits at the JMVF, and any other Fe-deposits formed in similar settings.

This study's findings of a layer comprised of unique bundled fibres, and of Y-guys which exhibit distinct differences to Y-guys previously discovered in similar deposits (e.g. Kato (2009); Emerson & Moyer (2011); Chan et al., 2011; 2016; Johannessen et al., 2017) implies the possibility that other, as-of yet undiscovered textural features and associated microorganisms

could be present in low-temperature hydrothermal Fe-deposits throughout the deep ocean, awaiting discovery.

Implications for cataloguing ancient mineralization and depositional processes

Jasper deposits tend to plot in the same chondrite-normalized REE distribution regions as many modern hydrothermal oxyhydroxides (e.g. Davidson et al., 2001; Şaşmaz et al., 2012), implying that they were formed from similar processes as modern hydrothermal Fe-deposits. Indeed, ancient seafloor deposits will retain much of the original geochemical fingerprint of the source fluid (e.g. Mclean and Kranidiotis, 1987; Grenne and Slack 2003a; 2003b; Grenne & Slack, 2005), assuming no significant alteration of the deposits has occurred. As such, the analysis of chondrite-normalized REE patterns have been suggested as an effective way of studying ancient jasper formation mechanics (Johannessen et al., 2017). This study found that distinct variations in MnO and chondrite-normalized REE contents and patterns reflect variations in depositional processes between low-temperature modern Fe-deposits at the JMVF. This may potentially add valuable insight when differentiating between formation processes of ancient jaspers that formed in environments similar to the Troll Wall and Perle & Bruse hydrothermal systems.

Utilization of similar geochemical analysis of scavenged elements in modern and ancient Si-Fe-oxyhydroxide deposits might provide us with a cost-effective way of gathering data concerning the original hydrothermal fluid, depth, and mineral occurrence of active and ancient hydrothermal systems. Therefore, the application of chemical analysis of modern and ancient Fe-deposits may be relevant for surveying in industries which traditionally rely on expensive drilling and core sampling techniques to obtain geochemical data of subsurface hydrothermal systems.

Microaerophilic chemolithoautotrophic Fe-oxidizing bacteria likely are responsible for a large amount of the oxidation of ferrous iron in the investigated Fe-deposits, especially in the deposits from the Perle & Bruse field. The FeOB biomineralize extensively and leave behind hollow, branching clustered structures, among other morphologies. Similar twisting and branching filamentous structures have also been detected in ancient jasper deposits (e.g. Juniper and Fouquet, 1988; Duhig et al., 1992; Davidson et al., 2001; Little and Thorseth, 2002; Boyce et al., 2003; Little et al., 2004; Slack et al., 2007), which signify that these may represent low-temperature hydrothermal vent communities. This study can subsequently aid the search for Fe-oxidizing bacteria in the rock record by providing additional details about the geochemistry and microtextures of hydrothermal systems that host modern Fe-oxidizing communities. For example, the long bundles of fibres (Figs. 4.3A 4.3B, 4.4C, and 4.6E), the ribbon-like twisted stalks (Fig. 4.7G), and densely colonizing Y-guys (Fig. 4.6F) show striking resemblance to the sinusoidal filaments detected in the Ballynoe Jasper deposits (Little et al., 2004), and thin, branching filaments of Løkken jaspers originally interpreted to form biotically during Fe-Si-gel maturation on the seafloor (Grenne & Slack, 2003a; 2003b). This implies that modern analogues to such textures may be preserved in the rock record, and used as indicators

of likely ancient microbial activity. However, further studies are needed to determine whether these textures are unique to the Fe-oxidizing metabolism and can be regarded as robust biosignatures in ancient Fe-deposits.

Not only are ancient Fe-deposits in the rock record such as Jaspers believed to be archives of paleoenvironmental data of ancient earth (e.g. Juniper and Fouquet, 1988; Duhig et al., 1992; Ravizza et al., 1999; Davidson et al., 2001; Grenne and Slack, 2003a 2005; Little, 2004; Slack et al., 2007), but also of other planets where hydrothermal activity could have occurred, such as Mars or Venus (e.g. Horton et al., 2004; Little et al., 2004). Hence, this study's deciphering of microtextures in modern Fe-deposits such as the extremely dense colonies of Y-guys (Fig. 4.6F), massive, 50-300um long filamentous structures (Figs. 4.5F and 4.6G), and as-of yet undiscovered bundled stalks (Figs. 4.4C, 4.5G, 4.7A) may help future work studying ancient geological processes, and also aid in the search for biosignatures in the rock record on earth and other planets.

6. Summary and conclusions

The Fe-deposit investigated in this study reveal a complex formation history, which is recorded in the pronounced textural and geochemical traits. These traits manifest as repeated sequences of layers and laminae of distinct colour, texture and porosity. Each of the sequences of laminated layers are separated by internal cavities. The innermost layer in each sequence is usually a light brown layer. A yellow <1mm thick lamina is evident above the light brown layer in most samples. A semi-continuous, massive glass-like lamina is located above the yellow and light brown laminae. The glass-like lamina is usually anchored to a 5-15mm thick overlying brown layer. Making up most of the mounds, this brown layer contains varying, laminated internal structures and abundant distinct morphologies. The top layer of a sequence is dark brown to black in colour and is around 0.5-1 mm thick.

A distinct framework consisting of 10-50 μm thick, 200 μm to >1000 μm long bundles of 300-1000nm wide fibres fill up most of the cavities. The high phosphorous content of semi-bundled fibres comprising the yellow lamina suggests the bundles of fibres formed abiotically, through nucleation of an enriched pulse of hydrothermal fluid to pre-existing EPS. Mineral coatings and twisted stalks associated with secondary colonizers of FeOB cover some of the fibre bundles in the light brown layer however, implying the bundles in the light brown layer evolved through several stages: a fist stage of abiotic precipitation onto EPS, followed by formation of the coating, and later colonization and further growth by biomineralizing FeOB.

Located mainly around openings in the glass-like laminae and certain parts of the brown and light brown layers, most of the observed biosignatures were concentrated deep inside the Fe-mounds, however. This imply that the physiochemical conditions for biomineralizing FeOB were likely optimal deeper inside the mounds, where oxygen contents were low, and the redox gradient favoured $Fe(II)$ over $Fe(III)$. Conversely, the outer sections of the mounds mainly consist of abiotically mediated microtextures such as massive, unidirectional filamentous structures, globules of Fe-precipitates, and detritus, along with 10μm wide, 20μm long tubes inferred to represent aerobic eukaryotes. These microstructures suggest the outer layer was too oxic for FeOB to thrive.

Morphologies produced by FeOB were generally more abundant in the Perle & Bruse sample. This is probably due to the Perle & Bruse deposits receiving a more stable influx of reducing, hydrothermal fluids, which would provide excellent growth conditions. Indeed, the Y-guys in and around the glass-like laminae in the Perle & Bruse sample displayed much stronger branching (i.e. cell division), than similar Y-guys in the Troll Wall sample, suggesting better growth conditions for FeOB at Perle & Bruse.

The investigated Fe-mound deposits mainly consist of Fe-oxyhydroxides and SiO_2, implying that they were formed from fluids that were strongly enriched in Fe and Si, and therefore depleted in H_2S. Enrichment of Mn and Co accompanied by elevated amounts of detrital fragments in crustal layers of samples from both vent sites indicate periods of hydrothermal quiescence at

both the Troll Wall and Perle & Bruse fields. Lower REE and higher MnO contents in the Troll Wall sample relative to Perle & Bruse sample area indicate a more sporadic influx of less altered hydrothermal fluids at the Troll Wall site, leading to less REE scavenging and more time for Mn-oxyhydroxides to accumulate onto the crustal layer, likely through seawater scavenging and microbial Mn-oxidation. Conversely, the Perle & Bruse site which display high REE contents and low MnO contents likely experienced a more continuous hydrothermal influx. Chondrite-normalised REE patterns for the Troll Wall Fe-deposit (average La/Yb ~1.6) display striking similarities to that of Jan Mayen seawater and low-temperature hydrothermal fluid previously reported for the Troll Wall material. This suggests the hydrothermal circulation cell feeding the Fe-mounds at the Troll Wall field is likely shallow, with hydrothermal fluids circulating in subsurface sediments filling the rift valley. Mixing between hydrothermal fluids and seawater probably occur in the subsurface of the Troll Wall, giving the fluid, and thus the Fe-oxyhydroxide mounds its seawater REE signature. The REE patterns for the Fe-deposits at Perle & Bruse (average La/Yb ~23) does not display REE signatures of seawater, instead showing similarities to REE patterns of Jan Mayen basalts, along with generally higher REE concentrations. The Perle & Bruse Fe-mounds are therefore likely precipitated from hydrothermal fluid strongly influenced by leaching at higher temperatures. However, negative Eu anomalies in both samples strongly imply that neither of the hydrothermal fluids that formed the sampled deposits reached temperatures of 200-250C or associated crustal depths.

This study provides the first ever detailed analysis of Fe-mounds from Perle & Bruse, and the first data taken from the fault wall at the Troll Wall. This data, combined with fluid and mound deposit data previously acquired from the Troll Wall field allow for the construction of a formation model for laminated, hydrothermal Fe-deposits, which incorporate and explain new features discovered in this study, such as formation of an internal, light brown layer in Fe-mounds. Although the textural and geochemical characteristics of the samples indicate that hydrothermal influx rates, hydrothermal fluid chemistry, and microtextures vary somewhat between the Troll Wall and Perle & Bruse deposits, they still display the same general characteristics such as similar types of layers and laminae, coloration, and many similar microstructures. As such, a single three-stage development model may be used to describe the formation process of Fe-deposits at both sites. However, the flow rate, lifetime, and chemistry of each hydrothermal pulse likely vary, and result in deposition of slightly or strongly varied hydrothermal sequences with certain layers or laminae being more or less pronounced in each sequence within each Fe-deposit. Differences in inter- field textural and chemical composition also exist between the investigated Fe-deposits, especially in the abundance of biotically vs abiotically mediated microtextures, and these differences are caused by the variation in venting styles and physicochemical signatures of the diffuse, hydrothermal fluids supplying the Fe-deposits.

By comparing the differing textures and geochemistry of the samples from the Troll Wall and Perle & Bruse venting fields, this study demonstrates that hydrothermal fluctuations and

associated shifts in the position of the redox-gradient and nutrient availability over time exert the primary control on the formation of laminae and the activity of Fe-oxidizing bacteria in marine hydrothermal Fe-deposits. The study also adds to earlier suggested models of hydrothermal low-temperature Fe-mound development, and provide a detailed description and formation model for the bundled fibres comprising the light brown layer, a microtexture not previously described in detail. The suggested formation processes in the respective vent-fields may also provide insight into the formation mechanics, and abiotically and biotically mediated structures of other modern seafloor Fe-oxyhydroxide deposits, and potentially also of ancient iron formations on earth and on other planets.

Future work

In the future, multiple distinct low-temperature venting Fe-deposits should be compared and analysed to increase our understanding of how discharge fluxes in hydrothermal fields affects fluid and deposit compositions, structures, and composition of microbial communities.

To avoid contamination from other layers when investigating the geochemical composition, TEM-EDS (Transmission Electron Microscopy) techniques should be used for separating and analysing the millimetre-thin glass-like laminae in the deposits. Additionally, electron diffraction by TEM of the crystalline part of the glass-like laminae could assert whether the precipitate there also likely contain gypsum or anhydrite, and what this means for the development history of the associated Fe-deposits.

The exact mechanisms behind the formation of ribbon-like stalks, massive filled unidirectional filamentous structures and bundles of fibres are still ambiguous and should be resolved. A challenge lies in evaluation of biotic vs. abiotic precipitation mechanics of oxyhydroxide microstructures, and whether they are primary or secondary structures. One way to identify if these structures are of biotic origin is to apply microbiological methods like microbial community analysis, using 16SrRNA analytical techniques such as FISH on fresh samples, which contain living microorganisms. Another method would be cultivating and isolating Fe-oxidizing bacteria that produce other morphologies than the characteristic twisted stalks, although this would require mimicking the environments found at hydrothermal settings, which have previously proved challenging (e.g. Toner et al., 2009). Hydrothermal fluid from the Perle & Bruse and the Troll Wall sample sites need to be collected and analysed to confirm the suggestions on fluid geochemistry, notably negative Eu anomalies, differences in HREE/LREE content between Perle & Bruse and the Troll Wall, and temperature and redox variations between the two investigated sites. Mound cavity fluid and fresh mound samples should be sampled, adequately stored, and analysed to more accurately determine which type of microbes and processes are involved in the formation of the bundled structures comprising the light brown (1) layers. Of the sample sites, sampling of hydrothermal fluids from within and discharge close to the Perle & Bruse hydrothermal Fe-mounds should be prioritized, as no previous samples or analyses of diffuse, hydrothermal fluid from this area exists.

Future research should also address whether sporadic, decoupled hydrothermal input to shallow hydrothermal systems are a common, global feature, and use comparisons between similar shallow hydrothermal fields to set the premises for microaerophilic Fe-oxidation in marine hydrothermal Fe-oxyhydroxide deposits globally and in the ancient rock record.

7. References

Allen, D.E., Seyfried, W.E. (2005). *REE controls in ultramafic hosted MOR hydrothermal systems: an experimental study at elevated temperature and pressure*. Geochimica et Cosmochimica Acta **69**, 675–683.

Alt, J.C. (1995). *Subseafloor Processes in Mid-Ocean Ridge Hydrothermal Systems*. Seafloor Hydrothermal Systems: Physical, chemical, biological, and geological interactions **91**, pp.85–114.

Alt, J.C. (1988). *Hydrothermal oxide and nontronite deposits on seamounts in the eastern Pacific*. Marine Geology **81**, 227–239.

Bach, W., Irber, W. (1998). *Rare earth element mobility in the oceanic lower sheeted dyke complex: evidence from geochemical data and leaching experiments*. Chemical Geology **151**, 309–326.

Bach, W., Roberts, S., Vanko, D.A., Binns, R.A., Yeats, C.J., Craddock, P.R., Humphris, S.E. (2003). *Controls of fluid chemistry and complexation on rare-earth element contents of anhydrite from the Pacmanus subseafloor hydrothermal system, Manus Basin, Papua New Guinea*. Mineralium Deposita **38**, 916–935

Bao S.-X., Zhou H.-Y., Peng X.-T., Ji F.-W. and Yao H.-Q. (2008) *Geochemistry of REE and yttrium in hydrothermal fluids from the Endeavour segment, Juan de Fuca Ridge.* Geochem. J. **42**, 359–370.

Barge L. M., Doloboff I. J., White L. M., Stucky G. D., Russell M. J. and Kanik I. (2011) Characterization of iron – *phosphate – silicate chemical garden structures.* Langmuir **28**, 3714–3721.

Baskar, S., Baskar, R., Thorseth, I. H., Ovreås, L., and Pedersen, R. B. (2012*). Microbially induced iron precipitation associated with a neutrophilic spring at Borra Caves, Vishakhapatnam, India*. Astrobiology **12**, 327–346.

Bau, M., 1991. *Rare-earth element mobility during hydrothermal and metamorphic fluid-rock interaction and the significance of the oxidation state of europium*. Chemical Geology **93**, 219–230.

Bau M. 1993 *Effects of syn- and post-depositional processes on the rare-earth element distribution in Precambrian iron-formations.* Eur. J. Mineral. **5**, 257-267.

Bau, M., & Dulski, P. (1996). *Distribution of yttrium and rare-earth elements in the Penge and Kuruman iron-formations, Transvaal Supergroup, South Africa.* Precambrian Research, **79**(1-2), 37-55.

Bau, M. (1999). *Scavenging of dissolved yttrium and rare earths by precipitating iron oxyhydroxide: experimental evidence for Ce oxidation, Y-Ho fractionation, and lanthanide tetrad effect.* Geochimica et Cosmochimica. Acta **63**, 67–77.

Bau, M., Koschinsky, A. (2009). *Oxidative scavenging of cerium on hydrous Fe oxide: evidence from the distribution of rare earth elements and yttrium between Fe oxides and Mn oxides in hydrogenetic ferromanganese crusts.* Geochemical Journal **43**, 37–47.

Bemis, K., Lowell, R.P., Farough, A. (2012) *Diffuse Flow: On and Around Hydrothermal Vents at Mid-Ocean Ridges.* Oceanography **25**, 182–191.

Benz, M.; Brune, A; Schink, B. (1998). *Anaerobic and aerobic oxidation of ferrous iron at netural pH by chemoheterotrophic nitrate-reducing bacteria*. Archives of Microbiology, Vol.**169**(2), pp.159-165.

Biscoff L.L, and E.E. Seyfried (1978) *Hydrothermal chemistry of seawater from 25C to 350C*, Am. J. Sci. **278**, 838-860.

Blake, R.C., 2nd, Shute, E.A., Greenwood, M.M., Spencer, G.H., and Ingledew, W.J. (1993) Enzymes of aerobic respiration on iron. FEMS Microbiol Rev **11**: 9–18.

Boyce A. J., Little C. T. S. and Russell M. J. (2003) *A new fossil vent biota in the Ballynoe barite deposit, Silvermines, Ireland: evidence for intracratonic sea-floor hydrothermal activity about 352 Ma.* Econ. Geol. **98**, 649–656.

Boyd T. D. and Scott S. D. (2001) *Microbial and hydrothermal aspects of ferric oxyhydroxides and ferrosic hydroxides: the example of Franklin Seamount, Western Woodlark Basin,* Papua New Guinea. Geochem. Trans. **2.**

Brian Jones, Kurt O. Konhauser, Robin W. Renaut, Raymond S. Wheeler (2004) *Microbial silicification in Iodine Pool, Waimangu geothermal area, North Island, New Zealand: implications for recognition and identification of ancient silicified microbes.* Journal of the Geological Society, ***161****, 983–993.*

Bennett, S.A., Hansman, R.L., Sessions, A.L., Edwards, K.J. (2011). *Tracing iron-fueled microbial carbon production within the hydrothermal plume at the Loihi seamount.* Geochimica et Cosmochimica Acta **75**, 5526–5539.

Beukes, N. (2005). *Biogeochemistry: Early options in photosynthesis.* Nature **431**, 522-523.

Boynton, W.V. (1984). *Cosmochemistry of the rare earth elements: meteorite studies. Rare Earth Element Geochemistry.* Developments in Geochemistry 2 (Henderson, R., ed.), 89-92. Elsevier, Amsterdam.

Breier, J.A., Gomez-Ibanez, D., Reddington, E., Huber, J.A., Emerson, D. (2012). *A precision multi-sampler for deep-sea hydrothermal microbial mat studies.* Deep Sea Research Part I: Oceanographic Research Papers **70**, 83–90.

Byrne, R.H., Kim, Kihyun (1990) *Rare earth element scavenging in seawater.* Geochimica et Cosmochimica Acta, Vol.**54.**

Chan, C.S., Fakra, S. C., Edwards,D.C., Emerson, D., and Banfield, J.F. (2009). *Iron oxyhydroxide mineralization on microbial extracellular polysaccharides.* Geochim. Cosmochim. *Acta* 73, 3807–3818.

Chan, C.S., Fakra, S.C., Emerson, D., Fleming, E.J., Edwards, K.J. (2011). *Lithotrophic iron-oxidizing bacteria produce organic stalks to control mineral growth: implications for biosignature formation.* The ISME journal **5**, 717–727.

Chan, C.S., McAllister, S.M., Leavitt, A.H., Glazer, B.T., Krepski, S.T., Emerson, D. (2016). *The architecture of iron microbial mats reflects the adaptation of chemolithotrophic iron oxidation in freshwater and marine environments.* Frontiers in Microbiology **7**.

Kruber C. (2007) *Hydrothermal Deposits and Weathered Basaltic Glasses at the Mohns Ridge: Textures, Geochemistry and Microbial Effects.* University of Bergen.

Craddock P. R., Bach W., Seewald J. S., Rouxel O. J., Reeves E. and Tivey M. K. (2010) *Rare earth element abundances in hydrothermal fluids from the Manus Basin, Papua New Guinea: indicators of sub-seafloor hydrothermal processes in back-arc basins.* Geochim. Cosmochim. Acta **74**, 5494–5513.

Cooper, M.J., Elderfield, H., Schultz, A. (2000). *Diffuse hydrothermal fluids from Lucky Strike hydrothermal vent field: Evidence for a shallow conductively heated system. Journal of Geophysical Research*: Solid Earth **105**, 19369–19375.

Davidson, G.J., Stolz, A.J., Eggins, S.M. (2001). *Geochemical anatomy of silica iron exhalites: evidence for hydrothermal oxyanion cycling in response to vent fluid redox and thermal evolution (Mt. Windsor Subprovince, Australia).* Economic Geology **96**, 1201–1226.

Dekov V. M., Petersen S., Garbe-Scho¨nberg C.-D., Kamenov G. D., Perner M., Kuzmann E. and Schmidt M. (2010) *Fe-Sioxyhydroxide deposits at a slow-spreading centre with thickened oceanic crust: the Lilliput hydrothermal field (933'S, MidAtlantic Ridge).* Chem. Geol. **278**, 186–200.

Duhig, N.C., Davidson, G.J., Stolz, J. (1992). *Microbial involvement in the formation of Cambrian sea-floor silica-iron oxide deposits, Australia.* Geology **20**, 511–514.

Edwards K. J., Glazer B. T., Rouxel O. J., Bach W., Emerson D., Davis R. E., Toner B. M., Chan C. S., Tebo B. M., Staudigel H. *and Moyer C. L.* (2011) *Ultra-diffuse hydrothermal venting supports Fe-oxidizing bacteria and massive umber deposition at 5000 m off Hawaii.* ISME J. **5**, 1748–1758.

Edmond, J.M., Measures, C., Mangum, B., Grant, B., Sclater, F.R., Collier, R., Hudson, A., Gordon, L.I., Corliss, J.B. (1979). *On the formation of metal-rich deposits at ridge crests.* Earth and Planetary Science Letters **46**, 19–30.

Elderfield, H., Schultz, A. (1996). *Mid-ocean ridge hydrothermal fluxes and the chemical composition of the ocean.* Annual Review of Earth and Planetary Sciences **24**, 191–224.

Emerson, D., and Moyer, C. (1997). *Isolation and characterization of novel iron- oxidizing bacteria that grow at circumneutral pH.* Appl. Environ. Microbiol. **63**, 4784–4792.

Emerson D., Rentz J. A., Lilburn T. G., Davis R. E., Aldrich H., Chan C. and Moyer C. L. (2007) *A novel lineage of proteobacteria involved in formation of marine Fe-oxidizing microbial mat communities.* PLoS ONE **2**, e667.

Emerson, D., Fleming, E.J., McBeth, J.M. (2010). *Iron-oxidizing bacteria: an environmental and genomic perspective.* Annual review of microbiology **64**, 561–583.

Esther J, Sukla LB, Pradhan N, Panda S (2015) *Fe(III) reduction strategies of dissimilatory iron reducing bacteria.* Korean J Chem Eng **32**:1–14.

Fehn U, K.E. Green, R.P. Von Herzen, L.M. (1983) Cathles *Numerical models for the hydrothermal field at the Galapagos Spreading Center* J. Geophys. Res., **88**pp. 1033-1048.

Fehn U and Lawrence M.C. (1986) *The influence of plate movement on the evolution of hydrothermal convection cells in the oceanic crust* Tectonophysics Vol. **125**, Issue 4, 15 May 1986, p. 289-312.

Fleming, E.J., Cetinić, I., Chan, C.S., King, D.W., Emerson, D. (2014). *Ecological succession among iron-oxidizing bacteria.* The ISME journal **8**, 804–815.

Forget N. L., Murdock S. A. and Juniper S. K. (2010) *Bacterial diversity in Fe-rich hydrothermal sediments at two South Tonga Arc submarine volcanoes.* Geobiology **8**, 417–432.

German, C.R., Legendre, L.L., Sander, S.G., Niquil, N., Luther, G.W., Bharati, L., Han, X., Le Bris, N. (2015). *Hydrothermal Fe cycling and deep ocean organic carbon scavenging: Model-based evidence for significant POC supply to seafloor sediments.* Earth and Planetary Science Letters **419**, 143–153.

Gonzalez-Toril, E., Llobet-Brossa, E., Casamayor, E.O., Amann, R., and Amils, R. (2003) *Microbial ecology of an extreme acidic environment, the Tinto River.* Appl Environ Microbiol **69**: 4853–4865.

Grenne, T., Slack, J.F. (2003a). *Bedded jaspers of the Ordovician Løkken ophiolite, Norway: seafloor deposition and diagenetic maturation of hydrothermal plume-derived silica-iron gels.* Mineralium Deposita **38**, 625–639.

Grenne T., and Slack J. F. (2003b). *Paleozoic and Mesozoic silica-rich seawater: Evidence from hematitic chert (jasper) deposits.* Geology **31**, 319-322.

Grenne, T., Slack, J.F. (2005). *Geochemistry of jasper beds from the Ordovician Løkken ophiolite, Norway: origin of proximal and distal siliceous exhalites.* Economic Geology **100**, 1511–1527.
Gromet, L.P., Haskin, L.A., Korotev, R.L., Dymek, R.F. (1984). The *"North American shale composite": its compilation, major and trace element characteristics"*. Geochimica et Cosmochimica Acta **48**, 2469–2482.

Hallbeck, L., and Pedersen, K. (1990). *Culture parameters regulating stalk formation and growth rate of Gallionella ferruginea.* J. Gen. Microbiol. **136**, 1675–1680.

Handley K. M., Boothman C., Mills R. A., Pancost R. D. and Lloyd J. R. (2010) *Functional diversity of bacteria in a ferruginous hydrothermal sediment.* ISME J. **4**, 1193–1205.

Hanert, H. (1973). *Quantification of gallionella development under natural conditions.* Arch. Microbiol. **88**, 225–243.

Hannington M.D., C.E.J. de Ronde, S. Petersen, in: J.W. Hedenquist, J.F.H. Thompson, R.J. Goldfarb, J.P. Richards (2005) (Eds.), *Economic Geology 100th Anniversary Volume, Society of Economic Geologists*, Littleton, Colorado, pp. 111–141, includes Appendix in CD.

Hannington M.D., I.R. Jonasson, P.M. Herzig, S. Petersen, (1995) Physical and chemical processes of seafloor mineralization at mid-ocean ridges, Geophys. Monogr. Vol. **91** p115–157.

Hegler, F., Lösekann-Behrens, T., Hanselmann, K., Behrens, S., and Kappler, A. (2012). *Influence of seasonal and geochemical changes on the geomicrobiology of an iron carbonate mineral water spring*. Appl. Environ. Microbiol. **78**, 7185–7196.

Hekinian R., Hoffert M., Larque´ P., Chemine´e J. L., Stoffers P. and *Bideau D. (1993) Hydrothermal Fe and Si oxyhydroxide deposits from South Pacific intraplate volcanoes and East Pacific Rise axial and off-axial regions*. Econ. Geol. **88**, 2099– 2121.

Horton E. Newsom, Justin J. Hagerty, and Ivan E. (2004) *Location and Sampling of Aqueous and Hydrothermal Deposits in Martian Impact Craters*. Thorsos. Astrobiology, **1**(1): 71-88

Hrischeva, E., Scott, S.D. (2007). *Geochemistry and morphology of metalliferous sediments and oxyhydroxides from the Endeavour segment, Juan de Fuca Ridge.* Geochimica et Cosmochimica Acta **71**, 3476–3497

Jensen, H.S., Mortensen, P.B., Andersen, F., Rasmussen, E., Jensen, A. (1995). *Phosphorus cycling in a coastal marine sediment, Aarhus Bay, Denmark.* Limnology and Oceanography **40**, 908–917.

Johanston, J., and Williamson, E.D. (1916) Journ. Geology **24**, 729.

Johannessen, K.C., Vander Roost, J., Dahle, H., Dundas, S.H., Pedersen, R.B., Thorseth, I.H. (2017). *Environmental controls on biomineralization and Fe-mound formation in a low-temperature hydrothermal system at the Jan Mayen Vent Fields.* Geochimica et Cosmochimica Acta **202**, 101–123.

Johannesson, Kevin H.; Lyons, W. Berry; Fee, Jennifer H.; Gaudette, Henri E.; Mcarthur, John M. (1994), *Geochemical processes affecting the acidic groundwaters of Lake Gilmore, Yilgarn Block, Western Australia: a preliminary study using neodymium, samarium, and dysprosium* Journal of Hydrology, Vol.**154**(1), pp.271-289.

Juniper, S.K., Fouquet, Y., (1988). *Filamentous iron-silica deposits from modern and ancient hydrothermal sites.* The Canadian Mineralogist **26**, 859–869.

Juniper, S. K. and Tebo, B. M. (1995) *Microbe-metal interactions and mineral deposition at hydrothermal vents. In Microbiology of Extreme and Unusual Environments*, **2**: Deep-Sea Hydrothermal Vent Habitats, D. M. Karl (ed.), pp. 219-253. Telford Press, Caldwell, NJ.

Karl, D.M., McMurtry, G.M., Malahoff, A., Garcia, M.O. (1988). *Loihi Seamount, Hawaii: a mid-plate volcano with a distinctive hydrothermal system.* Nature **335**, 532-535.

Kato S, Kobayashi C, Kakegawa T & Yamagishi A (2009) Microbial communities in iron-silica-rich microbial mats at deep-sea hydrothermal fields of the southern Mariana Trough. Environ Microbiol **11**: 2094–2111.

Kelley DS, Baross JA, Delaney JR (2002) Volcanoes, fluids and life at mid-ocean
Kodaira S, R. Mjelde, K. Gunnarsson, H. Shiobara, H. Shimamura *Evolution of oceanic crust on the Kolbeinsey Ridge, north of Icealnd, over the past 22 Myr* Terra Nova, **10** (1998), pp. 27–31.

Kendall, B., Anbar, A.D., Kappler, A., Konhauser, K.O., 2012. *The global iron cycle.* Fundamentals of Geobiology 65–92.

Kennedy, C.B., Martinez, R.E., Scott, S.D., Ferris, F.G., 2003a. *Surface chemistry and reactivity of bacteriogenic iron oxides from Axial Volcano, Juan de Fuca Ridge, north- east Pacific Ocean.* Geobiology **1**, 59–69.

Kennedy, C.B., Scott, S.D., Ferris, F.G., 2003b. *Characterization of bacteriogenic iron oxide deposits from Axial Volcano, Juan de Fuca Ridge, northeast Pacific Ocean.* Geomicrobiology Journal **20**, 199–214.

Kilias S. P., Nomikou P., Papanikolaou D., Polymenakou P. N., Godelitsas A., Argyraki A., Carey S., Gamaletsos P., Mertzimekis T. J., Stathopoulou E., Goettlicher J., Steininger R., Betzelou K., Livanos I., Christakis C., Croff Bell K. and *Scoullos M. (2013) New insights into hydrothermal vent processes in the unique shallow-submarine arc volcano, Kolumbo (Santorini), Greece.* Sci. Rep. **3**, 1–13.

Konhauser, K. O., 1998. *Diversity of bacterial iron mineralization.* Earth-Science Reviews, **43**, 91-121.

Krepski, S.T., Emerson, D., Hredzak-Showalter, P.L., Luther, G.W., Chan, C.S. (2013). *Morphology of biogenic iron oxides records microbial physiology and environmental conditions: toward interpreting iron microfossils.* Geobiology **11**, 457–471.

Krepski, S.T., Hanson, T.E., Chan, C.S., 2012. *Isolation and characterization of a novel biomineral stalk-forming iron-oxidizing bacterium from a circumneutral groundwater seep.* Environmental microbiology **14**, 1671–1680.

*Lee, J. S.; McBeth, J. M.; Ray, R. I.; Little, B. J.; Emerson, D. (2013). Iron cycling at corroding carbon steel surfaces. Biofouling. **29** (10): 1243–1252.*

Little C. T. S. and Thorseth I. H. (2002) *Hydrothermal vent microbial communities: a fossil perspective.* Cah. Biol. Mar. **43**, 317–319.

Little, C.T., Glynn, S.E., Mills, R.A. (2004). *Four-hundred-and-ninety-million-year record of bacteriogenic iron oxide precipitation at sea-floor hydrothermal vents.* Geomicrobiology Journal **21**, 415–429.

Lottermoser, B.G. (1992). *Rare earth elements and hydrothermal ore formation processes.* Ore Geology Reviews **7**, 25–41.

*McBeth, J. M.; Little, B. J.; Ray, R. I.; Farrar, K. M.; Emerson, D. (2010). Neutrophilic Iron-Oxidizing "Zetaproteobacteria" and Mild Steel Corrosion in Nearshore Marine Environments. Applied and Environmental Microbiology. **77** (4): 1405–1412.*

MacLean W. H. and Kranidiotis P. (1987) *Immobile elements as monitors of mass transfer in hydrothermal alteration: Phelps Dodge massive sulfide deposit, Matagami, Quebec.* Econ. Geol. **82**, 951–962.

McAllister, S. M., Davis, R. E., McBeth, J. M., Tebo, B. M., Emerson, D., and Moyer, C. L. (2011). *Biodiversity and emerging biogeography of the neutrophilic ironoxidizing Zetaproteobacteria.* Appl. Environ. Microbiol. **77**, 5445–5457.

Michard A., Michard G., Stu¨ben D., Stoffers P., Chemine´e J.-L. *and Binard N. (1993) Submarine thermal springs associated with young volcanoes: the Teahitia vents, Society Islands, Pacific Ocean.* Geochim. Cosmochim. Acta **57**, 4977–4986.

Moeller, K., Schoenberg, R., Grenne, T., Thorseth, I.H., Drost, K., Pedersen, R.B. (2014). *Comparison of iron isotope variations in modern and Ordovician siliceous Fe oxyhydroxide deposits.* Geochimica et cosmochimica acta **126**, 422–440.

Morgan J. J. (2005) *Kinetics of reaction between O_2 and Mn(II) species in aqueous solutions.* Geochim. Cosmochim. Acta **69**, 35– 48.

Mosier D. L., Berger V. I. & Singer D. A. (2009) *Volcanogenic massive sulfide deposits of the world-database and grade and tonnage models.* USGS Open-File Rep. 2009–1034, 46p.

Mukhopadhyay J., Gutzmer J., Beukes N. J, Hayashi K. I. (2008). *Stratabound magnetite deposits from the eastern outcrop belt of the Archaean Iron Ore Group, Singhbhum craton, India. Applied Earth Science.* Transcripts of the Institution of Mining and Metallurgy, Section B, **117**, 175–186.

Murray, J.W., Dillard, J.G. (1979). *The oxidation of cobalt (II) adsorbed on manganese dioxide.* Geochimica et Cosmochimica Acta **43**, 781–787.

Nakamura, K., Takai, K. (2014). *Theoretical constraints of physical and chemical properties of hydrothermal fluids on variations in chemolithotrophic microbial communities in seafloor hydrothermal systems.* Progress in Earth and Planetary Science **1**, 5.

Olsen, B.R, Økland, I.E, Thorseth, I.H, Pedersen, R.B, Rapp, H.T. (2016). *Environmental challenges related to offshore mining and gas hydrate extraction.* Miljødirektoratet.

Pedersen, R. B., Thorseth, I. H., NygåRd, T. E., Lilley, M. D. and Kelley, D. S. (2010) *Hydrothermal Activity at the Arctic Mid-Ocean Ridges, in Diversity of Hydrothermal Systems on Slow Spreading Ocean Ridges* (eds P. A. Rona, C. W. Devey, J. Dyment and B. J. Murton), American Geophysical Union, Washington, D. C.

Pedersen, R. B., I. H. Thorseth, B. Hellevang, A. Schultz, P. Taylor, H. P. Knudsen, and B. O. Steinsbu (2005), *Two vent fields discovered at the ultraslow spreading Arctic Ridge System*. Eos Trans. AGU, **86**(52), Fall Meet. Suppl., Abstract OS21C 01.

Pedersen, R.B., Thorseth, I.H., Nygård, T.E., Lilley, M.D., Kelley, D.S. (2010). *Hydrothermal Activity at the Arctic Mid-Ocean Ridges.* In Rona, P., Devey, C. and Murton, B. (eds.): Diversity of hydrothermal systems on slow spreading ocean ridges. Geophysical monograph 188, Washington D.C., American Geophysical Union, 67-89.

Peng X., Ta K., Chen S., Zhang L. and Xu H. (2015) *Coexistence of Fe(II)- and Mn(II)-oxidizing bacteria govern the formation of deep sea umber deposits.* Geochim. Cosmochim. Acta **169**, 200–216.

Poulton, S.W., Canfield, D.E. (2006). *Co-diagenesis of iron and phosphorus in hydrothermal sediments from the southern East Pacific Rise: Implications for the evaluation of paleoseawater phosphate concentrations.* Geochimica et Cosmochimica Acta **70**, 5883–5898.

Li, J., Zhou, H., Peng, X., Wu, Z., Chen, S., Fang, J. (2012). *Microbial diversity and biomineralization in low-temperature hydrothermal iron–silica-rich precipitates of the Lau Basin hydrothermal field.* FEMS microbiology ecology **81**, 205–216.

Lovley, D. R., and E. J. P. Phillips. (1986). *Organic matter mineralization with the reduction of ferric iron in anaerobic sediments*. Appl. Environ. Microbiol. **51**:683-689.

Resing, J.A., Sedwick, P.N., German, C.R., Jenkins, W.J., Moffett, J.W., Sohst, B.M., Tagliabue, A. (2015). *Basin-scale transport of hydrothermal dissolved metals across the South Pacific Ocean.* Nature **523**, 200–203.

Rollinson H. (1993). *Using Geochemical Data: Eveluation, Presentation, Interpretation*. Routledge, New York.

Scholten J. C., Scott S. D., Garbe-Scho¨nberg D., Fietzke J., Blanz T. and Kennedy C. B. (2004) *Hydrothermal Iron and Manganese Crusts from the Pitcairn Hotspot Region. In Oceanic Hotspots. Intraplate Submarin Magmatism and Tectonisms* (eds. R. Hekinian, P. Stoffers and J.- L. Chemine´e). Springer-Verlag, Berlin. pp. 375–405.

Scott, J.J., Breier, J.A., Luther III, G.W., Emerson, D., (2015). *Microbial iron mats at the MidAtlantic Ridge and evidence that Zetaproteobacteria may be restricted to iron-oxidizing marine systems.* PLoS One **10**, e0119284.

Sherrell, R.M., Field, M.P., Ravizza, G. (1999.) *Uptake and fractionation of rare earth elements on hydrothermal plume particles at 9 45′ N, East Pacific Rise*. Geochimica et Cosmochimica Acta **63**, 1709–1722.

Sleep N.H. (1991) Hydrothermal circulation, anhydrite precipitation, and thermal structure at Ridge axes, J. Geophys. Res., **96**, 2735-2397.

Slack J. F. (1993) *Descriptive and grade-tonnage models for Besshi-type massive sulphide deposits. Geol. Assoc*. Canada Spec. Pap. **40**, 343–371.

Slack, J.F., Grenne, T., Bekker, A., Rouxel, O.J., Lindberg, P.A. (2007). *Suboxic deep seawater in the late Paleoproterozoic: evidence from hematitic chert and iron formation related to seafloor-hydrothermal sulfide deposits, central Arizona, USA.* Earth and Planetary Science Letters **255**, 243–256.

Stein C. A and Stein S. (1994). Constraints on Hydrothermal Heat flux through the Oceanic *Lithosphere from Global Heat Flow. Journal of Geophysical research*, Vol. **99**, no. B2, p.3081-3095.

Stein, C.A., S. Stein, and A. Pelayo, (1995), Heat flow and hydrothermal circulation. In: *Seafloor Hydrothermal Systems: Physical, Chemical, Biological, and Geological Interactions* (S. E. Humphris, R. A. Zierenberg, L. S. Mullineaux, and R. E. Thomson, eds.). AGU Monograph Series, No. 91. American Geophysical Union, Washington, DC, pp. 425-445.

Straub, K.L.; Buchholz-Cleven, Berit E.E. (1998). Enumeration and Detection of Anaerobic Ferrous Iron-Oxidizing, Nitrate-Reducing Bacteria from Diverse European Sediments. Applied and Environmental Microbiology, Vol. 64(12), p.4846.

Stumm, W., Morgan JJ. (1998). *Aquatic Chemistry: Chemical Equilibria and Rates in Natural Waters, **3rd** ed.* Wiley, New York.

Svellingen, W. (2004). *Submarin vulkanisme i Jan Mayen området.* M. Sc. Thesis, Department of Earth Science, University of Bergen.

Sverjensky, D.A. (1984) *Europium redox equilibria in aqueous solution.* Earth and Planetary Science Letters **67**, 70–78.

Sun Z., Li J., Huang W., Dong H., Little C. T. S. and Li J. (2015) *Generation of hydrothermal Fe-Si oxyhydroxide deposit on the Southwest Indian Ridge and its implication for the origin of ancient banded iron formations.* J. Geophys. Res. Biogeosci. **120**, 187–203.

Tagliabue, A., Bopp, L., Dutay, J.-C., Bowie, A.R., Chever, F., Jean-Baptiste, P., Bucciarelli, E., Lannuzel, D., Remenyi, T., Sarthou, G. (2010). *Hydrothermal contribution to the oceanic dissolved iron inventory.* Nature Geoscience **3**, 252–256.

Takai K, Nakamura K, Toki T, Tsunogai U, Miyazaki M, Miyazaki J, Hirayama H, Nakagawa S, Nunoura T, and Horikoshi K (2008). *Cell proliferation at 122°C and isotopically heavy CH_4 production by a hyperthermophilic methanogen under high-pressure cultivation. PNAS.* **105** (31): 10949–51

Taylor, S.R., McLennan, S.M. (1985). *The continental crust: its composition and evolution.* Blackwell Scientific Publications, Oxford.

Tebo B. M., Johnson H. A., McCarthy J. K. and Templeton A. S. (2005) *Geomicrobiology of manganese(II) oxidation.* Trends Microbiol. **13**, 421–428.

Templeton A. S., Staudigel H. and Tebo B. M. (2005) *Diverse Mn (II)-oxidizing bacteria isolated from submarine basalts at Loihi Seamount.* Geomicrobiol. J. **22**, 127–139.

Thorseth, I. H., R. B. Pedersen, C. Kruber, and J. Kosler (2007). Low-temperature hydrothermal deposits at the 71°N vent fields at the Arctic Mid-Ocean Ridge: Architecture, microtextures, and geochemistry, *Eos Trans. AGU*, **88**(52), Fall Meet. Suppl., AbstractOS43A-0996.

Tivey M. K. (2007). *Generation of seafloor hydrothermal vent fluids and associated mineral deposits.* Oceanography, Vol. **20**, Number 1.

Toner, B. M. *et al. Biogenic iron oxyhydroxide formation at mid-ocean ridge hydrothermal vents: Juan de Fuca Ridge. Geochim. Cosmochim. Acta* **73**, 388–403 (2009).

Wood S. A. (1990). The aqueous geochemistry of the rare-earth elements and yttrium, 2. Theoretical predictions of speciation in hydrothermal solutions to 350 C at saturation water vapor pressure. Chem. Geol. **88**, 99–125.

Other references:

https://microbewiki.kenyon.edu

Personal communications with P.h.d Karen C. Johannessen and Professor Ingunn Thorseth at the Centre for Geobiology at the University in Bergen, during the year 2017.

Konhauser (2007) Introduction to Geobiology. Chapter 8 p.105-111.